Form-Function Relation: Implications of Synaptic Design on Neuronal Function

A thesis

Submitted in partial fulfillment of the requirements

Of the degree of

Doctor of Philosophy

By

NISHANT SINGH
Roll No. 20153393

IISER PUNE

INDIAN INSTITUTE OF SCIENCE EDUCATION AND RESEARCH PUNE

2022

Some seeds need deep roots
Before their flowers bloom.

DEDICATION

For *maa*.

She has been a constant source of joy, encouragement and support.
It makes me happy to know that she will be the happiest to see this thesis complete.

DECLARATION

I declare that this written submission represents my ideas in my own words and where others' ideas have been included, I have adequately cited and referenced the original sources. I also declare that I have adhered to all principles of academic honesty and integrity and have not misrepresented or fabricated or falsified any idea/data/fact/source in my submission. I understand that violation of the above will be cause for disciplinary action by the Institute and can also evoke penal action from the sources which have thus not been properly cited or from whom proper permission has not been taken when needed.

निshant सिngh

(Signature)

Nishant Singh
(Name of the Student)

Roll No. 20153393

Date: 29/03/2022

CERTIFICATE

Certified that the work incorporated in the thesis entitled "Form-Function Relation: Implications of Synaptic Design on Neuronal Function" submitted by Mr. Nishant Singh was carried out by the candidate, under my supervision. The work presented here or any part of it has not been included in any other thesis submitted previously for the award of any degree or diploma from any other University or institution.

(Supervisor)

29/03/2022

Date:

ACKNOWLEDGEMENT

I would like to extend my gratitude to Suhita for her unwavering support throughout this journey. She has helped me grow in so many ways that I consider her my mentor, not merely my PhD supervisor.

I would not have gotten this far if not for the constant support from my family, especially maa, papa, Nishu, Raju mama, Niranjan mama, Raja mama, nani and nana. Their love has been a big force that kept me going on difficult days.

Collins, thank you for genuinely appreciating my jokes, when no one would.

Rohan has been that presence who, with his ease, makes my problems seem small.

All my labmates have helped me in my research and personal development. I would especially like to mention Anup, Arun, Gaurang, and Subhadra.

My heartiest thanks to Neo for bearing with me during my most troubled days, as I wrote my thesis.

I am grateful to Surabhi and Shweta for reading through my thesis, and bringing cakes and happiness to the lab.

I would like to thank my school principal Mrs Tanuja Samal, and Dr. S P Khastgir, my Physics professor at Khagarpur for inspiring me.

Some of my closest friends, in their own way, have shaped me. I learnt how to learn from CeeBee (aka Chaitanya Bayanwala); A special word for Patel (Saurabh Patel) who taught me to seek hobbies – and be more – by simply being himself. Shyamji's appetite for life will always stay with me. And from Gopal, I learnt how not to worry.

Four years ago, Yashwantji knocked on my door to complain about my newest hobby. So much for being inspired by Patel! In hindsight, I agree it is not OK to practise your flute at 6 in the morning but well, who knew what was in store for us: over the coming months, Yashwantji and I would be close enough to consider each other family. Thank you for your support and wisdom.

I would also like to extend my gratitude to my RAC members for their support and guidance: Dr. Nixon and Dr. Girish.

I would like to thank INSPIRE and WELLCOME-DBT India Alliance for funding this research.

ABSTRACT

In the world around us, form and function are closely linked together. Each continually directing the other. Our brain is no exception. Its neural circuitry dictates behavior and our daily experiences, in turn, rewire the brain. In the same spirit, I have explored the intricate relation between the form and function of hippocampal synapses in my thesis.

The hippocampus, a deep structure in the limbic system, plays an essential role in storing and recollecting episodic memories. I have chosen to study two distinctly different synapses from the trisynaptic loop in this brain structure: the Schaffer collaterals and the mossy fibers to enable a comparative understanding of the inner workings of the systems. One of the most important properties of these synapses, which enables memory formation, is plasticity — the ability to modulate their synaptic strength in an activity-dependent manner. I have focussed on investigating the mechanistic cause behind a specific kind of plasticity called short-term plasticity (STP).

Schaffer collaterals originate in the CA3 and project onto CA1 creating a small synapse containing a single active zone, with barely ten vesicles in the readily releasable pool (RRP). The endoplasmic reticulum (ER) is extensively present in the axons. Mossy fibers, on the other hand, are large, hosting tens of active zones that incorporate hundreds of vesicles in their RRP. Rapid short-term plasticity manifests in both these synapses, but very differently, owing to their distinct form. Short bursts of stimuli increase synaptic efficacy in both cases although mossy fibers sustain the elevated synaptic strength for much longer. Sustained stimulus, on the other hand, depresses Schaffer collaterals while it strengthens mossy fibers. Despite decades of research into these synapses, our understanding of their form-function is still murky.

I have employed a computational approach to shed light on their underlying mechanisms. We developed physiologically realistic spatial models of the CA3 pyramidal neuron and the mossy fiber bouton to explore the role of synaptic form in orchestrating calcium signaling and plasticity. Such in-silico methods provide us with the ability to probe complex interactions between multiple components in small spaces that are difficult to study otherwise.

Our model predicts that presynaptic ER is critical in generating the observed STP in CA3-CA1 synapses. SERCA pumps maintain low release probability and contribute to residual calcium. Blocking ER disrupts facilitation as seen in animal models of Alzheimer's, underscoring the importance of ER in normal function. At the mossy fiber synapse, the crosstalk between active zones, local buffer saturation, and the calcium sensor synaptotagmin-7 make distinct contributions to STP. With subsequent stimuli, the local capacity to buffer calcium decreases and the residual calcium increases, so does the spatial extent of the calcium signal, which ultimately increases the overlap with nearby active zones. This cross-talk further elevates residual calcium levels, augmenting vesicle release. In addition, synaptotagmin-7 shows progressive increase in bound calcium with each subsequent calcium influx, leading to increased asynchronous release. The combined effect of these phenomena results in a sharp increase in neurotransmitter release that is capable of triggering an action potential in the postsynaptic terminal. Moreover, we find that STP is essential in decorrelating input signals in MF, thereby confirming its role in temporal pattern separation.

TABLE OF CONTENTS

Page

List of Figures **xvii**

1 Introduction **1**

1.1 The hippocampus 2

1.1.1 Functional organization of hippocampal circuitry 4

1.1.2 Pattern separation and completion 5

1.2 Synaptic transmission and neuronal plasticity 6

1.2.1 Synaptic transmission 6

1.2.2 Plasticity 7

1.2.3 Long-term synaptic plasticity 8

1.2.4 Short-term plasticity 9

1.3 Hippocampus in health and disease 10

1.4 Research questions 11

1.5 Organization of the thesis 12

2 Role of Secondary Calcium Source in Small Hippocampal Neurons in Health and Disease **13**

2.1 Introduction 13

2.2 Model construction 16

2.2.1 Chronology of events in response to a single action potential . . 19

2.3 ER is essential for short-term plasticity 19

2.3.1 Blocking ER increases transmitter release probability 19

2.3.2 Disruption of internal calcium store diminishes short-term plasticity 21

2.3.3 Altered calcium signaling disrupts STP 24

2.3.4 RyR contributes minimally to STP 29

2.4 Increased reliability mediated by stores machinery 29

2.5 Calcium overload in ER disrupts STP similar to genetic models of Alzheimer's disease . . . 32
2.5.1 Model reproduces established experimental observations . . . 34
2.6 Discussion . . . 36

3 Presynaptic Design Influences Short-term Plasticity in Hippocampal Mossy Fiber 39
3.1 Introduction . . . 39
3.2 The MFB model . . . 41
3.2.1 Chronology of events . . . 41
3.3 Degeneracy in synaptic design . . . 44
3.4 Probing the plasticity mechanism . . . 45
3.4.1 Role of calcium buffer, synaptotagmin and cross-talk in STP . . . 45
3.4.2 Interplay of calcium buffer and cross-talk leads to enhanced residual calcium . . . 49
3.4.3 Synaptotagmin-7 shows larger increase in neurotransmitter release . . . 49
3.5 Conditional detonation . . . 52
3.6 Implication of the design: temporal pattern separation . . . 52
3.7 Discussion . . . 52

4 Model Construction 57
4.1 CA3 bouton . . . 57
4.1.1 Simulations . . . 59
4.2 Hippocampal mossy fiber . . . 59
4.2.1 Spatial model of mossy fiber bouton . . . 60
4.2.2 Stochastic model of vesicle release . . . 61
4.2.3 CA3 phenomenological model . . . 61
4.2.4 CA3 inhibitory interneuron model . . . 62
4.3 Molecular components . . . 62
4.3.1 Voltage-dependent calcium channels . . . 62
4.3.2 Calcium sensors (synaptotagmin 1 and 7) . . . 63
4.3.3 Ryanodine receptor . . . 63
4.3.4 IP3 receptor . . . 63
4.3.5 SERCA pumps . . . 63
4.3.6 Calbindin-D28k . . . 64

4.3.7 Plasma membrane calcium ATPase pump 64
4.4 Tools used in the study 66
4.4.1 MCell 66
4.4.2 STEPS 67
4.4.3 Brian 67
4.4.4 Python, gnuplot, GNU parallel 67
4.5 Computing facility 67

5 Discussion **69**
5.1 Summary 69
5.2 Computational approaches to problems in neuroscience 71
5.3 Future prospects of the study 72

Publication **73**

Bibliography **75**

LIST OF FIGURES

FIGURE **Page**

1.1 Levels of investigation . . . 2
1.2 The hippocampal formation . . . 3
1.3 Circuitry of the hippocampal formation . . . 4

2.1 Model of the CA3 neuron bouton. . . . 17
2.2 Presence of ER in CA3 axons . . . 18
2.3 Chronology of events . . . 20
2.4 Release probability . . . 22
2.5 Facilitation . . . 23
2.6 Calcium buffering by calbindin-D28k and SERCA . . . 25
2.7 Calcium signal in response to a pair of APs . . . 26
2.8 Calcium signal in response to train stimulus . . . 27
2.9 Neurotransmitter release . . . 28
2.10 Negligible contribution of RyR to STP . . . 30
2.11 Reliability of synapses with ER . . . 33
2.12 STP dysregulation in Alzheimer's disease . . . 35
2.13 Comparison of simulation results with experimental data . . . 37

3.1 Model of the mossy fiber bouton . . . 42
3.2 Chronology of events . . . 43
3.3 Degeneracy in mossy fiber design . . . 46
3.4 Facilitation in mossy fiber . . . 47
3.5 Distribution of facilitation . . . 48
3.6 Calcium dynamics in the MF bouton . . . 50
3.7 Synaptotagmin activity . . . 51
3.8 Conditional detonation of CA3 pyramidal neuron . . . 53
3.9 Temporal pattern separation . . . 54

4.1 Model of the CA3 neuron bouton. 58
4.2 Model of the mossy fiber bouton 60
4.3 Kinetic schemes 65

CHAPTER 1

INTRODUCTION

Our brain, in broad terms, is a computing device: it takes sensory information from the external world, processes it and generates responses. This processing occurs at multiple levels: from the central nervous system all the way down to the neurons, synapses and molecules (see Figure 1.1). Consequently, probing our brain demands various levels of investigation.

Understanding how the brain performs such a magnanimous task is an important problem not only for our scientific curiosity, but also to tackle various brain disorders, and perhaps, even to enhance or augment its function in the near future.

The current approach to understanding the brain is much like the story of the blind men who come across an elephant and try to describe it based on their limited experience. One of the men gets hold of its leg and says the elephant is like a tree stump. The other who held its trunk likens it to a huge python. The neuroscience community has also been probing and prodding different parts of the brain in an attempt to comprehend its functional underpinnings for more than a century now: while Ramon y Cajal looked into the anatomy of neurons, Alan Hodgkin and Andrew Huxley investigated the origin of electrical signals in neurons. Stephen W. Kuffler elucidated light reception in mammalian retinal ganglion cells, and Mosers investigated the encoding of space in rodent brains. Some have explored which brain regions are responsible for what behaviors while others have examined how peripheral neurons sense the world around us. Probing and prodding various parts of the brain at various levels, we aim to, someday, have a cohesive understanding of it, and see the elephant for what it is.

Humbly, I contribute towards this grand aim by exploring the inner workings of synapses in the hippocampus.

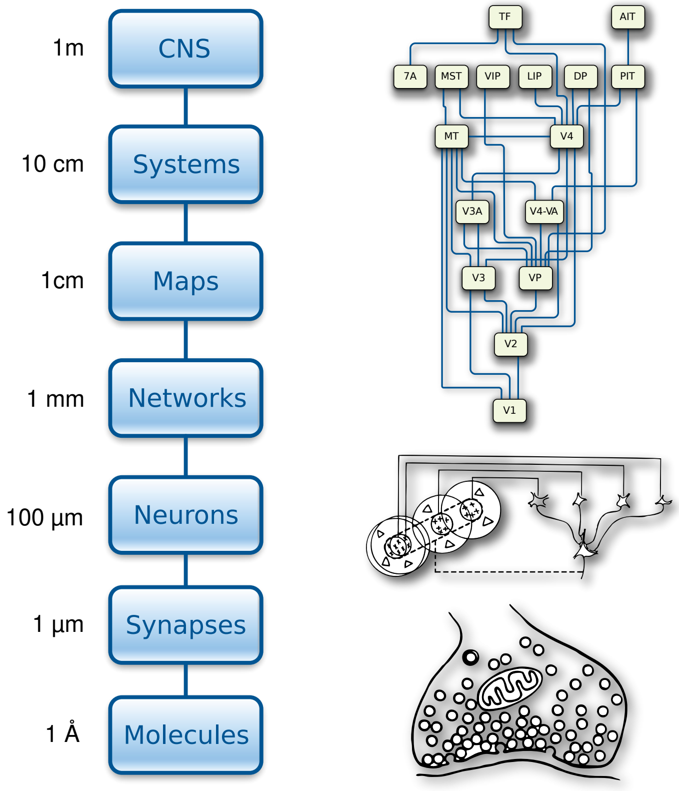
1m
CNS
10 cm
Systems
1cm
Maps
1 mm
Networks
100 µm
Neurons
1 µm
Synapses
1 Å
Molecules
TF
AIT
7A
MST
VIP
LIP
DP
PIT
MT
V4
V3A
V4-VA
V3
VP
V2
V1

Figure 1.1: **Levels of investigation.** source: https://cnl.salk.edu

1.1 The hippocampus

The hippocampus has intrigued scientists for centuries. Its first documented description is credited to Julius Caesar Arantius (Giulio Cesare Aranzi), a sixteenth-century surgeon and anatomist, from Italy [Bir et al., 2015]. Arantius called this brain structure "hippocampus" given its resemblance to a seahorse. (*Hippos* means "horse" and *kampos* means "sea monster" in Greek.) He also likened it to a silkworm, but "bombycini" or "bombyx" never caught on. In 1742, De Garengeot coined a new term for the hippocampus: "cornu ammonis" or Ammon's horn after the Egyptian god, Amun Kneph. Although the term was rarely used for hippocampus, its subdivisions are referred to as abbreviations of cornu ammonis (CA1, CA2 and CA3).

Located deep within the medial temporal lobe of the mammalian brain, the hippocampus is an integral part of the limbic system (see Figure 1.2). It is not an independent structure, but acts in concert with neighboring structures: the dentate gyrus, subiculum, presubiculum, parasubiculum and entorhinal cortex. Together, these regions form a functional unit called the hippocampal formation.

Phylogenetically, the hippocampus is one of the oldest parts of the brain. Although its shape and size are different in rats, monkeys and humans (the volume of human hippocampus is about 10 times more than that of a monkey's, and about 100 times more than that of a rat's), the basic architecture and connectivity among the neurons are highly conserved across mammalian hippocampus [Per et al., 2009].

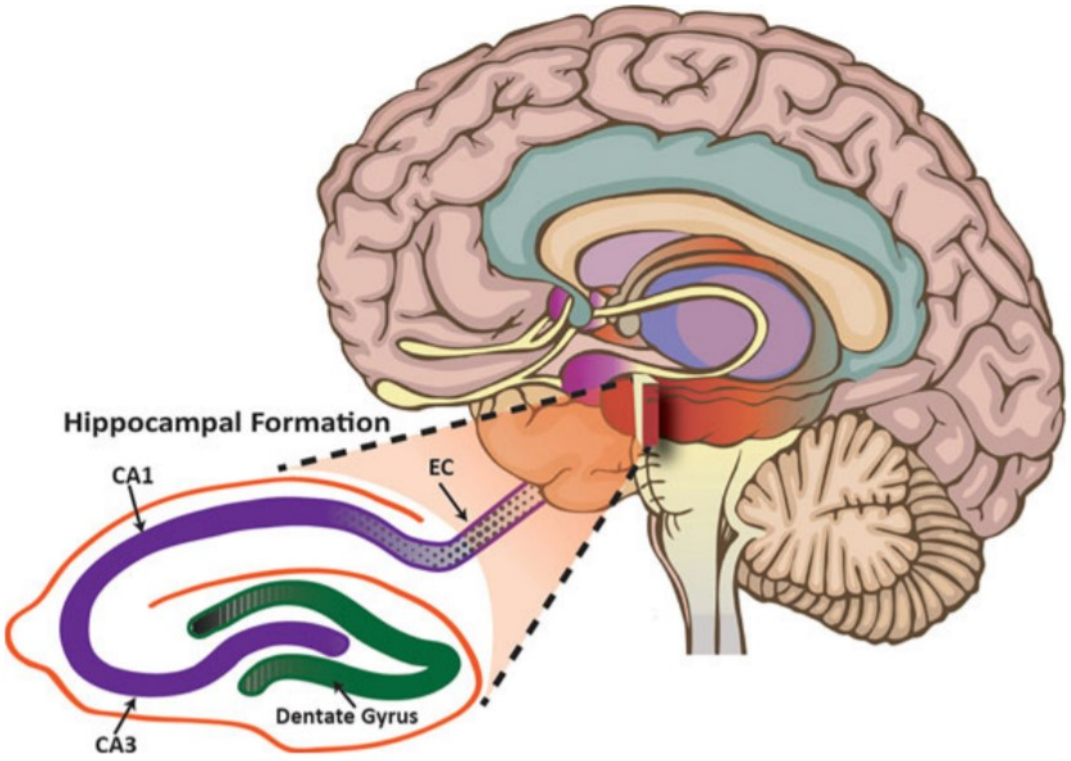

Figure 1.2: **The hippocampal formation.** It lies deep in the medial temporal lobe. Its major components are the entorhinal cortex, dentate gyrus and hippocampus proper (CA1, CA2 and CA3). source: https://www.creative-diagnostics.com/blog/index.php/what-is-hippocampus

The hippocampus is a quintessential memory and learning machine. It is involved in episodic memory formation and its retrieval, and spatial navigation. Episodic memory includes the ability to learn, store, and retrieve events from our daily experiences [Burgess et al., 2002]. Over the past few decades, many different functional cells have been discovered in the rodent hippocampus: place cells, head direction cells and grid cells. These provide a spatiotemporal framework to represent our daily conscious experiences [Bird and Burgess, 2008; McNaughton et al., 2006; Miller et al., 2013]. The hippocampal circuitry is well designed to support the complex task of encoding and retrieving episodic memories.

1.1.1 Functional organization of hippocampal circuitry

Neuronal network in the hippocampus has a characteristic directional connectivity [Witter et al., 1989]. The trisynaptic circuit is a major unidirectional highway in the hippocampus. It begins in the entorhinal cortex and projects onto the dentate gyrus via the perforant pathway. Mossy fibers from dentate gyrus further project onto the CA3 field that further passes on the signals to the CA1 field, and then back to the entorhinal cortex (see Figure 1.3). This is starkly different from the neocortex that has a largely reciprocal connectivity between different regions [Harris and Mrsic-Flogel, 2013; Ko et al., 2011].

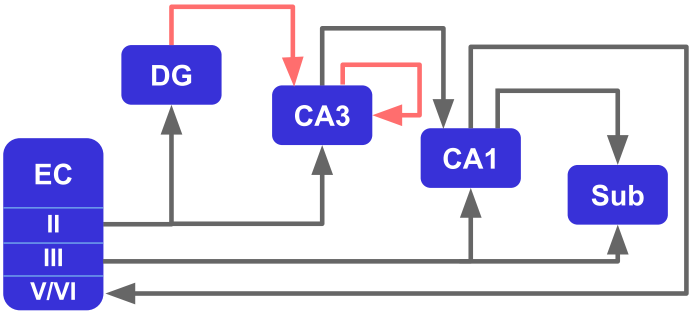

Figure 1.3: **Circuitry of the hippocampal formation.** EC: entorhinal cortex, DG: dentate gyrus, CA: cornu ammonis, Sub: subiculum.

The entorhinal cortex establishes a major gateway between the cortex (or neocortex) and the hippocampus, providing essential, raw data. It receives multimodal sensory input from the cortex. The perforant fibers arise principally in layers II and III of the entorhinal cortex (EC), with minor inputs from the deeper layers IV and V. Layer II and IV provide inputs to the granule cells in the dentate gyrus and pyramidal neurons in the CA3 field. Layer III and V project onto pyramidal neurons of the CA1 and subiculum. The perforant path is often subdivided into lateral and medial pathways, depending on their region of origin: lateral or medial entorhinal cortex [Strange et al., 2014; Van Strien et al., 2009].

Dentate gyrus is unique in its ability to generate new neurons in the adult brain. It is one of the two established neurogenic niches, the other is the subventricular zone of the lateral ventricles [Ming and Song, 2011]. Dentate granule cells (GDC) decorrelate the input activity patterns it receives from the entorhinal cortex and send them down to CA3 via mossy fibers. These fibers travel through hilar, the region where they make en passant synapses with mossy cells, before entering CA3 hippocampal subfield. In the CA3 region, these fibers make two different kinds of synapses. Giant mossy fiber boutons (MFB) make synapses with CA3 pyramidal neurons. A single DGC axon contacts about 15 different CA3 pyramidal neurons, providing only one contact per neuron. Each CA3 pyramidal neuron receives input from about 50 DGC [Amaral et al., 1990]. Filopodial extensions of MFB give rise to small synapses with interneurons (mostly GABAergic). These interneurons provide feedforward inhibition to CA3 pyramidal neurons [Acsady et al., 1998; Rollenhagen et al., 2007; Toth et al., 2000].

CA3 region primarily receives three prominent forms of excitatory inputs. Apart from the aforementioned perforant pathway from the entorhinal cortex and mossy fibers from the dentate gyrus, they receive inputs from other CA3 pyramidal neurons. These recurrent axons make extensive interconnections among the neighboring pyramidal neurons as well as inhibitory interneurons. It is a prominent feature of the region [Amaral et al., 1990; Per et al., 2009]. Pyramidal neurons in the CA3 further project signals onto CA1 via Schaffer collaterals. CA1 pyramidal neurons are similar to their CA3 counterparts in properties. These neurons further send projections to the subiculum as well as back to EC in layer V/VI.

1.1.2 Pattern separation and completion

Dentate gyrus contains a larger number of granule cells relative to CA3 neurons, and a single granule cell contacts only a few CA3 neurons. This configuration is ideally suited for what is known as pattern separation. It is the minimization of overlap between patterns of neuronal activity that represent similar experiences. Genetic and lesion studies in rodent hippocampus [Kesner et al., 2016; McHugh et al., 2007; Neunuebel and Knierim, 2014] strongly indicate the role of dentate gyrus as a pattern separator. Two overlapping input activity patterns in dentate gyrus elicit distinct cell-population activity in the CA3. Theoretical and computational modeling studies also suggest that DG separates cortical input patterns before sending it to CA3 [O'reilly and McClelland, 1994; Rolls, 2010; Treves and Rolls, 1994]. However, DG could be receiving decorrelated activity representations from upstream structure: the entorhinal cortex. Some electrophysiological studies show decrease in spatial correlation of activity representations in DG compared to EC [Knierim and Neunuebel, 2016; Leutgeb et al., 2007; Neunuebel et al., 2013].

Pattern completion is a complementary process of pattern separation. A memory is represented as a specific activity pattern in the neurons. A partial or degraded input is able to restore the original pattern that inscribed the memory. For example, a network may output the complete address of a house when presented with only the street name as a cue. This pattern completion is often ascribed to CA3 [Knierim and Neunuebel, 2016]. The dense recurrent collaterals in CA3 provide an anatomical basis for an autoassociative network. Such a network can encode non-overlapping input from dentate gyrus as unique firing patterns of pyramidal cells in CA3 [Rolls, 2013].

1.2 Synaptic transmission and neuronal plasticity

Another essential property of these hippocampal neurons that allows them their function is plasticity. Arguably, hippocampal neurons exhibit the largest amount of plasticity, both short-term and long-term. Before we delve into plasticity, let's take a look into synaptic transmission at a chemical synapse in the hippocampus.

1.2.1 Synaptic transmission

It is an intricately orchestrated process. An action potential generated at the proximal end of an axon travels to the presynaptic bouton. Sudden membrane depolarisation of the bouton due to an AP lasts only about a millisecond. It changes the conformation of voltage-dependent calcium channels (VDCCs) and renders them open, transiently. VDCCs are localized around active zones. Opening of these channels allow free movement of calcium ions across the neuronal membrane of the presynaptic bouton. A large difference of four orders of magnitude in calcium concentration across the neuronal membrane causes a large influx of calcium ions into the cytosol during an action potential. This calcium signal through VDCCs is spatially limited by fast calcium buffers and temporally by the small timespan of action potentials. Calcium sensors present at the active zones, upon binding calcium ions, start the chain of events in the SNARE proteins that fuses neurotransmitter-containing vesicles with the plasma membrane, thus, releasing its content, neurotransmitters, into the synaptic cleft. Glutamate is the most commonly found neurotransmitter in excitatory hippocampal neurons.

On the postsynaptic side, neurotransmitters released in the synaptic cleft are received by α-amino-3-hydroxy-5-methyl-4-isoxazolepropionic acid (AMPA) and N-methyl-D-aspartate (NMDA) receptors. Postsynaptic membrane on the dendritic spine is enriched with AMPA and NMDA receptors. These receptors are highly dynamic in nature and synaptic activity determines their quantity present on the membrane. AMPA receptors are formed by 4 subunits in a dimer-of dimers form. Glutamate, upon binding to the receptor, opens a pore that allows sodium and potassium ions to pass through, in accordance with their electrochemical gradient. A rare combination of subunits allows passage of calcium ions also [Chater and Goda, 2014; Jurado et al., 2010].

NMDA receptors are glutamate binding channels composed of NR1, NR2 and NR3 subunits. Extracellular magnesium ions can bind to the receptor, blocking its activity. Mg^{2+} ions are dislodged by sufficient depolarisation of the postsynaptic membrane which allows it to conduct calcium and sodium ions into the dendritic spine. Sustained stimulus can depolarise the membrane due to the action of AMPA receptors, such that NMDA receptors allow calcium influx. Rise in calcium levels in the postsynaptic terminal can lead to a plethora of downstream signaling.

1.2.2 Plasticity

Plasticity, in general, refers to the capability of being deformed or molded continuously in an irreversible manner. In the context of neuroscience, plasticity is associated with a neuron's ability to change its response in an activity-dependent manner. Such changes may manifest themselves in the form of new synapses or degradation of an old one (structural plasticity) or, in the modulation of synaptic properties that affect transmission (synaptic plasticity). Here, we will limit our discussion to synaptic plasticity. The term "synaptic plasticity" was first introduced by a Polish psychologist, Jerzy Konorski to describe persistent and activity-dependent changes in synaptic strength [Konorski, 1948]. Donald Hebb presented one of the earliest ideas suggesting activity-dependent modulation of neuronal signal transmission. Later, it came to be known as Hebb's rule of synaptic plasticity or Hebbian plasticity: repeated activity across a synapse should gradually strengthen the synapse, such that the learning-dependent changes are reflected in the strength of the synapse [Abbott and Nelson, 2000].

Many factors or processes modulate synaptic transmission, either enhancing or suppressing it. Plasticity keeps a track of the history of a neuron's activity, and is thought to provide a cellular basis for memory storage in the nervous system. For more than half a century, synaptic plasticity has been a focus of study among the neuroscience community. The most commonly studied forms of plasticity for learning and memory research are the Hebbian forms of plasticity: long-term plasticity and short-term plasticity (STP).

1.2.3 Long-term synaptic plasticity

Repeated stimulations bring about a long-term change in the synaptic efficacy that can last for hours to days. Long-term potentiation (LTP) and long-term depression (LTD) are two major forms of long-lasting synaptic plasticity. LTP is an activity-dependent, long-lasting increase in excitatory synaptic strength following a brief high-frequency (30-100 Hz) synaptic stimulation. On the other hand, LTD is a long-lasting reduction in synaptic efficacy following a prolonged low-frequency (0.5-5 Hz) synaptic stimulation [Bliss and Collingridge, 1993; Malenka et al., 1999]. Long-term plasticity has been established in all principal neurons of the hippocampus [Bliss and Collingridge, 2013, 1993; Malenka et al., 1999; Yang et al., 1999] and deemed essential for long-term memory [Abraham et al., 2019; Escobar and Derrick, 2007; Ge et al., 2010; Malenka and Bear, 2004].

LTP is initiated when a brief high-frequency stimulation results in opening of AMPA receptors which subsequently creates strong depolarization of the postsynaptic neuron. NMDA receptors require a strong depolarisation to remove the magnesium block and get activated; a single synaptic input is insufficient to induce a strong enough depolarisation. Activated NMDA causes a large influx of calcium ions into the cytosol [Malenka et al., 1989]. Elevated calcium into the postsynaptic bouton activates signaling cascades corresponding to long-term molecular changes [Franks and Sejnowski, 2002].

One of the major downstream cellular processes induced by elevated calcium involves the phosphorylation and activation of CAMKII kinase. Upon binding calcium, CAMKII gets activated and phosphorylates AMPARs, increasing their conductance and localizing additional AMPARs to the membrane [Barria et al., 1997; Lee et al., 2000]. CAMKII is known to have many more interactions with many other signaling candidates which cohesively determine the duration of early-LTP.

1.2.4 Short-term plasticity

Short-term plasticity refers to the rapid modulation of synaptic efficacy which quickly decays back to its initial state. It can last for tens of milliseconds to several minutes. It is thought to underlie information processing by alternating between a high-pass and low-pass filter in an use-dependent manner [Abbott and Regehr, 2004] and is essential for working memory and temporal pattern separation [Deng and Klyachko, 2011; Madar et al., 2019]. Almost all the factors responsible for the induction of STP are present in the presynaptic terminal [Regehr, 2012].

Most forms of short-term plasticity are marked by an increase in the presynaptic calcium level that modulates the probability of neurotransmitter release [Citri and Malenka, 2008]. Naturally, the release probability has emerged as a good measure for defining the short-term plasticity profile of synapses.

In response to two closely spaced presynaptic action potentials, the postsynaptic membrane potential is larger for the second pulse. The proposed mechanism behind this is the contribution of residual calcium from the first stimulus to additional neurotransmitter release after the second stimulus, thereby increasing release probability. Alternatively, synapses also undergo depression during prolonged stimulation, resulting from a transient depletion of vesicles from the readily releasable pool (RRP) or desensitization of postsynaptic receptors binding to neurotransmitters [Hennig, 2013; Rosenbaum et al., 2012; Schneggenburger et al., 2002].

The functional implications of STP remains a critical question in neuroscience. STP modulates the functional efficacy of synaptic transmission at a millisecond-to-seconds timescale. In the mammalian brain, STP plasticity influences the information processing function of synapses, enabling them to optimize network level computation [Pfister et al., 2010]. Synapses with a low intrinsic release probability are capable of potentiation and function as high-pass filters. The reverse is also true for high Pr synapses [Abbott and Regehr, 2004; Fortune and Rose, 2000; Klyachko and Stevens, 2006]. Other reported functions of STP include insulating postsynaptic terminal from direct stream of presynaptic activity, working memory, optimizing energy consumption and information transmission and spike sequence decorrelation, [Abbott et al., 1997; Cook et al., 2003; Goldman et al., 2002; Mahajan and Nadkarni, 2019; Mongillo et al., 2008].

1.3 Hippocampus in health and disease

Damage to the hippocampus impairs formation of new episodic memories [Covington et al., 2018; Rosenbaum et al., 2005]. These are exactly the faculties one loses at the onset of Alzheimer's disease (AD). AD is a multifaceted catastrophic disease that involves multiple brain areas resulting in a range of debilitating symptoms that increase in severity over time. It is marked by the aggregation of neurofibrillary tangles and amyloid plaques [Murphy and LeVine III, 2010]. Early symptoms of AD, the inability to navigate through space and loss of short term memory, suggest that the hippocampal formation is impacted first in the disease. Further, these cognitive deficits precede structural changes in the brain [Association et al., 2018]. The precise molecular mechanisms that underlie the constellation of deficits are not yet known. Put another way, the first signs of this disorder are seen in the hippocampus, and therefore, this region of the brain is essential to study.

Proposed by Khachaturian in 1989, disruption of intracellular calcium signaling, and therefore dysfunctional plasticity, has been implicated in the pathogenesis of Alzheimer's disease [Khachaturian, 1989]. Abnormal calcium regulation in the endoplasmic reticulum, disrupts calcium signal in the cytosol, and is linked to Alzheimer's. In addition, mutations linked to familial AD have been observed to interrupt intracellular calcium signaling pathways. Destabilization of calcium signaling seems to be central to the pathogenesis of Alzheimer's disease. Loss of short-term plasticity is among the very first manifestations of Alzheimer's disease [Berridge, 2010; LaFerla, 2002; Thibault et al., 2007]. Alterations in calcium signaling precedes the onset of AD pathology. SERCA channel blocker, thapsigargin, led to a perturbation in the intracellular calcium balance, reflecting the role of functional SERCA channel in maintaining calcium homeostasis [Bezprozvanny and Mattson, 2008]. Mutations in presenilins 1 and 2 (PS1 and PS2) are implicated in Familial AD (FAD) Bezprozvanny and Mattson [2008]; Zhang et al. [2013]. It is well documented now that functional presenilins form divalent cation channels in lipid bilayers which contribute to about 80% of the calcium leak from the ER [Tu et al., 2006]. Abnormal presenilin function, therefore, hampers their ability to conduct calcium ions efficiently [Nelson et al., 2007; Tu et al., 2006]. Increase in calcium response in PS-1 mutant mice is attributed to increased store filling, which reduces the overall excitability of the cell [Stutzmann et al., 2004]. These mutations disrupt calcium homeostasis in cytosol, however the precise mechanism is still not clear.

1.4 Research questions

In the world around us, form and function are closely linked together. Each continually directing the other. Our brain is no exception. The neural circuitry dictates behavior and our daily experiences, in turn, rewire the brain. In the same spirit, I have explored the intricate relation between the form and function of synapses in my thesis.

I have chosen to study two drastically different hippocampal synapses from the trisynaptic circuit: the Schaffer collaterals and the mossy fibers to enable comparative understanding of the systems. One of the most important properties of these synapses is plasticity. I have focused on exploring the mechanistic cause behind short-term plasticity.

Presynaptic bouton of Schaffer collaterals contains a single active zone, with barely 10 neurotransmitter-containing vesicles in the readily releasable pool. The endoplasmic reticulum is extensively present in axons, all the way to the terminals. Compare this with mossy fiber boutons. They are large, hosting tens of active zones that incorporate hundreds of vesicles in their RRP. MFBs also require large amounts of mitochondria to function effectively, and it is controversial whether they have an extensive endoplasmic reticulum. Rapid short-term plasticity manifests in both these synapses, but very differently, owing to their distinct form. Short bursts of stimuli increase synaptic efficacy in both cases although mossy fibers sustain the elevated synaptic strength for much longer. Sustained stimulus, on the other hand, depresses Schaffer collaterals while it strengthens mossy fibers. Despite decades of research into these synapses, our understanding of their function is still murky. So, I have employed a computational approach to shed some light on their underlying mechanisms.

Despite extensive presence of ER, in axons of CA3 pyramidal neurons, this intracellular calcium store has been neglected in studies probing STP. To this effect we have studied and looked into the molecular mechanisms that orchestrate short-term plasticity at this synapse. In Alzheimer's, ER has been found to be overloaded with calcium. In the familial case, mutations in presenilins have been implicated. Such mutations have been shown to decrease calcium leak from ER by 80% [Tu et al., 2006]. This results in calcium overload in ER. We further studied the disruption of STP in Alzheimer's disease caused by ER overload.

MF synapses can undergo substantial changes in synaptic strength, exhibiting marked short-term facilitation which has been deemed essential for its role as a transmission line and a pattern separator. Upon stimulation it rapidly transitions from a low release probability (Pr) to a high Pr synapse. However, the implication of this elaborate synaptic design on STP is not well understood. Numerous active zones have long been thought to act independent of each other. We investigate this assumption and the role of buffers and calcium sensors, elaborating on the complex interactions that modulate calcium signals that bring about the profound short-term plasticity that we observe at this synapse.

1.5 Organization of the thesis

In the upcoming chapters I have elaborated on the research that I have conducted during the course of my PhD. In the second chapter, I have explored, in detail, the mechanistic role of ER, the internal calcium store in orchestrating STP in CA3-CA1 synapses. Additionally, I have probed the mechanistic effect of ER calcium overload on STP, as seen in Alzheimer's. The third chapter explores the story of short-term plasticity in mossy fiber. Here, I have examined how cross-talk between active zones, reduction in local buffering capacity and synaptotagmins' properties come together to orchestrate STP. Further, I have looked into its implications on temporal pattern separation. I have addressed my questions using an in-silico approach to the above mentioned problems. Fourth chapter provides the details of the methodology used in the study. Finally, in the concluding chapter, I have set up the broad arena in which the results of my work fits, providing the rationale for the thesis' research and the future prospects of the work. Further I have explored the usefulness of a computational study in resolving experimentally difficult scientific questions. Lastly, I discuss the relevance of my work to the scientific community, and to the world and society.

CHAPTER 2

ROLE OF SECONDARY CALCIUM SOURCE IN SMALL HIPPOCAMPAL NEURONS IN HEALTH AND DISEASE

2.1 Introduction

One of the most historically studied synapses of the brain lie in the hippocampus. These are the synapses between CA3 and CA1 pyramidal neurons. The axonal fibers that originate from the CA3 pyramidal neurons, the Schaffer collaterals, form small en-passant synapses with CA1 pyramidal neurons. CA3-CA1 synapses are the last leg of the hippocampal highway, the trisynaptic circuit. This circuit consists of the entorhinal cortex that collates multimodal thalamocortical signals and passes it onto the dentate gyrus via perforant pathway. Granule cells from dentate gyrus further project onto CA3 via mossy fibers and then, from CA3 to CA1 regions [Witter et al., 1989]. The CA3 and CA1 hippocampal subfields are crucial for memory encoding and retrieval [Dimsdale-Zucker et al., 2018; Lee et al., 2005].

Presynaptic boutons of CA3 pyramidal neurons are relatively small. It possesses only one (on rare cases, two) active zone (AZ) and a small readily releasable pool containing 5-10 vesicles. A loosely coupled cluster of voltage-dependent calcium channels (VDCC) is associated with the active zone [Jensen et al., 2019; Vyleta and Jonas, 2014]. Brief membrane depolarisation during an action potential leads to rapid and large calcium influx from VDCCs. The manyfold increase in the local calcium concentration lasts only about a millisecond but leaves residual calcium ions which decays with a timescale of about 100 ms. In the cytosol, the calcium signal through VDCCs is highly restricted by a large concentration of fast calcium buffer, calbindin-D28k, both spatially and temporally. Extended separation of the VDCC cluster attenuates calcium concentration at the active zone that helps in maintaining a low vesicle release probability, typically about 0.2 [Dobrunz and Stevens, 1997; Nadkarni et al., 2010]. The large number of VDCCs guarantees abundant bulk calcium that modulates subsequent activity.

The low basal release probability is an important feature of the presynaptic bouton that allows the synaptic efficacy to be tunable. In small hippocampal neurons, such as the CA3 and CA1 pyramidal neurons, paired pulse facilitation follows an inverse relation with the release probability [Dobrunz and Stevens, 1997]. Thus, the CA3-CA1 synapse maintains a low release probability and shows significant paired pulse facilitation. This requires a delicate balance between facilitating synaptic transmission and conserving the small vesicle resource [Dobrunz, 2002] and short-term plasticity provides the means to do so.

Multiple studies show an extensive presence of endoplasmic reticulum (ER) all the way to the presynaptic terminal in CA3 pyramidal neurons [Bouchard et al., 2003; Harris et al., 2015b; Sharp et al., 1993; Shepherd and Harris, 1998; Westrum and Gray, 1986]. Other neurons also possess ER closely associated with the neuron terminal [Carter et al., 2002; Hartter et al., 1987; Lindsey and Ellisman, 1985; McGraw et al., 1980; Tsukita and Ishikawa, 1976; Villegas et al., 2014; Yalçın et al., 2017]. The endoplasmic reticulum is an internal calcium store that maintains calcium ions at a high concentration (~250 M) by capturing calcium ions through the Smooth Endoplasmic Reticulum Calcium transport ATPase (SERCA) pumps. ER membranes also contain presenilins (PS1 and PS2). These proteins form low-conductance divalent-cation-permeable ion channels that slowly leak calcium ions from ER into cytosol. This leak function of presenilins is independent of their γ-secretase activity [Tu et al., 2006]. The interplay between SERCAs and ER leak maintains the high calcium concentration in ER. A different class of calcium-induced-calcium channels clustered on the ER membrane are the ryanodine receptors (RyRs). The activation of RyRs is fast, but requires high calcium concentration [Saftenku et al., 2001]. Upon activation by calcium influx, via VDCCs, RyRs also release calcium into the cytosol, but from the ER. The presence of high calcium concentration in the ER, in conjunction with the aforementioned calcium channels in its membrane makes the ER a reliable secondary source of calcium upon neuronal stimulation.

The high calcium concentration in the ER is primarily maintained by SERCA pumps. Irreversibly blocking SERCA pumps with thapsigargin stops calcium uptake into the ER, and in over the next several minutes ER calcium leaks out. Under such a condition, experimental studies have observed an impaired STP in the Schaffer collaterals [Zhang et al., 2009]. The precise mechanism that orchestrates STP at this synapse is not well understood and studies have often neglected this secondary source of calcium when exploring the mechanism behind STP. The effect of this secondary calcium source on short-term plasticity remains unexplored, partly due to the experimental difficulty in disambiguating the contributions of different sources of calcium.

Alzheimer's disease (AD) is a multifaceted catastrophic disease that involves multiple brain areas resulting in a range of debilitating symptoms that increase in severity over time. Despite a century of investigation, the precise molecular mechanisms that underlie the constellation of deficits are not yet known. Early symptoms of AD; the inability to navigate through space and loss of short term memory, suggest that the hippocampal formation is impacted first in the disease. Furthermore, these cognitive deficits precede structural changes in the brain. Mutations in presenilins 1 and 2 (PS1 and PS2) are implicated in Familial Alzheimer's Disease (FAD) and are known to disrupt calcium homeostasis in the cytosol Bezprozvanny and Mattson [2008]; Zhang et al. [2013]. However, there is no scientific consensus over the mechanism. Moreover, the ER has been found to be overloaded with calcium, both in sporadic as well as in familial forms of the disease. In the familial case, mutations in presenilins have been shown to decrease calcium leak from ER by 80% [Tu et al., 2006], resulting in calcium overload in the ER [Nelson et al., 2007]. Experiments have also shown that knocking out presenilin reduces short-term plasticity [Zhang et al., 2009, 2010]. In our study we have explored the implication of ER calcium overload in the context of STP.

With the aim to investigate the contributions of ER and its components to calcium signaling and short-term plasticity in CA3-CA1 synapse, we developed a biophysically detailed 3D model of the CA3 presynaptic terminal based on reconstruction data [Harris et al., 2015a].

2.2 Model construction

In presynaptic boutons of neurons, calcium signaling is a localized phenomenon. Calcium concentrations vary in time as well as space: it is not a well-mixed system. We built two 3D, spatially explicit models of a CA3 pyramidal neuron to capture this heterogeneity. The realistic model has the shape of an actual neuron chosen from the neuropil (see Figure 2.1) and the canonical one has a simplified box-like shape that represents the average size of all the synapses in the neuropil. All the in-silico experiments are performed in the canonical model while some are simulated in the reconstructed model, to compare.

I have built upon a previous model of CA3 presynaptic bouton [Nadkarni et al., 2010]. Endoplasmic reticulum has elongated thin processes that are extensively present in axons, reaching into the neuronal boutons (see Figure 2.2a). In the 3D reconstruction of CA1 neuropil, the closest approach between active zone and ER was observed to be around 100 nm on average (see Figure 2.2b). Among its numerous functions, ER stores calcium in large concentrations and its surface hosts SERCA pumps and ryanodine receptors. Cytosol contains calcium at an extremely low concentration of 100 nM. In contrast, ER maintains about 250 μM.

The components of the bouton relevant for the study are calcium sensors (synaptotagmin-1 and synaptotagmin-7), voltage-dependent calcium channels, SERCA pumps, ryanodine receptors, calcium buffers (calbindin-D28k), PMCA pumps. Synaptotagmin-1 and synaptotagmin-7 are the major calcium sensors present in CA3 pyramidal neurons [Bacaj et al., 2013]. It incorporates calcium-dependent synchronous and asynchronous, and calcium-independent spontaneous modes of vesicle fusion. High-threshold Cav2.1 (P/Q-type) voltage-dependent calcium channels are incorporated in our model as characterized by [Bischofberger et al., 2002]. These channels are placed in a cluster at 350 nm from the active zone. Passage of calcium ions is governed by electrochemical gradient across the membrane. We have used the four state model for the SERCA pump described by [Higgins et al., 2006]. RyR incorporates low and high activity states as described by Saftenku et al. [2001]. The model for calbindin-D28k maintains two high affinity and two medium affinity calcium binding sites which has been taken from Nägerl et al. [2000]. Kinetic model for the PMCA pump has been incorporated from Brini and Carafoli [2009]; Penheiter et al. [2003]. It implicitly incorporates calcium leakage across the plasma membrane.

The AD model that incorporated elevated calcium concentration in the ER was

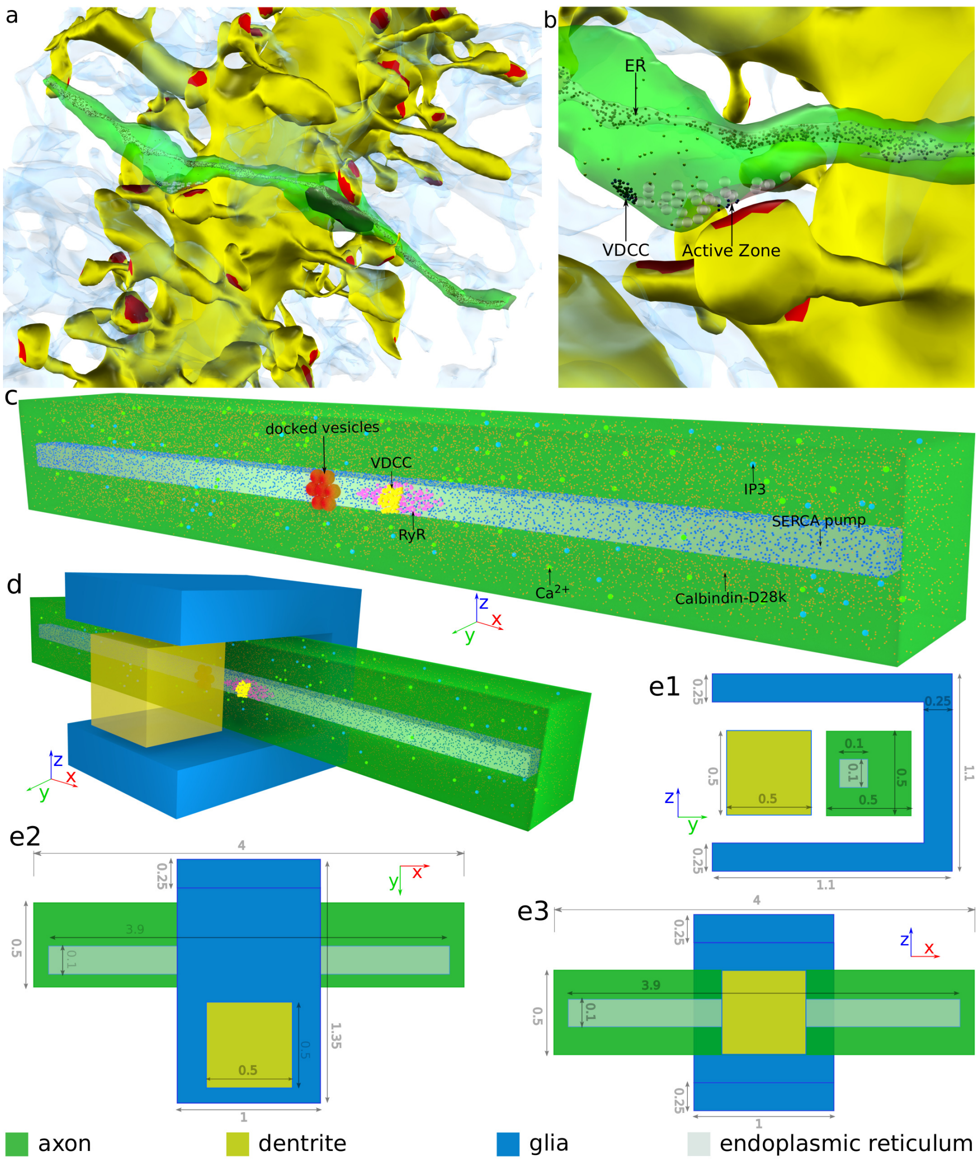
a
b
ER
VDCC
Active Zone
c
docked vesicles
VDCC
RyR
IP3
SERCA pump
Ca2+
Calbindin-D28k
d
z
x
y
e1
0.25
0.25
0.5
0.5
0.1
0.1
0.5
0.5
1.1
1.1
0.25
e2
4
0.25
3.9
0.5
0.1
1.35
0.5
0.5
1
e3
4
0.25
3.9
0.5
0.1
0.25
1
🟩 axon
🟨 dentrite
🟦 glia
⬜ endoplasmic reticulum

FIGURE 2.1. **Model of the CA3 neuron bouton. a.** Reconstruction of the CA3–CA1 neuropil in rat hippocampus. The dendrite of a CA1 pyramidal neuron is shown in yellow with red patches, indicating the postsynaptic densities. An axon of CA3 pyramidal neuron is shown in green (other axons in the vicinity have been made transparent for clarity). ER inside the axon is shown in gray. Astrocytes are shown as translucent blue structures. **b.** An en passant synapse formed by a CA3 axon onto a CA1 dendrite. **c.** Presynaptic terminal of the 3D canonical model showing the placement of key molecules. **d.** The complete view of the canonical model showing the relative arrangement of glia, presynaptic and postsynaptic terminals. **e1–3.** Dimensions (in m) of the model in orthographic projection. ER endoplasmic reticulum, VDCC voltage-dependent calcium channel, RyR ryanodine receptor, IP3 inositol (1,4,5)-trisphosphate.

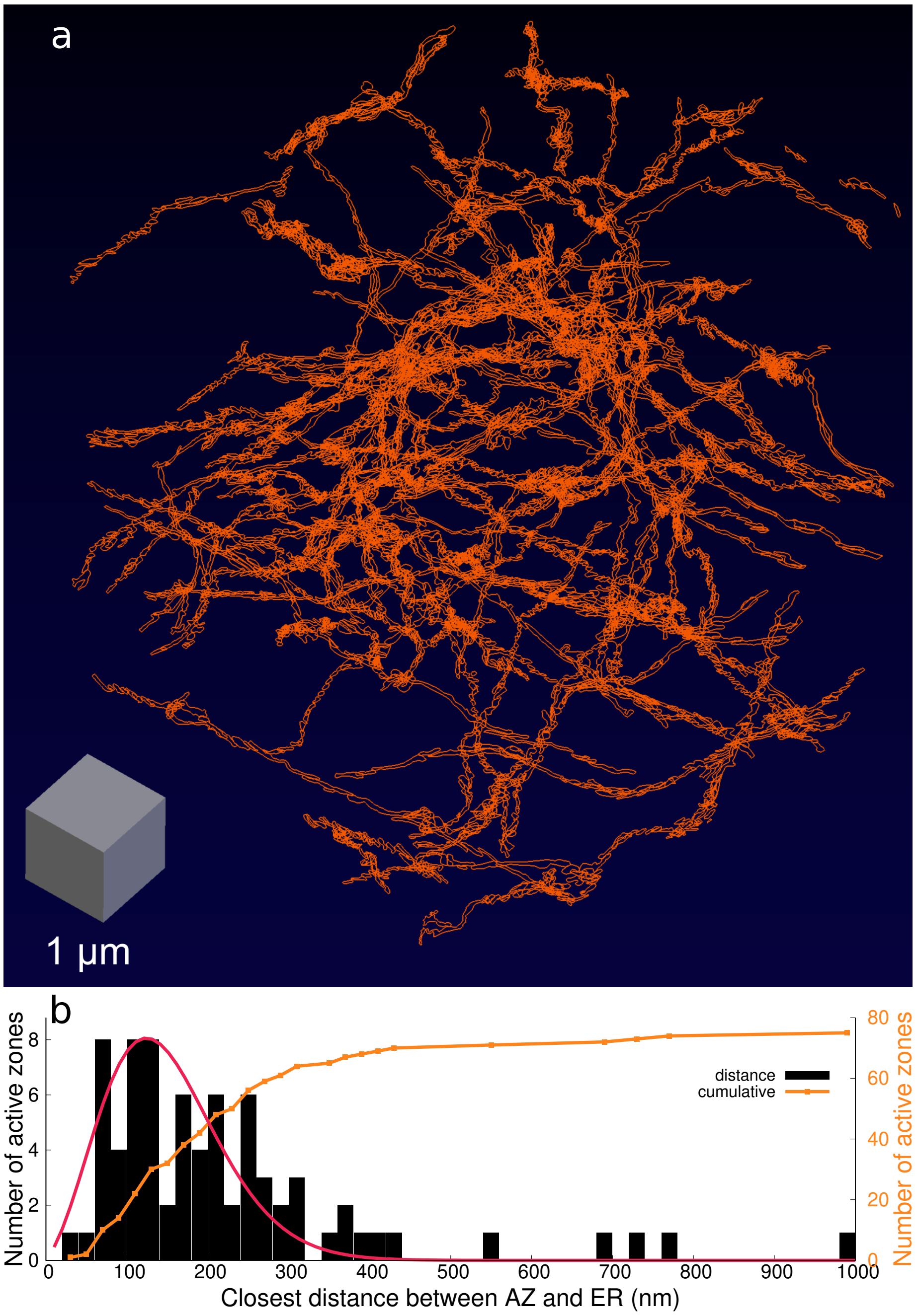

FIGURE 2.2. **Presence of ER in CA3 axons. a.** The hand segmented contours of smooth ER seen in a subsample of 69 of these axons are shown highlighted in orange. Smooth ER in axons of stratum radiatum of hippocampal area CA1 was observed in all of the 449 axons identified in a dense serial section electron microscopic 3D reconstruction. The scale cube is 1 micron on a side. **b.** Distribution of closest distance between AZ and ER in 75 axons. Peak of the distribution is around 100 nm (shown in red). Cumulative distribution is shown in orange.

implemented by modifying SERCA rates such that steady state calcium concentration in ER was 500 μM. For a complete description of the model implementation see Chapter 4.

2.2.1 Chronology of events in response to a single action potential

An action potential initiates synaptic transmission, triggering calcium influx from extracellular space into cytosol via VDCCs. Cytosolic calcium ions open ryanodine receptors further releasing calcium from endoplasmic reticulum (see Figure 2.3a). Due to its fast activation, opening of RyRs closely follows calcium influx through VDCCs, lasting only a few milliseconds (see Figure 2.3b). Calcium buffers present in the cytosol and SERCA pumps on ER rapidly capture a large fraction of the calcium ions (see Figure 2.3c). PMCA pumps further contribute in bringing the cytosolic calcium back to its basal level (see Figure 2.3d). This dynamic interaction of various synaptic components produces a large but short-lived and local calcium signal. Calcium concentration at the active zone shows a pronounced increase compared to the whole bouton (see Figure 2.3e). In response to such a calcium signal, two distinct vesicle release profiles are observed: a rapid and large synchronous release that decays quickly with the signal and a small but longer-lasting asynchronous release (see Figure 2.3f).

2.3 ER is essential for short-term plasticity

2.3.1 Blocking ER increases transmitter release probability

We conducted simulations in two sets of model conditions: control and stores-blocked. In control, ER and its associated components have normal functions while in stores-blocked, ER, the internal calcium store, is blocked (see Figure 2.4a). It can not take up or release calcium ions.

In one set of emphinsilico experiments, we stimulated the CA3 neuron with a pair of action potentials separated with a small inter-spike interval. For each action potential, neurotransmitter release probability was measured. As the number of VDCCs were increased in the neuron, release probability increased. This is expected because an increase in VDCCs would result in a higher transient calcium influx.

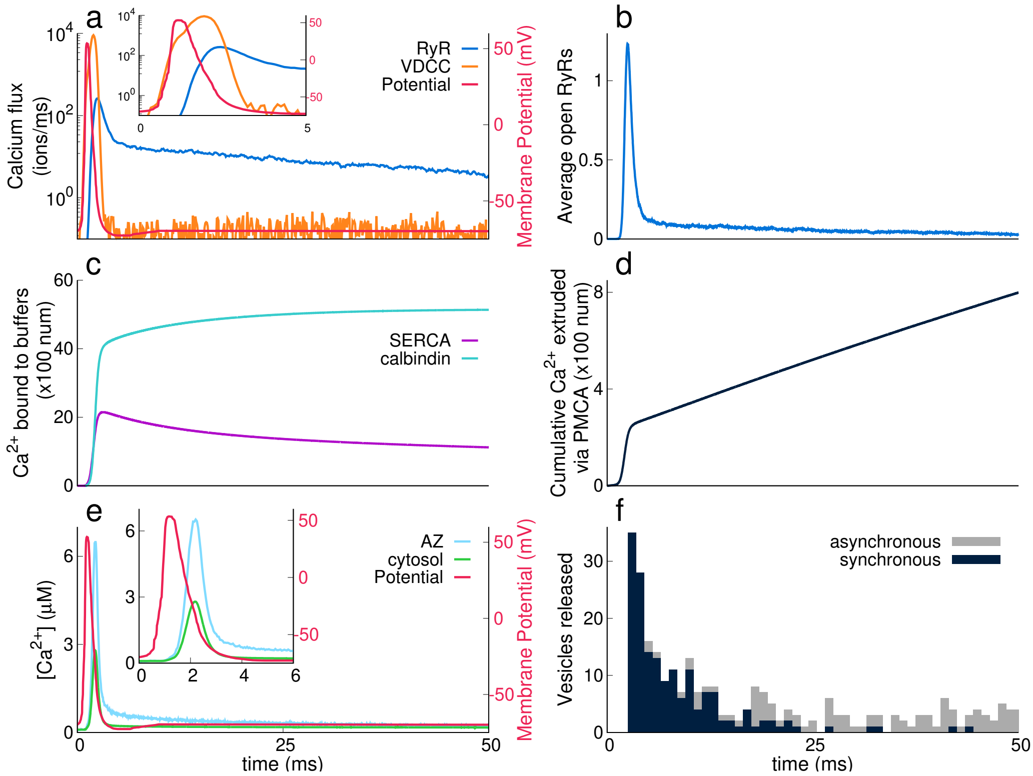

FIGURE 2.3. **Chronology of events. a.** Membrane depolarization due to AP (red, right “Y” axis) leads to an influx of Ca^{2+} ions via VDCC (orange) and subsequently via RyR (blue). Inset shows the first 5 ms of the simulation. **b.** Activity of RyR shows distinct responses to an AP. **c.** Calbindin-D28k (cyan) and SERCA pumps (pink) are seen to buffer a large part of Ca2+ influx from VDCC. **d.** PMCAs actively pump Ca2+ ions from the cytosol to maintain a base level $[Ca^{2+}]_{cyt}$of 100 nM. **e.** Calcium concentration at the active zone, $[Ca^{2+}]_{AZ}$ (light blue) measured 10 nm above the active zone and in the entire presynaptic bouton, $[Ca^{2+}]_{cyt}$ (light green). Inset shows the first 6 ms of the simulation. **f.** Stacked histogram of vesicle fusion (neurotransmitter release) events via synchronous (black) and asynchronous (gray) pathways in response to a single AP for 2000 trials. There were a total of 269 vesicle releases in 194 trials—some trials had multiple releases—(out of 2000) within the 50 ms of the simulation. The average release probability, in this case, is 194/2000 (fraction of successful trials).

However, in the stores-blocked case, rise in the Pr was drastically higher for the same number of VDCCs than their control counterparts. Experiments in both canonical as well as reconstructed models show similar trends (see Figure 2.4b-d).

Further, we stimulated our models with a train of 20 spikes at 10 Hz, 20 Hz and 50 Hz. As mentioned above, release probability in response to the first stimulus is higher in the stores-blocked case. We observe an initial rise in release probability in both the model conditions. However, stores-blocked shows a steeper rise as well as subsequent decrease (due to reduction in RRP) as the neuron is stimulated repeatedly. Steepness of rise and fall of Pr is, of course, dependent on the frequency of the stimulus (see Figure 2.4e-g). Reconstructed and canonical models both show similar Pr for a 20 Hz stimulation (see Figure 2.4h). The initial increase in vesicle release probability with stimulus number leads to a rapid depletion of the RRP. The decrease in release probability after the peak is dictated by the depletion of RRP (see Figure 2.4i-l).

2.3.2 Disruption of internal calcium store diminishes short-term plasticity

When stimulated with a pair of action potentials, facilitation was measured as paired-pulse ratio (PPR), defined as ratio of release probability of the second spike (Pr2) over the first (Pr1). In this protocol, blocking store activity reduced PPR at any given release probability compared to the control synapse. Since PPR inversely follows release probability, it is expected that the stores-blocked cases show lower short-term plasticity. Blocking stores changes the operating point of the neurons to a higher Pr. Sets of dark and light purple arrows indicate change in the operating points of two neurons with the same number of VDCCs in control and stores-blocked cases (see Figure 2.5b and d). Reconstructed model also shows reduction in PPR, similar to the canonical model (see Figure 2.5c). This effect is most prominent in the low release probability regime where most CA3–CA1 synapses operate. In this regime, disruption of PPR when stores are blocked is prominent across a large range of inter-spike intervals (see Figure 2.5e for canonical and fig. 2.5f for reconstructed models).

Further, we investigated facilitation in these models in response to a train stimulation at 10 Hz, 20 Hz and 50 Hz. Definition of facilitation was extended defining it as the ratio of vesicle release probability due to the nth stimulus to that of the 1st. Both synaptic configurations, control and stores-blocked, show a peak in facilitation that decays with subsequent stimuli. Although, facilitation is drastically reduced in the

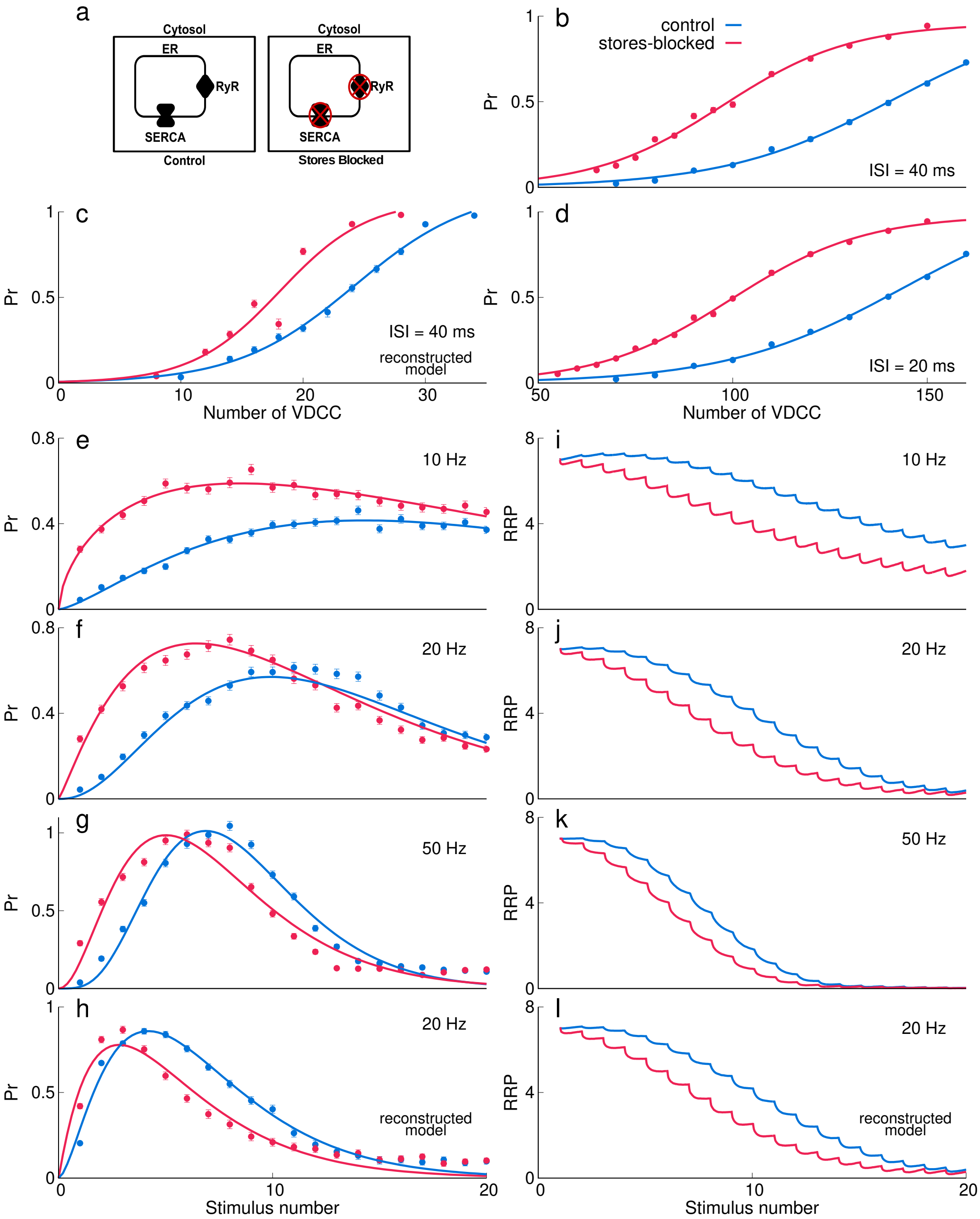

FIGURE 2.4. **Release probability. a.** Two model setups—“control”: ryanodine receptors and SERCA pumps are present on the ER; “stores-blocked”: SERCA pumps are blocked, therefore, no calcium ion is present in ER and RyR is redundant. **b-d.** Variation of release probability of a vesicle (Pr) with number of VDCCs. **e-h.** Release probability of a vesicle for each AP in a train stimulus at different input frequencies. **i-l.** Decrease in the RRP due to successive releases in response to a train stimulus at different input frequencies. All simulations are performed in canonical models unless "reconstructed model" is mentioned. Data are mean ± s.d.

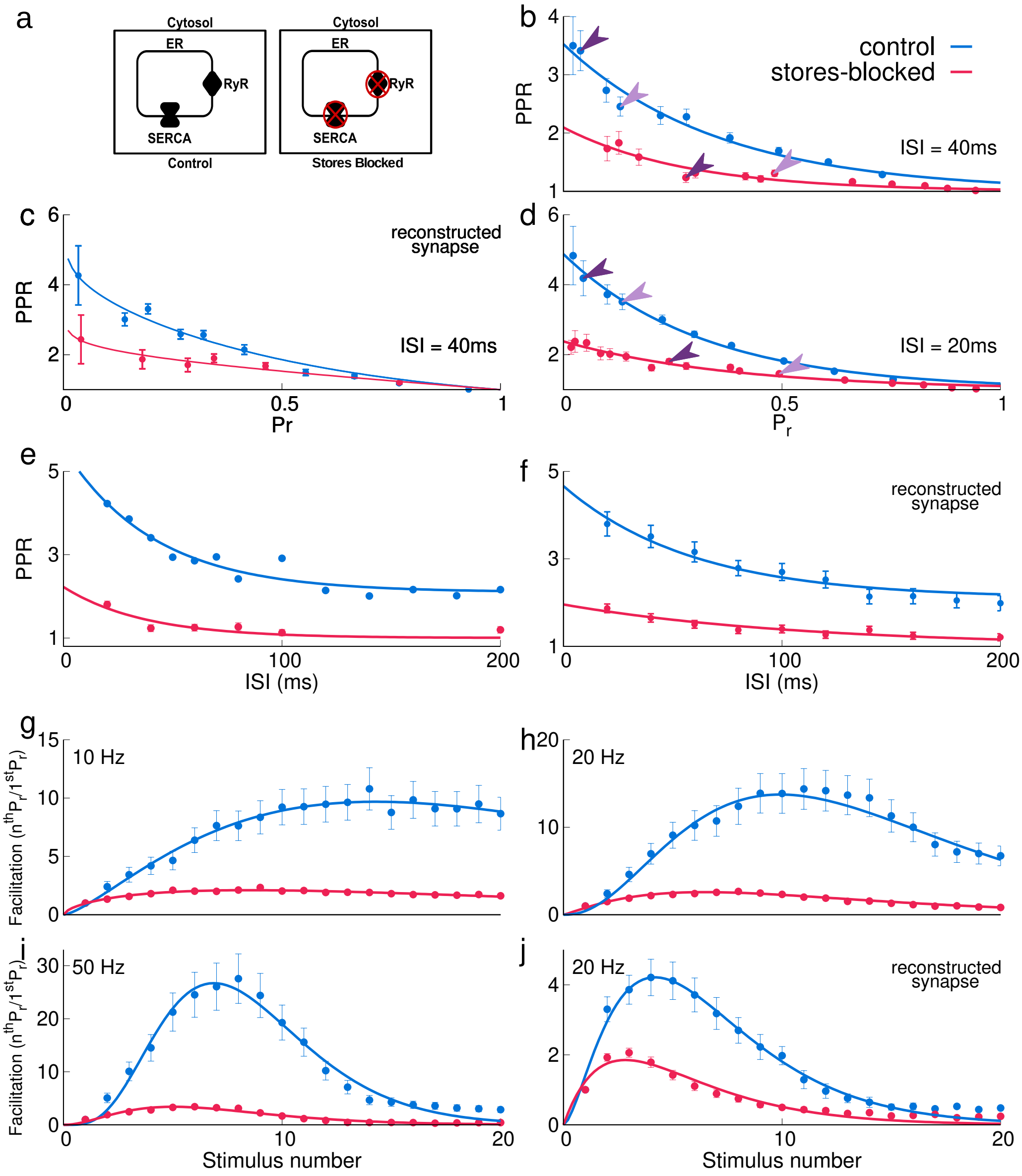

FIGURE 2.5. **Facilitation. a.** Two model setups—"control" and "stores-blocked". **b-d.** Inverse relation of paired-pulse ratio and intrinsic Pr for various synaptic configurations and for 20ms and 40ms inter-spike interval (ISI). Dark purple arrows indicate the PPR corresponding to 80 VDCCs, and light purple corresponds to 100 VDCCs for canonical synapse. **e,f.** Variation of paired-pulse ratio for different ISI. **g-j.** Facilitation in response to a train stimulus at different input frequencies. All simulations are performed in canonical models unless "reconstructed model" is mentioned. Data are mean ± s.d.

stores-blocked case for all the stimulus frequencies (see Figure 2.5g-i). Reconstructed and canonical models both show similar facilitation for a 20 Hz stimulation (see Figure 2.5j).

2.3.3 Altered calcium signaling disrupts STP

Calcium is the key element that ultimately triggers the neurotransmitter release. Also, it is sensitive to calcium concentration. In response to an action potential, VDCCs release a large amount of calcium ions that are quickly buffered by calbindin-D28k present in the cytosol (see Figure 2.6a-c). This restricts not only the amount of available free calcium, but also the spatial extent of the signal. However, the amount of calcium ions that bind to calbindin-D28k subsequently decreases with action potentials. This is due to the reduction in the binding capacity of calbindin-D28k. This then contributes to residual calcium ions that last much longer in the cytosol (~100 ms) than the calcium signal itself.

Another component that buffers calcium ions are the SERCA pumps, a rather surprising one. SERCAs deliver calcium ions into ER at a slow timescale (~10s; [Solovyova et al., 2002]). Yet they quickly bind a large quantity of calcium ions. SERCA pumps, characterized by high-affinity and fast-binding sites for calcium ions, can take-up a substantial amount of calcium arriving through VDCCs. Over the next tens of milliseconds, some of these bound calcium ions are transferred into ER while the rest is released back into the cytosol. Rapid binding and slow unbinding of calcium by SERCA pumps in response to two pulses separated by 40 ms are shown in Figure 2.6d-f). As with calbindin-D28k, SERCAs buffering capacity also tends to saturate with multiple stimuli. These results are robust to realistic variation of the binding rates and expression levels of SERCA pumps (see Figure 2.6g,h).

When stores are blocked, calcium uptake into ER and its release is abolished. As a result, the active zone experiences a larger amount of transient calcium ions that leads to high release probability as we saw earlier. As a consequence, the peak amplitude of calcium signal measured at the active zone, for the control synapse, is lower than it would be with stores blocked. The lower calcium peak that maintains a lower release probability for control synaptic configurations is seen consistently across a wide range of VDCC expressions (see Figure 2.7a1-2).

Yet the cumulative calcium concentration at the active zone is higher for the control case (see Figure 2.7b1-2). This is due to the subsequent unbinding of calcium ions

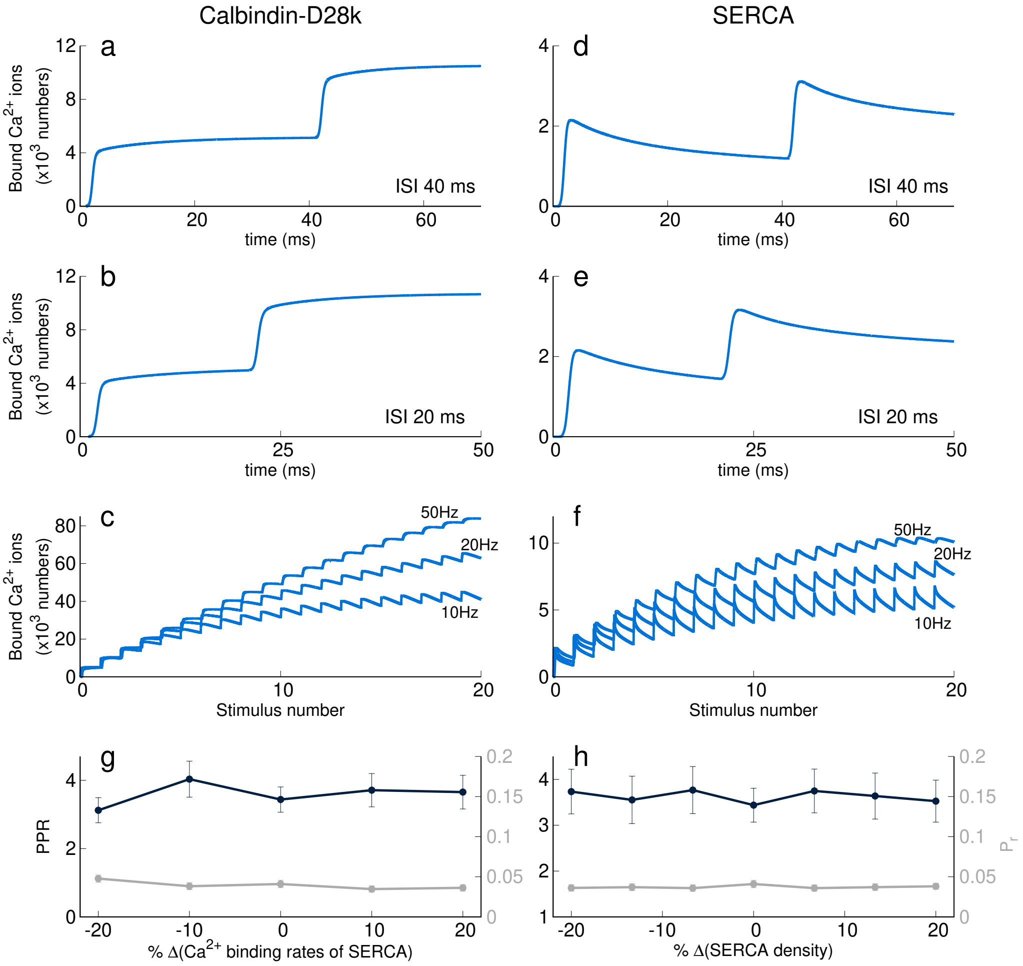

FIGURE 2.6. **Calcium buffering by calbindin-D28k and SERCA. a-c.** Amount of Ca^{2+} ions bound to calbindin-D28k in response to a paired pulse at an inter-spike interval of 20 ms and 40 ms, and in response to a train stimulus at 10Hz, 20 Hz and 50 Hz. **d-f.** Amount of Ca^{2+} ions bound to SERCAs for the above mentioned stimulations. **g.** PPR (black, left 'y' axis) and Pr (grey, left 'y' axis) for variation in calcium binding rates of SERCA. **h.** PPR (black, left 'y' axis) and Pr gray, left 'y' axis) for variation in SERCA pump density. Data are mean ± s.d.

from SERCAs back into the cytosol. It is clear from the observed longer-lasting increase in residual calcium at the active zone(see Figure 2.7c1-2) as well as in the bulk of the cytosol (see Figure 2.7d1-2). Similar trend is seen when the control and stores-blocked models are stimulated with a train of spikes at 10 Hz, 20 Hz and 50 Hz (see Figure 2.8).

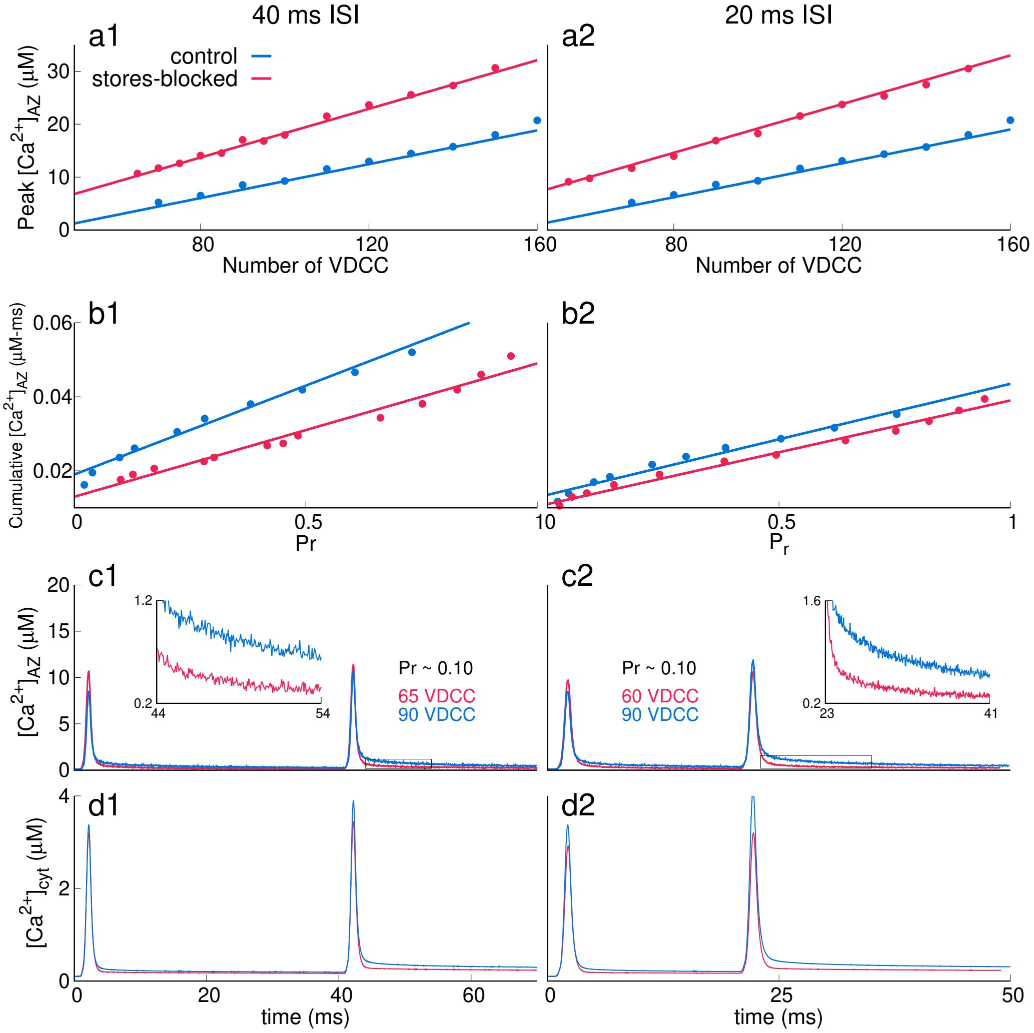

FIGURE 2.7. **Calcium signal in response to a pair of APs. a1-2.** Variation in peak calcium concentration with increasing amounts of VDCCs and in response to two APs. **b1-2.** Increase in cumulative calcium concentration with increase in Pr. **c1-2.** Calcium signal profile at active zone. **d1-2.** Bulk calcium signal in the bouton.

In summary, SERCAs quickly bind a large amount of calcium but slowly pump them into ER. As such, they act as fast calcium buffers. As a result, the peak calcium concentration during an action potential is lower in control, compared to stores-

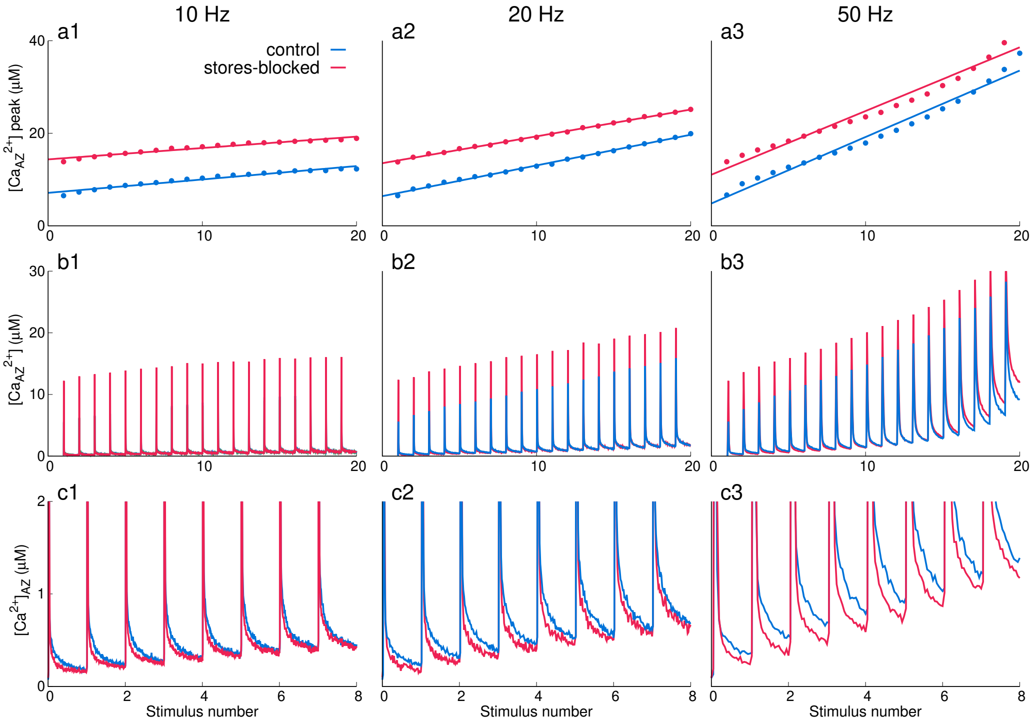

FIGURE 2.8. **Calcium signal in response to train stimulus. a1-3.** Variation in peak calcium concentration with increasing amounts of VDCCs and in response to a train stimulus. **b1-3.** Calcium signal profile at active zone. **c1-3.** Residual calcium profile at the active zone.

blocked. This maintains a low release probability. However, cumulative calcium concentration is higher in control because of the higher residual calcium compared to the stores-blocked case. Now, that happens because a fraction of the calcium buffered by SERCAs are released back into cytosol. Fast calcium buffering by SERCAs maintains a low release probability while assisting residual calcium. The effect of this buffering is evident from the synchronous and asynchronous vesicle release profiles. With stores blocked, we observe pronounced but shorter-lived synchronous release as compared to the control case due to higher release probability. This effect is seen for paired pulse protocol (see Figure 2.9a and b) as well as train stimulus (see Figure 2.9d and e). In addition, asynchronous release is diminished in response to lower residual calcium when stores are blocked (see Figure 2.9c and f). These results reveal an important and previously unaccounted role for SERCA in determining STP.

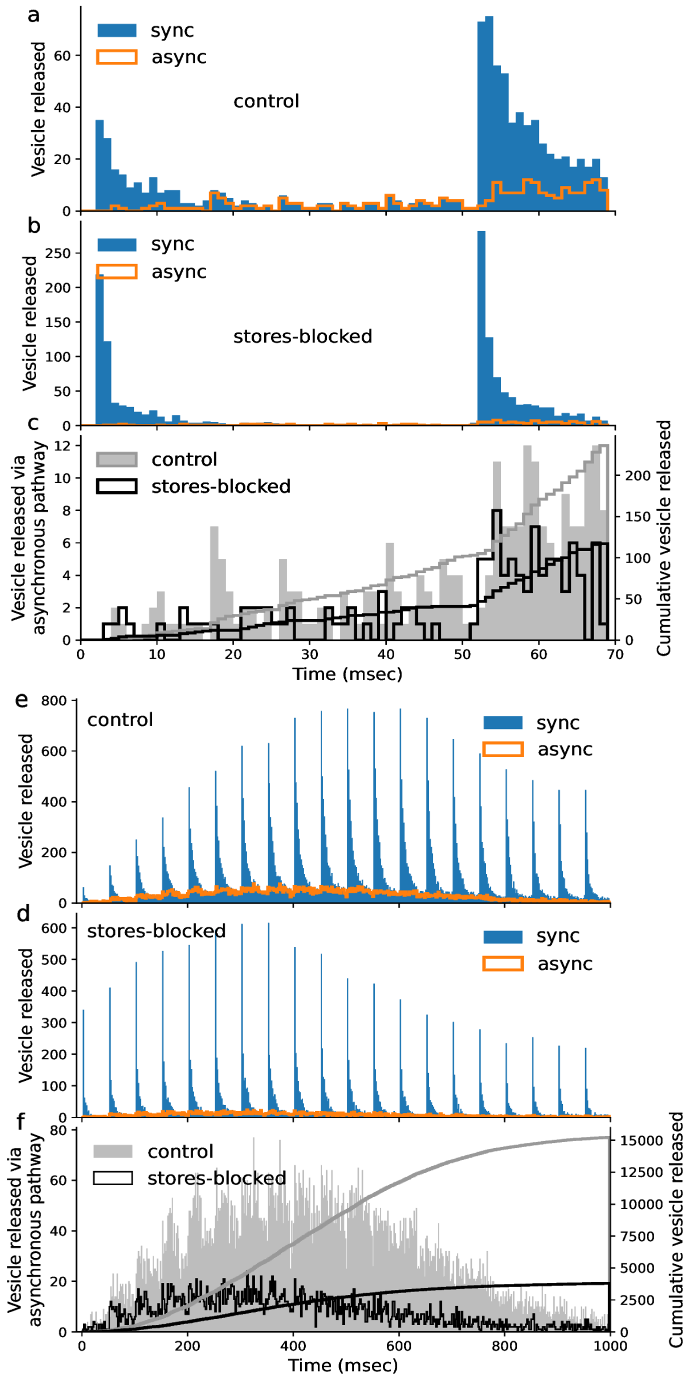

FIGURE 2.9. **Neurotransmitter release. a,b.** Total vesicles released via synchronous and asynchronous release pathways in 2000 trials of control and stores-blocked synapse in response to a pair of action potentials. **c.** Comparison of vesicle release between control and stores-blocked synapses. **d,e.** Total vesicles released via synchronous and asynchronous release pathways in 2000 trials of control and stores-blocked synapse in response to a train of 20 action potentials. **f.** Comparison of vesicle release between control and stores-blocked synapses.

2.3.4 RyR contributes minimally to STP

In another simulation condition, "RyR-blocked," we blocked ryanodine receptors (see Figure 2.10a). We find RyR does not contribute to the calcium signal sufficiently. Consequently, blocking RyR does not change Pr compared to the control case (see Figure 2.10b,c). Despite the close juxtaposition of RyR and VDCCs (50 nm), calcium release via RyRs opening is not a major contributor to timescales relevant to facilitation studied here. Facilitation was observed to be similar to the control model (see Figure 2.10d-f). Therefore, as expected, RRP as well as various calcium profiles (peak and basal calcium concentration at active zone) were comparable to the control case (see Figure 2.10g-l).

2.4 Increased reliability mediated by stores machinery

Despite the stochastic nature of synaptic activity of individual neurons that operate in the low probability regime, the firing activity rates are finely tuned. This is essential for encoding information in small hippocampal synapses, as suggested by experimental data on spatial navigation and sensory processing [Lu et al., 2013; Schmidt-Hieber and Häusser, 2013]. Here we show reduction in pulse-to-pulse variability of low Pr synapses in the presence of intracellular calcium stores and their associated components. In a facilitating synapse, Pr2 is larger than Pr1. Control synapses, as we saw before, facilitate much more compared to neurons where calcium stores are blocked (see Figure 2.11a).

In the context of neuronal firing activity, coefficient of variance (CV) is defined as the standard deviation of Pr2/(mean Pr2). It is one way to measure the reliability of the rate code that arises from the enhancement of release probability. CV remains lower in control synapses compared to the stores-blocked case (see Figure 2.11a). This indicates a less variable rate of vesicle release.

Uptill now we described properties of a population of CA3 presynaptic neurons rather than the relevance of synaptic activity as observed by a single neuron. Conditional probability, P11, refers to the probability of successful vesicle release in response to an action potential, which is followed by another successful release event in response to the next AP. P11 characterizes synapse-specific history of activity at the timescales of

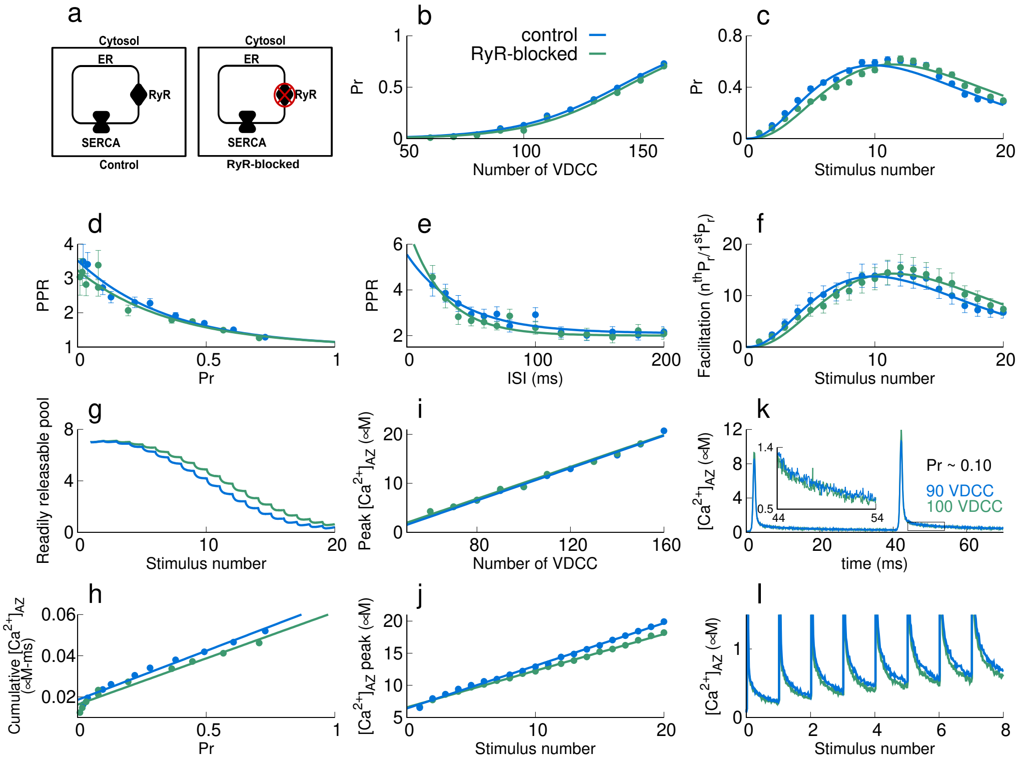

FIGURE 2.10. **Negligible contribution of RyR to STP. a.** Simulations are performed in canonical synapse for two model setups—'control': Ryanodine receptors and SERCA pumps are present on the ER; 'RyR-blocked': SERCA pumps are present on ER and RyR is blocked. **b,c.** Variation of release probability of a vesicle with number of VDCCs and in response to a train stimulus at 20 Hz. **d.** Paired pulse ratio at varying Pr at 40 ms ISI. **e.** Paired pulse ratio at varying ISI at 0.2 Pr. **f.** Facilitation in response to a train of stimulus at 20 Hz. **g.** Decrease in the RRP due to successive releases in response to a train stimulus. **h.** Increase in cumulative calcium concentration with increase in Pr. **i-j.** Increase in peak calcium concentration with increasing amounts of VDCCs and in response to a train stimulus. **k,l.** Calcium concentration profiles in response to a pair of action potentials and train stimulus. All simulations are performed in canonical models unless "reconstructed model" is mentioned. Data are mean ± s.d.

short-term plasticity [Hanse and Gustafsson, 2002; Stevens and Wang, 1994]. Various studies suggest that rapid synapse-specific modifications are crucial for hippocampal function. These changes guide the more gradual processes before being consolidated in the neocortical networks for permanent storage [Bhalla, 2017; Eichenbaum, 2017; Kitamura et al., 2017; Letellier et al., 2016].

Vesicle depletion negatively influences P11 in response to the previous release. Although, the effect is identical for both the types of synapses (assuming the same amount of vesicles in the RRP). However, noisy, nonbinary presynaptic residual calcium signal that persists even after the stimulus, also affects P11. As a result we observe that the conditional probability, P11, is higher in synapses with functional ER and it is true for a large range of intrinsic release probability (see Figure 2.11b). It is also higher for a wide range of inter-spike intervals in control synapses compared to those without stores (see Figure 2.11c). In essence, intracellular calcium stores help retain a better history of calcium dynamics and vesicle release.

Short-term plasticity enables estimation of non-discrete signals arriving at CA3 efferent synapses which are involved in critical computations [Pfister et al., 2010]. Our analysis suggests that control synapses, which show higher P11, are better at capturing this non-discrete nature of information (calcium signal) arriving at the synapse. Thus, the activity of intracellular calcium stores and the elevated residual calcium ensures a noisy synapse with low intrinsic release probability is a better predictor of ensuing neurotransmitter release.

In control synapses, a larger number of VDCCs are required to elevate the calcium levels enough for a vesicle release, compared to synapses with stores blocked (see Figure 2.4b). Hence, the coefficient of variation (CV) of the calcium signal is lower, maintained by a larger number of VDCCs (see Figure 2.11d).

Control synapse (with functional stores) clearly shows elevated residual calcium from the previous stimulus (see Figure 2.7c1-2). In control synapses, larger residual calcium and low CV of VDCCs contribute to the enhanced facilitation that manifests in P11. In addition to VDCCs, SERCAs also play a role in maintaining a less noisy calcium signal in control synapses. Amount of calcium binding to SERCAs keeps up with the noise in calcium peaks across trials. We can see it in the strong correlation between maximal % of SERCA-binding sites and peak calcium concentration during a paired-pulse stimulus (see Figure 2.11e for low Pr1 case and 2.11f for high Pr1). In addition, we show that for all intrinsic release probabilities, the CV of peak calcium concentration decays with an increase in SERCA occupancy (see Figure 2.11g). Each data point in Figure 2.11g corresponds to a specific release probability configuration of the synapse. In other words, for the whole range of Pr, SERCAs smooth out calcium fluctuations. The influence of SERCA pumps without the contribution of VDCCs in lowering the calcium variability can be seen in Figure 2.11h. Essentially, we simulated control and stores-blocked synapses with an identical number of VDCCs. The effect of SERCA is clearly seen between the pulses wherein the CV of calcium signal at the AZ remains lower for control synapses.

In summary, intracellular calcium stores allow synapses to operate at low intrinsic release probability and yet exhibit large, facilitated release with a lower CV caused by longer-lasting and less noisy residual calcium. The less noisy calcium signal associated with synapse with functional stores may have downstream implications in other calcium-dependent signaling involving vesicle recycling [Wu and Wu, 2014].

2.5 Calcium overload in ER disrupts STP similar to genetic models of Alzheimer's disease

The calcium hypothesis of Alzheimer's disease points to disruption of neuronal calcium signaling as one of the earliest manifestations of the disease. In order to gain a mechanistic understanding of this high-dimensional disease, we focus our investigations on these early pathological calcium dysregulations in hippocampal synapses [Popugaeva et al., 2018]. These perturbations modify the plasticity of synapses that ultimately may have a causal link to cognitive and memory deficits.

Calcium overload in ER is one such dysfunctional calcium signal caused by loss of presenilin function due to its mutation [Nelson et al., 2007; Tu et al., 2006]. Another study by Wu et al. [2013] suggested mutations in presenilins lead to reduction of RyR expression causing reduced calcium influx from ER. Thereby, disrupting STP. While a contradicting study suggested an increase in RyR expression [Chan et al., 2000].

We tested these hypotheses in our computational model. We set up six simulation conditions:

- Control, the normal functioning synapse

- 50 % RyR underexpression

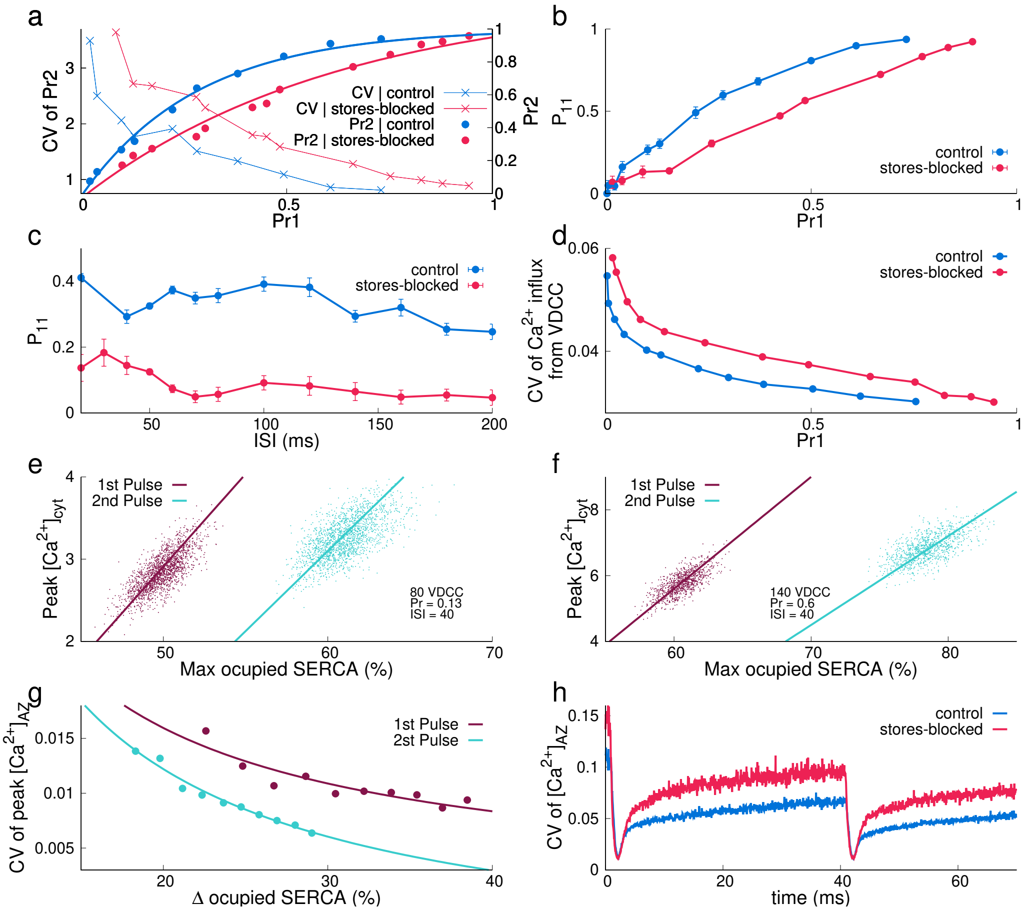

FIGURE 2.11. **Reliability of synapses with ER. a.** Release probability of a vesicle in response to the second pulse (Pr_2, right “y“ axis) in a paired-pulse protocol and coefficient of variation of Pr_2 (left “y“ axis) as a function of release probability in response to the first pulse (Pr_1). **b.** Conditional probability (P_{11}) as a function of Pr_1. **c.** P_{11} for a range of interspike interval, ISI (20–200 ms) with an intrinsic release probability, Pr ~ 0.14. **d.** CV of calcium flux through VDCCs as a function of Pr_1. The larger number of VDCCs contribute to release in Control synapses resulting in a lower CV of calcium flux. e,f. Correlation between peak cytosolic calcium concentration ($[Ca^{2+}]_{cyt}$) and the % maximum occupancy of SERCA pumps for synapses with intrinsic Pr ~ 0.13 and Pr ~ 0.6 (2000 and 1000 trials, respectively). **g.** Decreasing trend of CV of the peak of calcium concentration at the active zone, $[Ca^{2+}]_{AZ}$, as a function of %Δ occupied SERCA sites. %Δ occupied SERCA = ((max occupancy initial occupancy) × 100/total SERCA-binding sites). **h** CV of $[Ca^{2+]}_{AZ}$ across 2000 trials for a synaptic configuration with 80 VDCCs. Data are mean ± s.d.

- 300 % calcium overload in ER
- 300 % calcium overload in ER + 50 % RyR underexpression
- 300 % calcium overload in ER + 200 % RyR overexpression
- Blocked calcium stores

We found that reduction in RyR expression had no significant effect on STP while ER overload drastically impaired STP. Increased calcium influx through ER due to overload during stimulus raises neurotransmitter release probability, thereby, decreasing facilitation (see Figure 2.12a). Increase in peak calcium concentration in ER overload condition, although small, had a large effect on transmitter release probability as Pr has highly nonlinear dependence of 4th power of calcium peak concentration (see Figure 2.12b). In addition, due to high Pr, faster depletion of RRP was also observed.

2.5.1 Model reproduces established experimental observations

So far we have elaborated on the mechanism by which SERCA pumps and the other components associated with calcium signaling from ER orchestrate short-term synaptic plasticity. Here, we compare the predictions of our model with experimental observations of short-term plasticity at CA3–CA1 synapses [Dobrunz et al., 1997; Murthy et al., 1997].

Two independent experiments have measured the inverse relation between PPR and Pr at two different inter-spike intervals: 40 Hz and 50 Hz [Dobrunz et al., 1997; Murthy et al., 1997]. Our control model that includes presynaptic calcium stores arrives at a similar relation for a large range of Pr and is in better agreement than the stores-blocked case (see Figure 2.13a). As the inter-spike interval increases, the amount of influence by residual calcium from the first AP on the release due to the second AP is expected to decrease. This is consistent with experiments in CA3-CA1 synapses Dobrunz and Stevens [1997]. In the experiment, the ensemble of neurons has a distribution of release probabilities. We implemented the same distribution in our model study and the result closely followed experiment for the control model. As expected, PPR response in stores-blocked model was reduced drastically and was not in agreement with the experimental data (see Figure 2.13b).

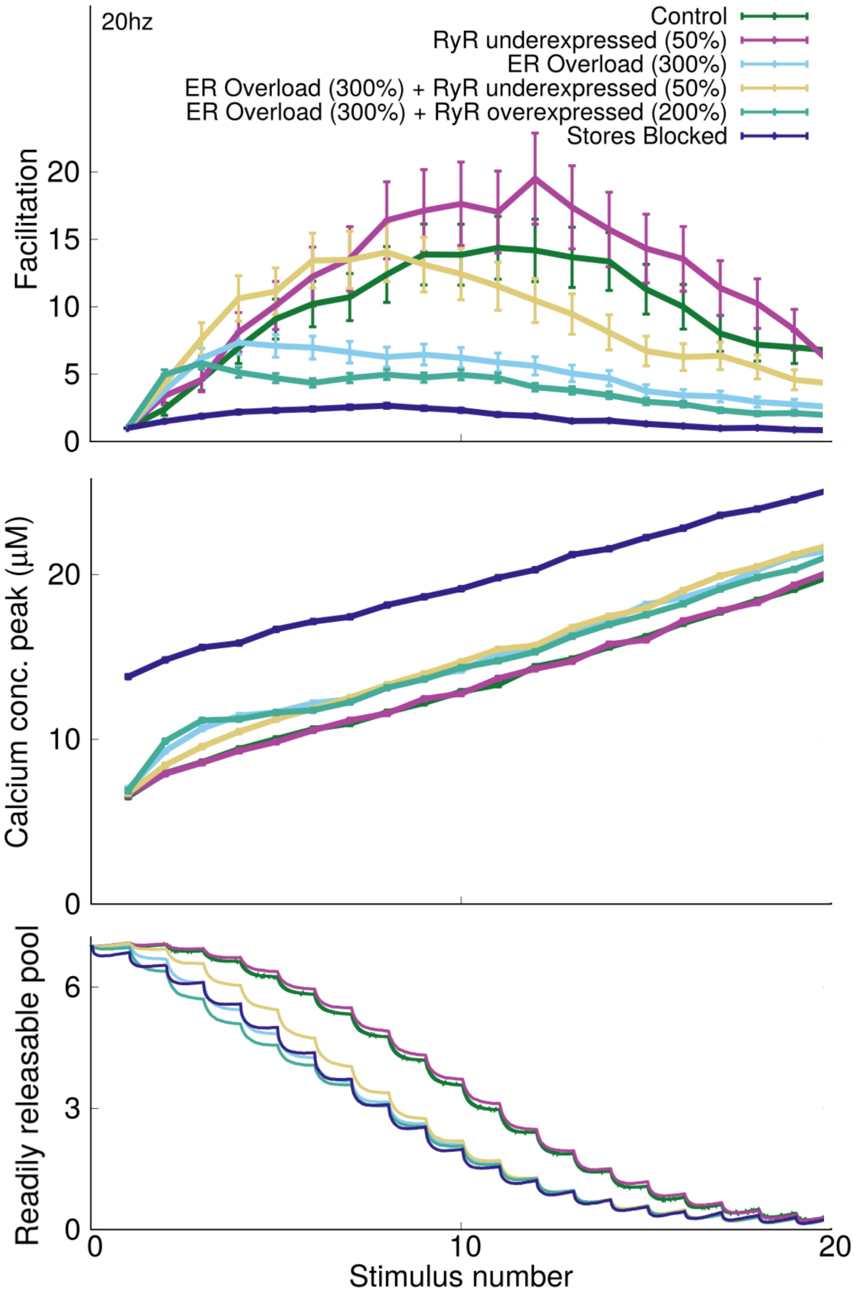

FIGURE 2.12. **STP dysregulation in Alzheimer's disease. a.** Facilitation in response to 20 action potentials at 20 Hz for six different simulation conditions. **b.** Peak calcium concentration in response to each of the action potentials. **c.** Vesicle depletion from RRP. Data are mean ± s.d.

In an experiment that measured release probability as a function of RRP size, high extracellular calcium concentration of 4 mM was used to minimize the amount of facilitation [Dobrunz et al., 1997]. We incorporated the same higher extracellular calcium concentration for both the control and stores-blocked synapses. Control synapse showed better agreement with experiment, while Pr was much higher when the stores were blocked (see Figure 2.13c). This higher Pr response is attributed to the absence of buffering by SERCAs when the stores are blocked.

Finally, the timescales for vesicle recycling can critically modify both PPR and release probabilities. The vesicle recovery in our model after depletion (see Figure 2.13d) is in agreement with experimentally observed replenishment timescale: τ_{model} = 2.94 s, $\tau_{experiment}$ = 2.8 s [Dobrunz et al., 1997].

2.6 Discussion

The presence of ER is reported in both axonal and dendritic compartments [Bouchard et al., 2003; Mattson et al., 2000; Rollenhagen et al., 2007]. However, only about 20% of CA1 spines have ER and is over-represented in the larger, stronger synapses [Bourne and Harris, 2008]. In contrast, the ER in CA3 axons extend through all boutons. ER can modulate several downstream calcium signaling cascades. Here, we report on the distinct role of extensively present presynaptic ER, in making a crucial contribution to STP. This is predominantly via the buffering action of SERCA pumps on the ER membrane.

SERCAs have a characteristic fast action and high binding affinity and these are ER calcium refilling [Higgins et al., 2006]. SERCA2b isoform is the most prevalent form in the hippocampus [Baba-Aïissa et al., 1996; Baba-Aïssa et al., 1996]. Structural analysis shows that these have the highest calcium affinity [Vandecaetsbeek et al., 2009]. These intrinsic properties make SERCA capable of quickly capturing a large amount of calcium ions lowering Pr. At the CA3 presynaptic terminal, the inverse relation between PPR and Pr is well established [Dobrunz et al., 1997; Hanse and Gustafsson, 2001]. Synapses with ER have low Pr (but not in stores-blocked synapses) which ensures high facilitation. The contribution of calcium release from RyR over these shorter time scales is minor.

There is a trade-off between synaptic reliability and STP in CA3 neurons. Sensory information and spatial location are encoded by firing rates of hippocampal neurons.

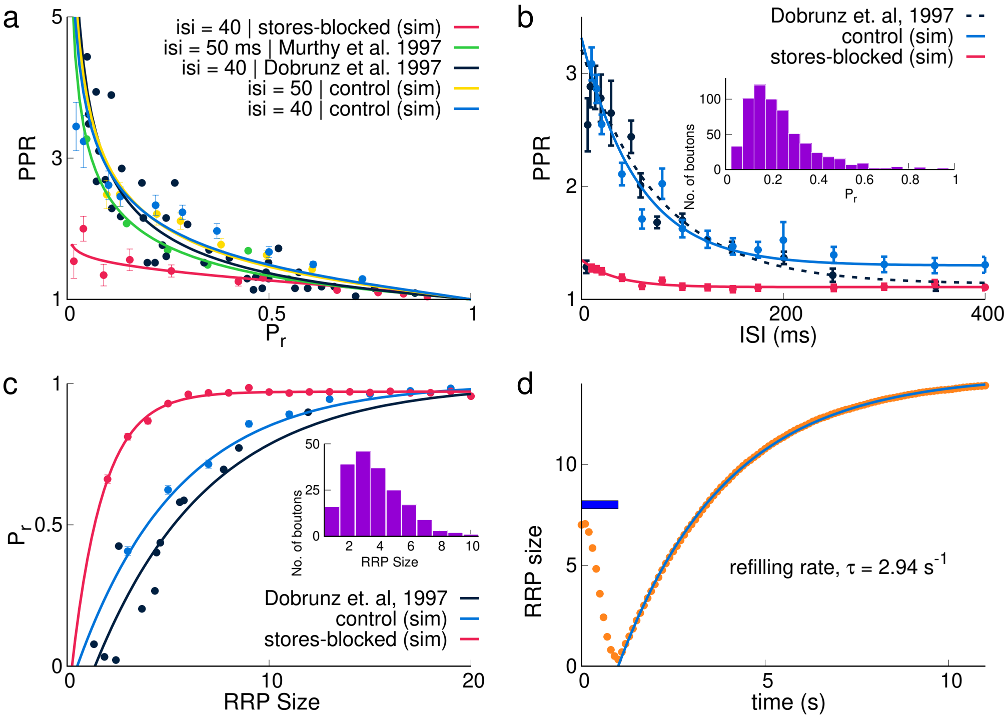

FIGURE 2.13. **Comparison of simulation results with experimental data. a.** Inverse relation of paired-pulse ratio (PPR) with intrinsic release probability (Pr) for 40 ms ISI (experiment, black; simulation, blue) and 50 ms ISI (experiment, green; simulation, yellow), and stores-blocked (simulation, red) (experimental data from Dobrunz and Stevens [1997]; Murthy et al. [1997]). **b.** PPR decreases with increasing ISI for all synapses: control (blue), stores-blocked (red), and experiment (dashed, black). Inset shows the distribution of Pr in synapses used in the experimental result (data from Murthy et al. [1997]) and in simulations. **c.** Variation of Pr with readily releasable pool (RRP) size for control (blue), stores-blocked (red), and experimental data (black). The distribution of the RRP size used for simulations is shown in inset [Murthy and Stevens, 1999]. **d.** RRP (shown in orange) was depleted by a 20 Hz stimulus for 1 s (indicated by horizontal blue bar) and vesicle refilling was observe and fitted to an exponential curve (blue) (replenishment timescale τ = 2.94 s). Data are mean ± s.d.

Sensory discrimination is compromised when hippocampal leisions impair rate code [Lu et al., 2013]. Reliable firing rates can be maintained despite the stochasticity of vesicle release if a large number of synapses are activated with bursts of spikes rather than isolated spikes. However, location is encoded and represented by the activity of a small number of neurons [Ahmed and Mehta, 2009]. The alternative strategy would be to operate at high Pr which is energy inefficient and small RRP can not sustain it. ER allows synapses to operate in low Pr regime yet still exhibit relatively higher reliability in its activity.

Earliest indications of various forms of dementia is perturbed short-term plasticity. [Selkoe, 2002]. In presenilin double knockout animal models of Alzheimer's disease facilitation in Schaffer collaterals was reduced in comparison to control synapses. Also, blocking presynaptic ER in normal synapses resulted in a similar reduction in facilitation [Zhang et al., 2009, 2010]. Furthermore, the effect of ER blocking was occluded in AD synapses. These studies suggest compromised plasticity in AD is linked to disruption of ER calcium signaling. This supports our prediction on ER's role in normal functioning of STP.

CHAPTER 3

PRESYNAPTIC DESIGN INFLUENCES SHORT-TERM PLASTICITY IN HIPPOCAMPAL MOSSY FIBER

3.1 Introduction

Dentate gyrus (DG), a part of the classic trisynaptic circuit, forms an important junction for information processing in the hippocampus. Its major functions include processing, storage, and recall of spatial information, and temporal and spatial pattern separation [Chawla et al., 2005; Lee and Kesner, 2004; Leutgeb et al., 2007; Madar et al., 2019].

Granule cells in DG send sparse but powerful unidirectional projections via mossy fibers that synapse with proximal apical dendrites of CA3 pyramidal neurons. Mossy fiber (MF) boutons are morphologically highly complex structures and make multiple contacts with the postsynaptic terminal. Multiple active zones are present across the synaptic surface with an average inter-AZ distance of about 450 nm. Each active zone is associated with a large readily releasable pool (RRP) and a loosely coupled cluster of voltage-dependent calcium channels (VDCC) [Rollenhagen et al., 2007; Vyleta and Jonas, 2014]. In addition to feedforward excitation, CA3 neurons also receive feedforward inhibition from interneurons that are excited via filopodial extensions of MF boutons [Acsady et al., 1998]. A single granule cell contacts about 15 different CA3 pyramidal neurons via MFBs, and about 50 different mossy fiber axons provide input to a single CA3 pyramidal neuron [Amaral et al., 1990]. As we can see, this is a different beast altogether when compared to CA3 pyramidal neurons.

To encode two similar experiences, the neural representations require low overlap. This is performed by dentate gyrus. Two similar input activity patterns in DG elicit distinct cell-population activity in the CA3. This is known as pattern separation. Pattern separation minimizes overlap between patterns of neuronal activity that represent similar experiences. The fact that the DG contains a large number of granule cells relative to CA3 neurons and that one granule cell contacts only a few CA3 neurons is ideally suited for pattern separation. Theoretical work suggests that the dentate gyrus (DG) performs this role for memory processing, but a direct demonstration is lacking [Madar et al., 2019; Rolls, 2010; Treves et al., 2008].

MF synapses can undergo substantial changes in synaptic strength, exhibiting marked short-term facilitation which has been deemed essential for its role as a transmission line and a pattern separator. Upon stimulation it rapidly transitions from a low release probability (Pr) of about 0.2 to a high Pr synapse [Lawrence et al., 2004; Salin et al., 1996], and a single synaptic event is capable of detonating, i.e. triggering an action potential in the CA3 pyramidal neuron [Chamberland et al., 2018; Henze et al., 2002; Vyleta et al., 2016]. Previous studies have shown involvement of many molecular mechanisms in STP: buffer saturation [Blatow et al., 2003; Vyleta and Jonas, 2014], adenosine receptor activity [Moore et al., 2003], calcium release from internal stores, synaptotagmin-7 [Jackman et al., 2016], AP broadening [Geiger and Jonas, 2000], modulation of VDCC activity through mGluR, differential spatial distribution and properties of P/Q and N type VDCC [Chamberland et al., 2017], and synchronous multivesicular release [Chamberland et al., 2014]. Another study showed synaptic information transfer employs action potential counting strategy [Chamberland et al., 2018]. Individual active zones in MF have long been considered to be independent of each other. However, Rollenhagen et al. [2007] suggested, based on the morphology, that synaptic cross-talk may contribute to the efficacy of hippocampal mossy fiber synapses.

Despite decades of study, the implication of this elaborate synaptic design on STP is not well understood. What is missing is a coherent understanding of how all these elements interact together to orchestrate the distinct detonating nature of this synapse. It is in this regard, we took to computational modeling study to provide insights to resolve and better understand the working of the synapse. We built a physiologically realistic spatial model of the MF bouton to explore the role of the structural and functional properties that orchestrate synaptic signaling and STP. This synapse makes use of most of the same components that we saw in the CA3 neuron: voltage-dependent calcium channels, calcium buffer, PMCA pumps and calcium sensors, synaptotagmin-1 and -7.

3.2 The MFB model

EM reconstruction study by [Rollenhagen et al., 2007] has elucidated various structural and spatial properties of MF boutons in adult rats. It provided us with the bouton's shape and size (volume and surface area), ranges for the number of active zones and RRP size, the inter-active-zone distance, and so on. The model heavily relies on these insights provided by the study.

The mossy fiber bouton model consists of several active zones spread across the membrane at the presynaptic and postsynaptic apposition zone with an inter-AZ distance of 450 nm (see Figure 3.1a,b). Each active zone has an associated cluster of VDCCs and contains a large number of neurotransmitter-containing vesicles in their readily releasable pool. The cytosol is populated with calcium ions at 100 nM. It has been found to be the major prominent fast buffer in MF, with a concentration of about 45 μM [Müller et al., 2005]. The plasma membrane hosts PMCA pumps for calcium ion extrusion. PMCA activity, however, is comparatively much slower than other calcium capturing processes. The exact number of active zones, vesicles in the RRP of an active zone, VDCCs in a cluster and its coupling distance from its associated active zone are varied in different simulations, as described below. For further details of the model, see chapter 4: Model Construction.

3.2.1 Chronology of events

The key to neurotransmitter release is the presynaptic calcium signal and its major contributors are VDCCs. Since kinetics of VDCCs are dependent on the membrane potential, the calcium signal is sensitive to the action potential waveform. We modeled the AP and VDCC kinetics based on the whole-cell patch-clamp recordings from mossy fiber boutons of therat hippocampus [Bischofberger et al., 2002].

First, we stimulated the mossy fiber bouton with a single action potential. Momentary depolarisation of the membrane changes VDCC conformation, increasing conductance that closely follows AP waveform. As a result, calcium concentration rises sharply

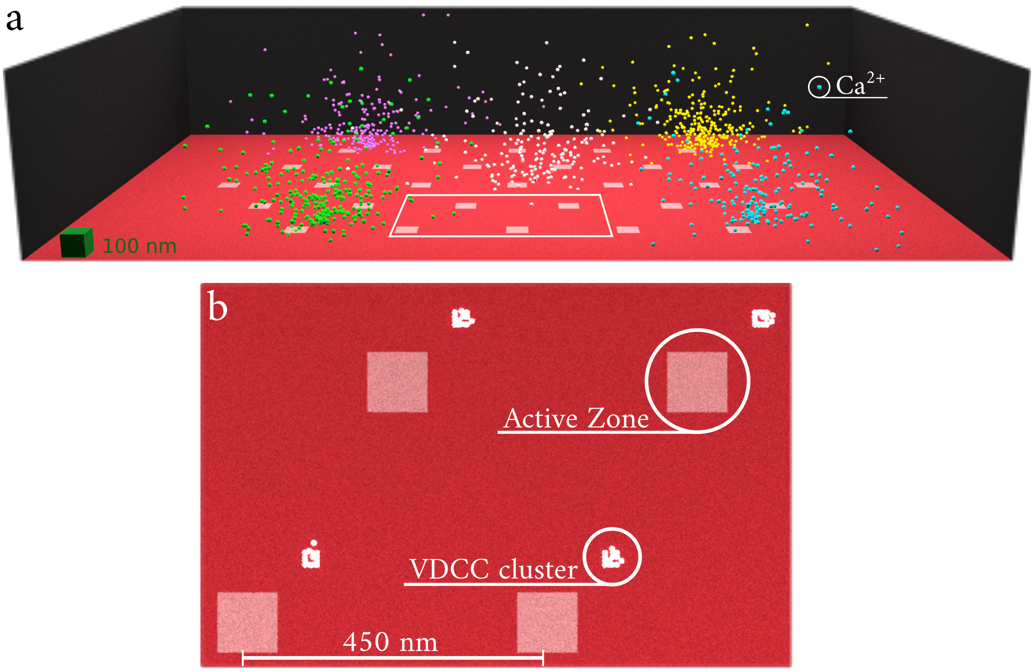

FIGURE 3.1. **Model of the mossy fiber bouton. a.** MF bouton from an oblique perspective. The two front surfaces have been made transparent. The red surface hosts active zones shown as white patches of squares. Calcium influx from 5 representative VDCC clusters is shown in different colours. **b.** The area enclosed in white boundary in **a** is zoomed in and shown here. Scale is represented by the green cube of 100 nm.

around the active zones (see Figure 3.2a). However, this rise is limited in time, amount and space. Calcium influx lasts for only about a millisecond and the ions are quickly captured by fast buffers (calbindin-D28k). Buffers not only limit the amount of free calcium, but also the spatial extent of the signal (see Figure 3.2c). Consequently, the average calcium concentration in the bouton remains much lower than around the active zones (see Figure 3.2a). Additionally, we observe a small and local decrease in the buffering capacity of calbindin-D28k (see Figure 3.2d). (We will see the effect of multiple stimuli on the buffering capacity and its effect on synaptic efficacy later). Finally, a small but significant amount of free calcium persists in the bouton after the AP for much longer. It decays at a timescale of around 100 ms (see Figure 3.2a). PMCA pumps present on the membrane maintain the calcium concentration gradient across the plasma membrane on a longer timescale.

Calcium ions bind to calcium sensors — synaptotagmin 1 and 7, present on the vesicle in mossy fiber axon terminals — resulting in neurotransmitter release.

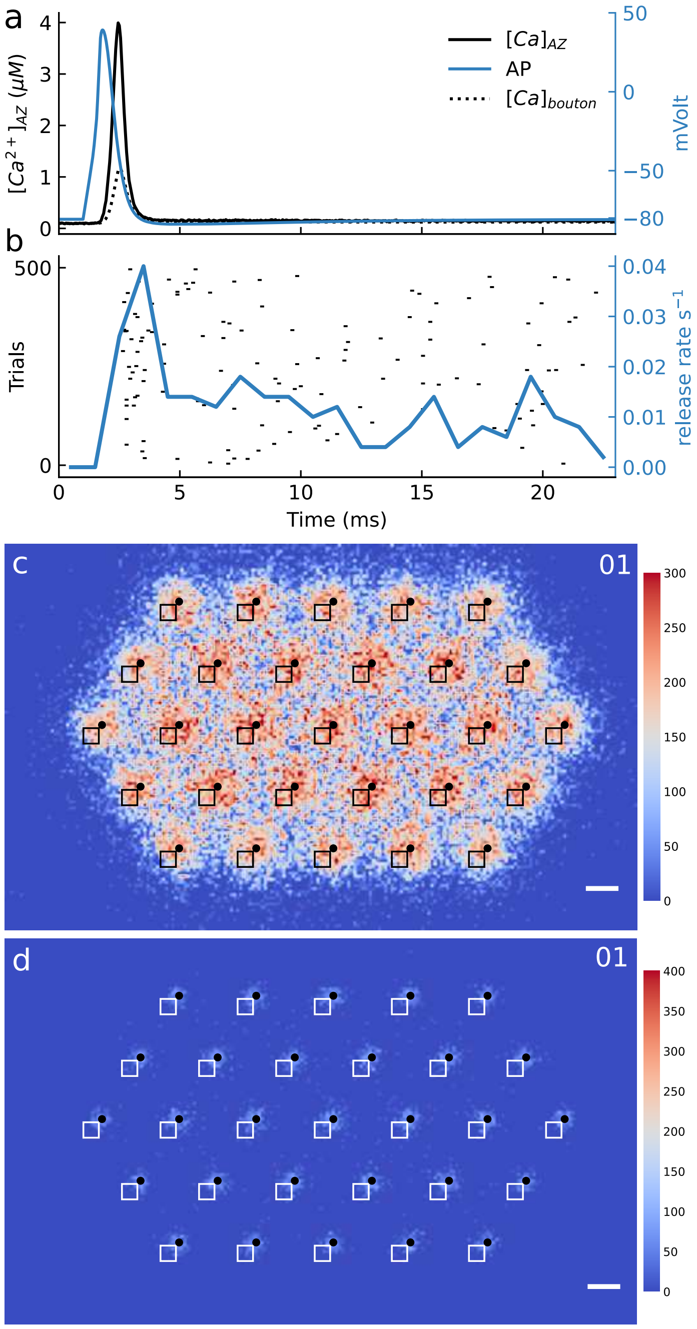

FIGURE 3.2. **Chronology of events. a.** Average calcium concentration at active zones and in the bulk of the bouton is shown in response to an AP. **b.** Raster plot of vesicle release from 500 trials in response to the above shown AP and the vesicle release rate. **c.** Bouton surface with active zones (black squares) and associated VDCC clusters (black filled circles) are demarcated here. When calcium is released from VDCCs, their concentrations decrease with distance. The colour here represents the height (in nm) of the imaginary surface below which **c** the calcium concentration is above 1 μM and **d** buffering capacity of calbindin-D28k has reduced by more than 20%.

Synaptotagmin-1 is responsible for fast synchronous release [Bacaj et al., 2013; Xu et al., 2007] while synaptotagmin-7 triggers asynchronous release [Bacaj et al., 2013; Luo and Südhof, 2017]. A single AP releases only a small amount of vesicles due to low basal release probability (see Figure 3.2b).

3.3 Degeneracy in synaptic design

Mossy fiber boutons show large variations in their presynaptic organization of vesicle release machinery. To study the implications of these variations on synaptic properties we chose four synaptic attributes or parameters:

- Number of active zones: **nAZ** (7-29:2)
- Number of VDCCs in a single cluster: **nVDCC** (2-14)
- Distance between AZ and associated VDCC cluster: **dVAZ** (60-220:20 nm)
- Number of vesicles in RRP of each active sone: **nRRP** (5-40:5)

Each combination of the above parameters represents a synaptic design. There are 11232 designs that we simulated with an action potential over 500 trials and calculated the vesicle release probability. Most of the designs are not relevant as their release probability is either too high or too low. Yet, a significantly large spread of designs reproduce the physiological release probability of ~0.2 (see Figure 3.3a). In other words, we observe a large degeneracy in the parameter sets that result in physiological Pr. However, there are some clear constraints to the design. For a constant number of VDCCs in a cluster and coupling distance, RRP size follows an inverse relation with the number of active zones (see Figure 3.3a). Larger coupling distance favors larger numbers of VDCCs in a cluster and vice versa (see Figure 3.3b).

Next, we divided each synaptic attribute into three categories — low, mid and high. We got 81 parameter sets based on their attributes/parameters, and counted the fraction of parameter sets that belong to each category. Interestingly, the physiological designs, the ones with Pr in the range 0.2 to 0.28, only occupy 33 of these parameter sets. The colour value shows the percentage of sets that occupy a category. We can begin to see that there is a preference among the designs. A large fraction of parameter sets for physiological Pr favors nVDCC, dVAZ and RRP on the higher side (see Figure 3.3c).

Due to large degeneracy in parameter sets, we chose one representative parameter set from each block to further probe the underlying mechanism of short-term facilitation in the mossy fiber bouton.

3.4 Probing the plasticity mechanism

3.4.1 Role of calcium buffer, synaptotagmin and cross-talk in STP

In the high Pr regime, the ratio of Pr_n to Pr_1 fails to capture facilitation faithfully due to saturation of Pr. Therefore, we have used $nRel_n$, the total number of vesicles released in response to n^{th} AP, averaged over all the trials. The ratio of $nRel_n$ to $nRel_1$ is a better measure of facilitation in MFB for two reasons: it does not saturate with increase in vesicle release and it accounts for multiple releases — a characteristic feature of this synapse. Throughout this study, facilitation refers to $\frac{nRel_n}{nRel_1}$ unless otherwise mentioned.

With the aim to probe into the mechanism of STP, we designed five simulation conditions — control, without crosstalk, nonsatBuffer, syt7KO and nonsatBuffer + syt7KO:

- **control**: bouton with normal properties of the components.
- **without crosstalk**: each active zone sees calcium only from its own VDCC cluster.
- **nonsatBuffer** (short for non-saturating buffers): calcium buffer is modeled with constant concentration that remains constant.
- **syt7KO**: neurotransmitter release from synaptotagmin-7 is abolished.
- **nonsatBuffer + syt7KO**: calcium buffers do not saturate and neurotransmitter release from synaptotagmin-7 is abolished.

Each of the 33 parameter sets were simulated for all the simulation conditions. While control shows highest increase in Pr, nRel and facilitation with subsequent stimuli, nonsatBuffer + syt7KO completely abolishes facilitation. Other three cases — without crosstalk, nonsatBuffer and syt7KO — show different degrees of reduction compared

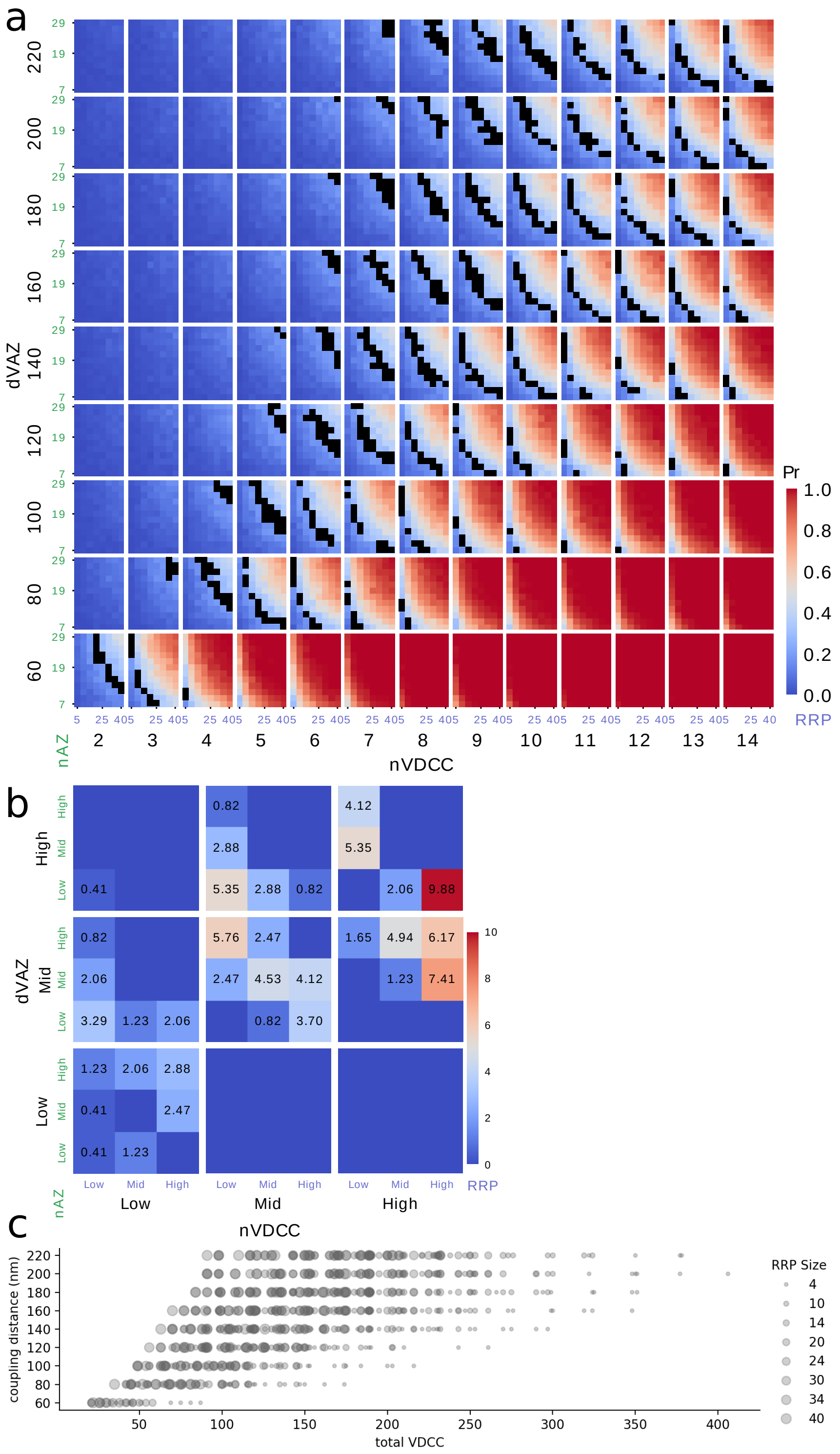

FIGURE 3.3. **Degeneracy in mossy fiber design. a.** Release probability of MF with different parameters: nVDCC, dVAZ, nAZ and RRP. Black spots refer to synaptic configurations with Pr within 0.20 - 0.28. **b.** Each parameter range was divided in three categories: low, mid and high. Percent of simulation configurations with physiological Pr (within 0.20 - 0.28) that fall in a category is shown. **c.** Degeneracy in design considering total VDCCs in the system.

to control (see Figure 3.4a-c). Therefore, crosstalk among active zones, occupation of local buffering sites and synaptotagmin-7, each contribute to presynaptic STP in mossy fiber bouton.

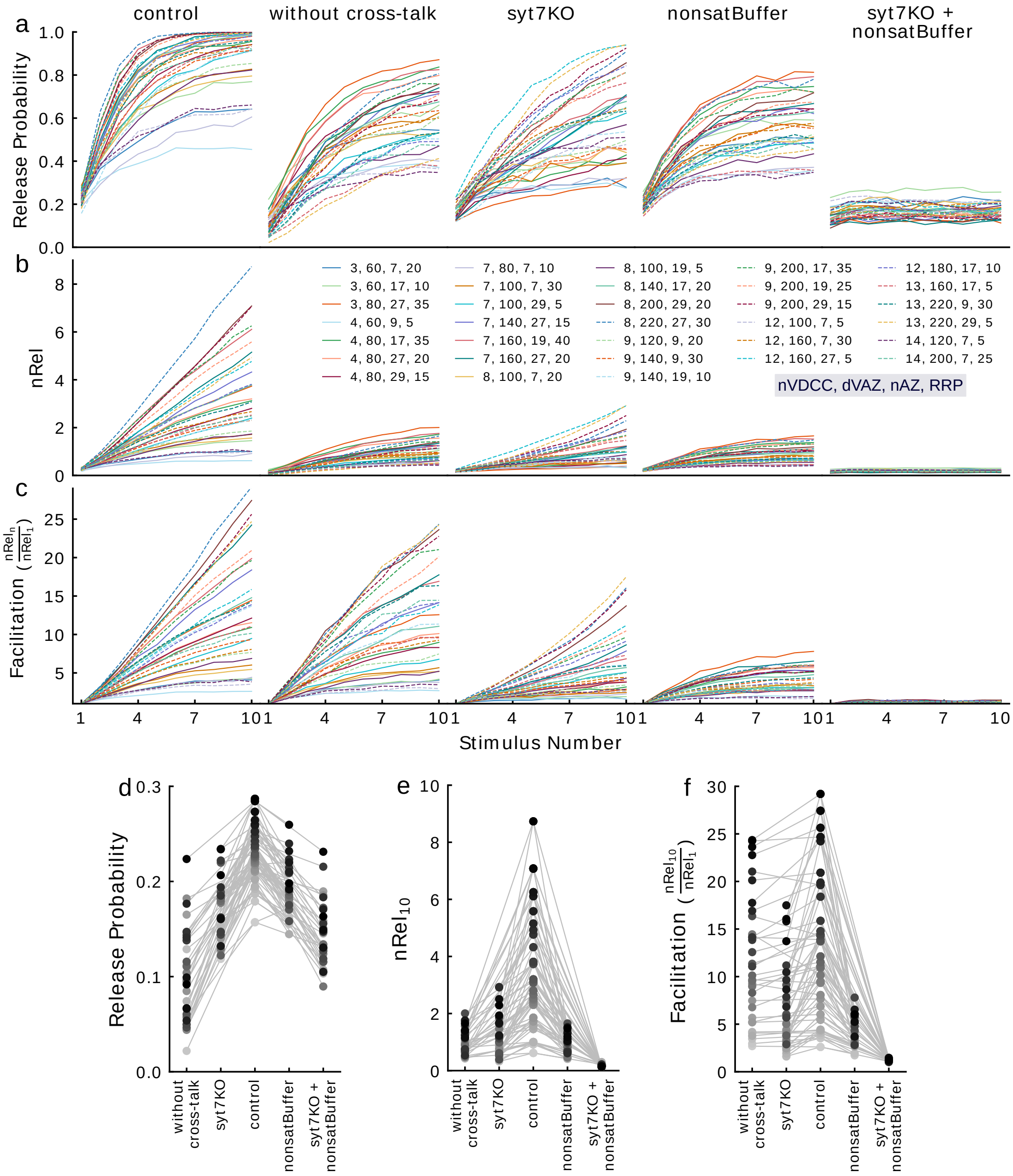

FIGURE 3.4. **Facilitation in mossy fiber. a-c.** Release probability, total vesicle releases per active zone and facilitation for each synaptic configuration and parameter sets. **d-f.** Comparison of initial Pr, $nRel_{10}$ and facilitation after 10th stimulus for each of the synaptic configurations.

Compared to control, each condition shows a small reduction in release probability and facilitation, and large reduction in $nRel_{10}$ (total number of vesicles released in response to 10^{th} action potential, averaged over 2000 trials) (see Figure 3.4d-f). High facilitation is favored by nVDCC, dVAZ and RRP on the higher side of the range for control, without crosstalk and syt7KO (see Figure 3.5a-c). While nonsatBuffer prefered smaller coupling distance between AZs and VDCC clusters as larger distance prohibits calcium signal (see Figure 3.5b). Interestingly, the categories that contain high fraction of parameter sets with physiological Pr are the ones that show high facilitation in control.

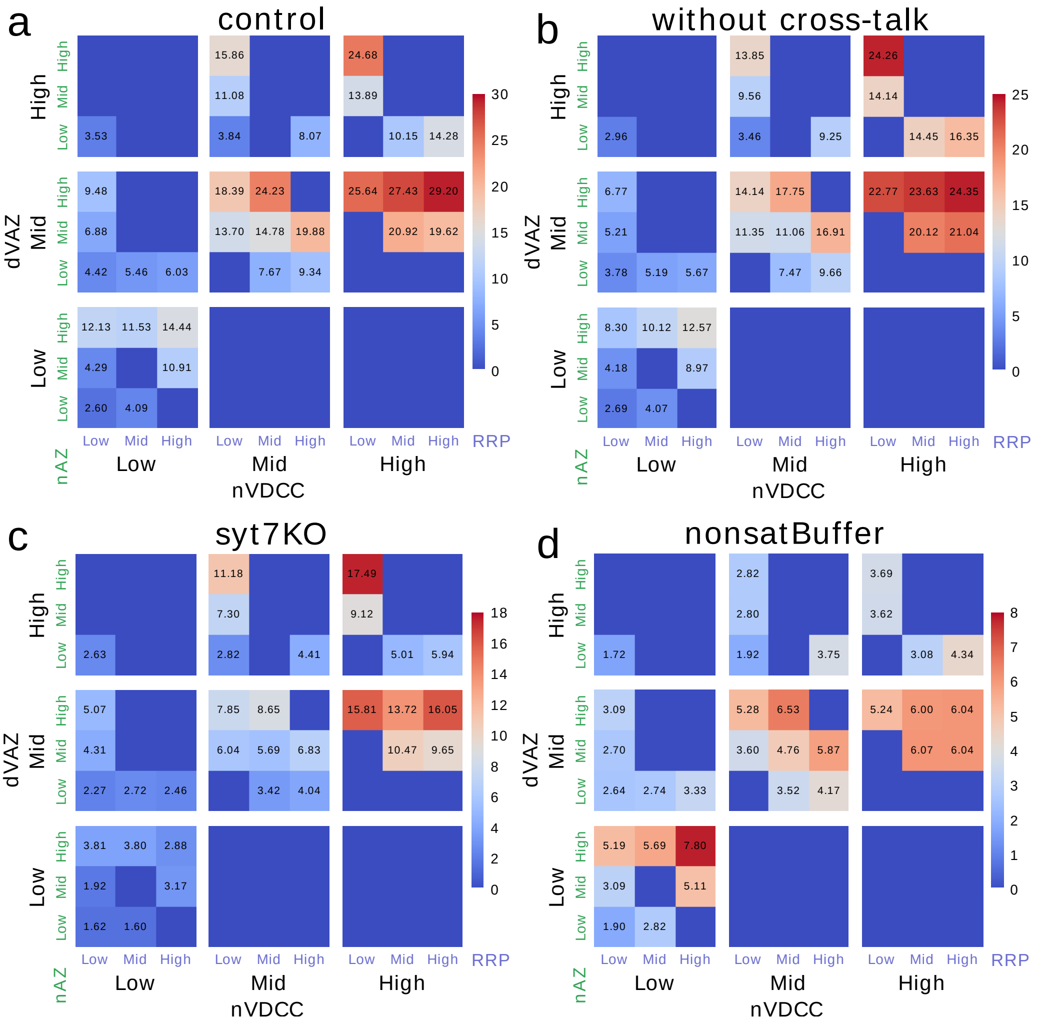

FIGURE 3.5. **Distribution of facilitation** after 10th stimulus across parameter sets for different synaptic configurations. Data for without crosstalk + syt7KO is not shown as there is practically no facilitation.

3.4.2 Interplay of calcium buffer and cross-talk leads to enhanced residual calcium

In response to an action potential, calcium concentration transiently rises (see Figure 3.6). In Figure 3.6a, we are looking at the presynaptic surface. Black squares are active zones and the smaller black circles are the associated VDCC clusters. The colour indicates the height of the surface below which the calcium concentration is greater than 1 μM. This snapshot is taken at the 1st peak of calcium influx from VDCCs. We notice that each VDCC cluster has its own calcium bubble that does not interact much with the nearby active zones. By the time it receives the 5th stimulus, the individual calcium bubbles have merged, and more so by the 10th stimulus. This shows that active zones are initially uncoupled, but with multiple stimulus, the cross-talk increases and cannot be neglected.

This happens due to subsequent decrease in calcium buffering capacity of calbindin-D28k. The color in Figure 3.6b shows the surface height below which buffering capacity has decreased by 20%. Subsequent stimuli increase the bubble size of calbindin-D28k where buffering capacity has decreased. This increases local residual calcium, and when local calcium signals start to overlap, cross-talk further contributes to elevated residual calcium concentration. Its overall effect can be seen in the average calcium concentration at the active zones. Control synapse shows an increasing calcium peak and its residual calcium is most enhanced compared to the other cases (see Figure 3.6c,d). Compare residual calcium concentration between control and when cross-talk is abolished after the tenth AP Figure 3.6f).

3.4.3 Synaptotagmin-7 shows larger increase in neurotransmitter release

Synaptotagmin-7 has low affinity for calcium, as opposed to synaptotagmin-1. As a result, synaptotagmin-1 quickly binds and unbinds calcium in response to a short-lived calcium pulse (see the blue trace in Figure 3.7), while synaptotagmin-7 shows progressive increase in bound calcium in response to subsequent calcium influx, as you can see in the orange trace in Figure 3.7. Consequently, synchronous release via synaptotagmin-1 remains the same after each stimulus. While, asynchronous release via synaptotagmin-7 shows a steady increase. That is how synaptotagmin-7 facilitates increase in vesicle release. Since mossy fibers have a large RRP size, vesicle

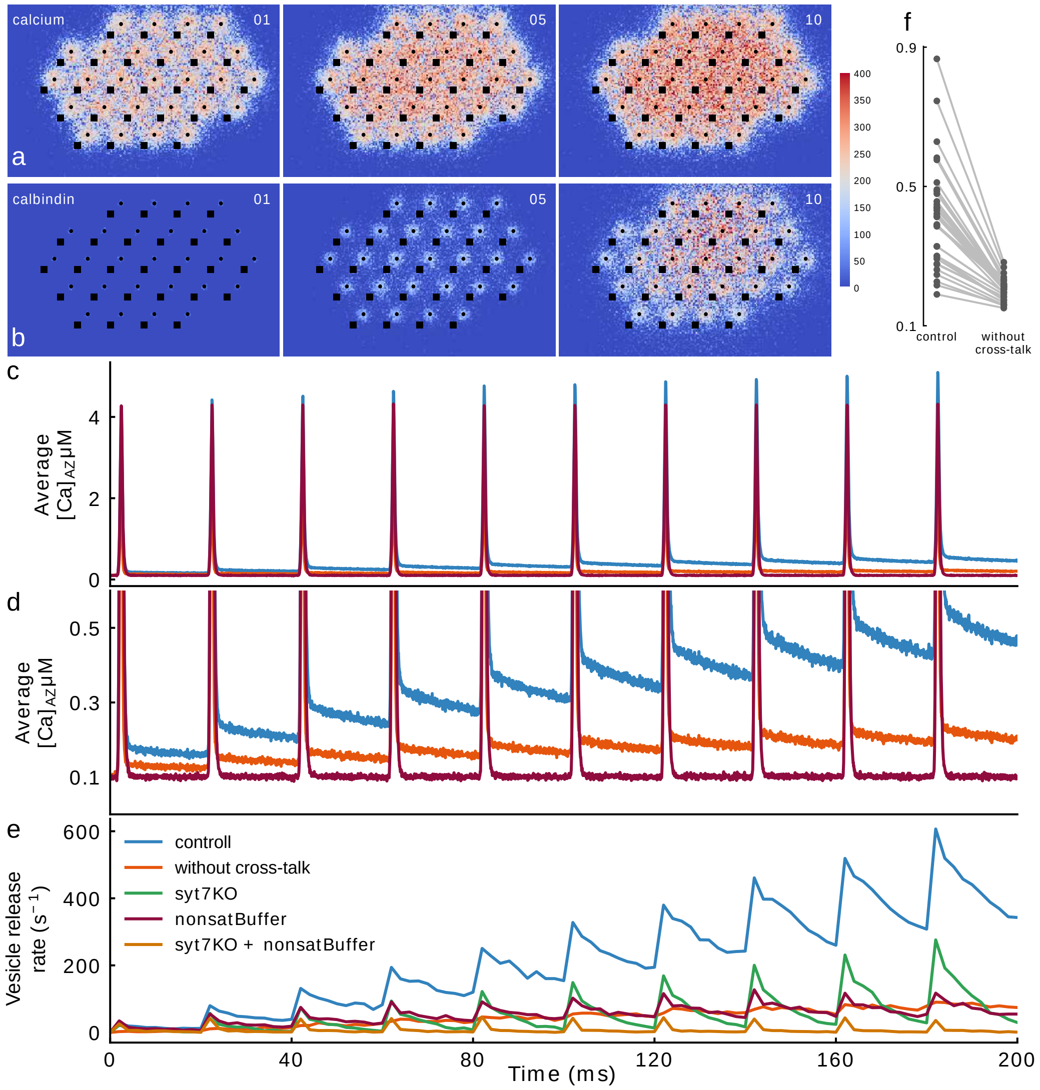

FIGURE 3.6. **Calcium dynamics in the MF bouton. a.** The heatmap shows the height (in nm) of the surface below which calcium concentration is above 1 μM during an AP. **b.** The heatmap shows the height (in nm) of the surface below which at least 20% of calcium binding sites in the calbindin-D28k is occupied during an AP. The three heatmaps (for both a and b) correspond to 1st, 5th and 10th AP, respectively, as indicated by numerals at the top right. **c.** Average calcium concentration profile at the active zones. **d**. Zoomed-in snapshot of c, showing residual calcium concentration. **e.** Total vesicle release rate in all the simulation conditions in response to 10 action potential at 50 Hz. **f.** Comparison of residual calcium after 10 stimuli. All the data shown here are for a specific design (nVDCC = 8, dVAZ = 220 nm, nAZ = 27, RRP = 30) that shows high facilitation.

depletion does not take over as in CA3-CA1 synapses, unless they are stimulated with unreasonably long and high frequency stimuli.

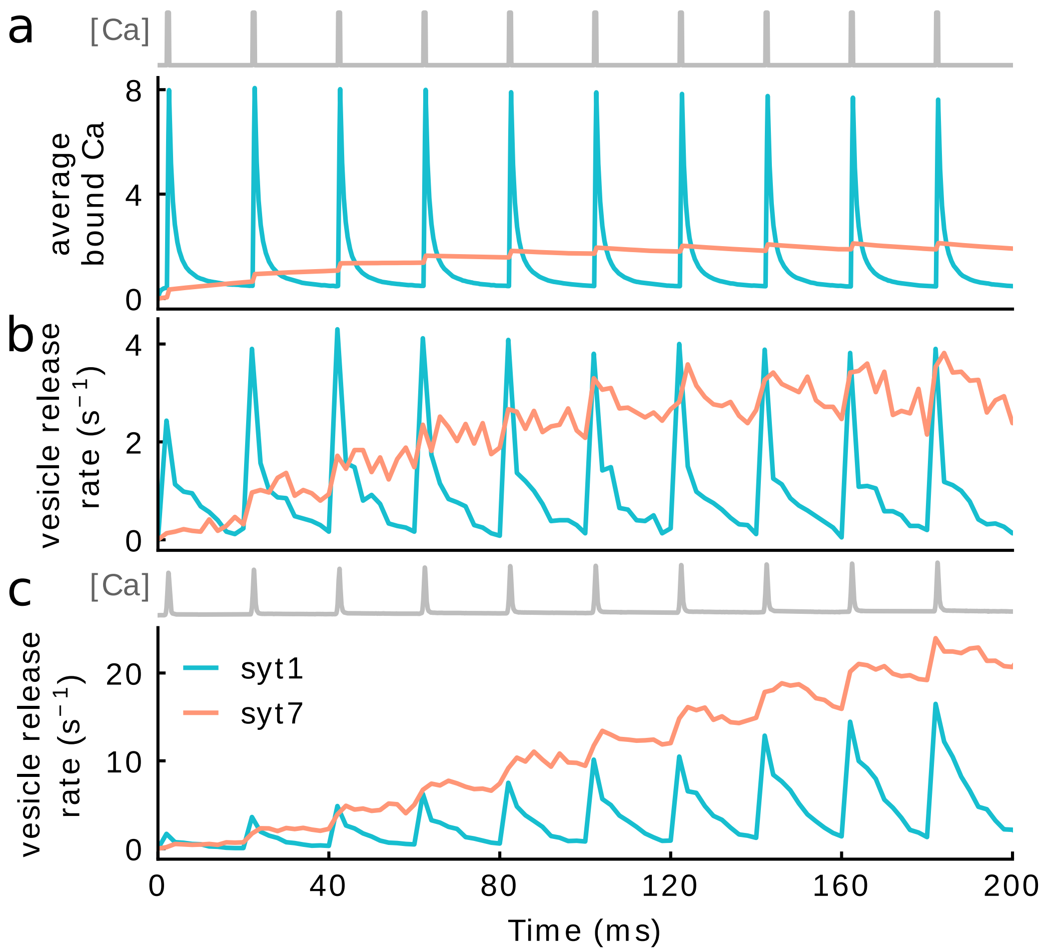

FIGURE 3.7. **Synaptotagmin activity. a,b.** average calcium ions bound to syt1 and syt7, and vesicle release rate via syt1 and syt7 in response to an artificial calcium stimulus with peak height of 8 μM and a residual 300 nM. **c.** Vesicle release rate via syt1 and syt7 in response to modeled calcium influx from VDCCs.

The combined effect of these phenomena results in a sharp increase in neurotransmitter release that is capable of triggering an action potential in the postsynaptic terminal (see Figure 3.6e).

3.5 Conditional detonation

To further probe the postsynaptic side of the system, we built a phenomenological model of the inhibitory interneuron and the pyramidal neuron in CA3. The neurotransmitter released from the mossy fiber spatial model was fed to the CA3 neuron and the interneuron as current input. The interneurons have a high release probability of about 0.4 and directly inhibit pyramidal neuron (see Chapter 4: Model construction for implementation details). The purpose of the CA3 model was to study the generation of action potential on the postsynaptic side. In control, we see many designs showing sudden increases in AP probability. But it is drastically reduced when synaptotagmin-7 is knocked out, cross-talk is abolished or buffer capacity is kept steady. In summary, all these factors are essential for AP counting (see Figure 3.8a1-5). In control, the probability of generating the first AP is maximum at the 4th stimulus and is diminished in all other cases (see Figure 3.8b1-5).

3.6 Implication of the design: temporal pattern separation

First we probed into the workings of this synapse. Next, we looked at the implications of its plasticity. Mossy fibers have been shown to perform pattern separation. That is, reduction of overlap between neuronal activities that represent similar experiences. This is done by activating a distinct set of neurons for each experience. Another kind of pattern separation is reduction of correlation between two signals encoded by the same neuron. This is known as temporal pattern separation. In a recent study, mossy fibers were stimulated by correlated poisson stimulus, and corresponding output was recorded, as shown here. Pairwise correlation between output trains was shown to be always lower than input. We performed the same experiment in our model. We found that short-term plasticity is required for low output correlation. And this is consistent across a range of input spike rates (see Figure 3.9).

3.7 Discussion

Mossy fibers employ a sparse coding strategy to represent information. Therefore, it proves essential to faithfully respond to bursts of high frequency incoming signal, while filtering out stimuli generated by intrinsic synaptic stochasticity. The rapid

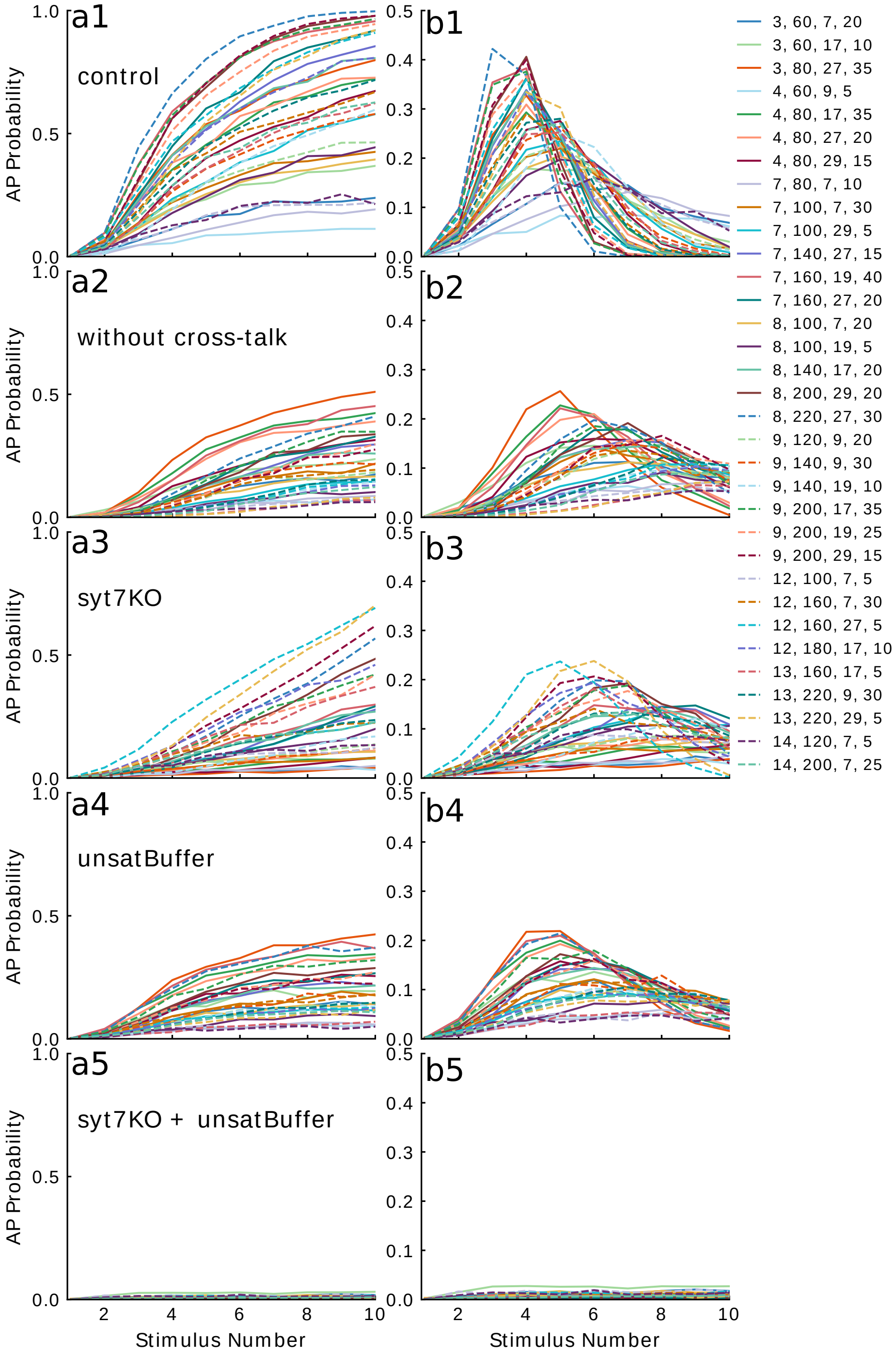

FIGURE 3.8. **Conditional detonation of CA3 pyramidal neuron. a1-5.** The CA3 pyramidal neuronal model was stimulated with synaptic current generated by neurotransmitters released from mossy fiber boutons. The probability of generating an action potential on the postsynaptic neuron is plotted for all the parameter sets and each synaptic configuration. **b1-5.** Probability of first AP in response to a train stimulus

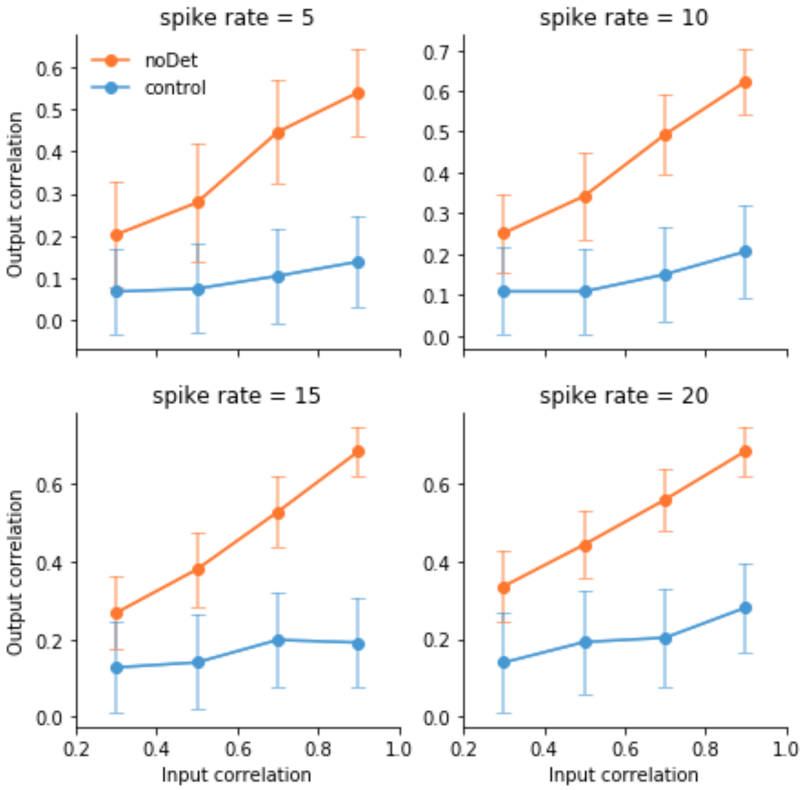

FIGURE 3.9. **Temporal pattern separation** Mossy fibers are stimulated with a correlated poisson spike train. Output correlation between CA3 activity, the output spike train, is measured and is shown for control as well the model where no plasticity is allowed, for four different input spike rate.

short-term plasticity of MFs allows them to respond in exactly the same fashion. The bouton is optimally designed for it; it is large for a reason. The large bouton hosts a large number of active zones. During low levels of activity, each active zone acts independently, given that they are separated from one another by considerable distance. In this case, the synapse acts like a collection of CA3 pyramidal neurons. The loose coupling between the active zones and their VDCC cluster ensures that the calcium levels remain low when a single AP is administered.

In the dentate gyrus, on the other hand, encoded signals arrive in short bursts of high frequency. Calbindin's capacity for calcium buffering gets reduced with this repeated influx with the result that calcium signals travel well beyond the VDCC cluster, ultimately overlapping multiple active zones. Active zones, at this point, no longer act independently. Both local decrease in buffering capacity and contributions from nearby VDCC clusters raise residual calcium drastically. In turn, large and rapid increase in synaptic efficacy ensues. It takes about three to six APs to make the synapse powerful enough to be a faithful signal transmitter that detonates postsynaptic CA3 neurons. All the while, large RRP size ensures that its vesicles do not get depleted even when the frequency of signals is high.

Additionally, because synaptotagmin-7 has a low affinity for calcium (as opposed to synaptotagmin-1), its response to the calcium influx steadily increases. As a result, asynchronous release via synaptotagmin-7 not only shows a steady increase, but it also spreads out the vesicle release over a larger range of time. This helps in the temporal decorrelation of similar activity patterns that may be encoding similar experiences. Both temporal and spatial pattern separation, as many models of CA3 associative network suggest, is essential for the faithful representation of memories in the CA3 neuronal activity.

Geiger and Jonas [2000] suggests broadening of AP profile as a mechanism for increasing calcium influx through VDCCs. Although the effect is significant only after stimulating the synapse with tens of APs at high frequency. This is not physiologically realistic and therefore we have ignored this effect in our study.

Mossy fibers are under the tonic influence of adenosine, which decreases the calcium flux through VDCCs, and maintains a low basal release probability in the bouton [Moore et al., 2003]. Although we did not include adenosine directly into our model, its effect is accounted for by the fact that the number of VDCCs is an open parameter in our study. Therefore, lower amounts of VDCCs account for the reduction in the influx due to adenosine.

Experimental results by Vyleta et al. [2016] show that three inputs at 20 Hz can rapidly increase the probability of a postsynaptic AP. Another study by [Chamberland et al., 2018] suggests six. According to our modeling study, every incoming AP contributes to a graded rise in the concentration of residual calcium as well as vesicle release by synaptotagmins. Although the presynaptic response is rapid, it is gradual, unlike a binary switch transitioning from off to on. For this reason, we suspect that the sudden increase in AP probability is due to factors beyond the presynaptic terminal. Besides directly exciting CA3 pyramidal neurons, mossy fiber suppresses them via feedforward inhibition. Inhibitory interneurons have high fidelity synapses and therefore, CA3 neurons are depressed in basal activity levels. Only when the CA3 excitation rises enough (due to increase in neurotransmitter release from MFs) to supersede suppression, AP probability shows a sudden rise.

A unique aspect of this synapse is the NMDA-independent LTP that is believed to be expressed presynaptically [Nicoll and Schmitz, 2005; Zalutsky and Nicoll, 1990], but see Kwon and Castillo [2008]. We have not explored LTP mechanism at this synapse. A logical extension of the present work would be to extend the model to explore LTP induction mechanisms and its implication at this important junction in the hippocampus.

CHAPTER 4

MODEL CONSTRUCTION

4.1 CA3 bouton

Canonical CA3 pyramidal neuron bouton is modeled as a cuboid of size $0.5\mu m \times 0.5\mu m \times 4.0\mu m$. This is the average size of the neurons seen in the reconstructed CA1 neuropil. Endoplasmic reticulum has a size of $0.1\mu m \times 0.1\mu m \times 3.8\mu m$, placed 50 nm from the active zone (see Figure 4.2). Along with canonical bouton, simulations were also performed in a realistic bouton reconstructed from EM images [Harris et al., 2015a]. The model was built using MCell, described in the "Tools used in the study" section.

The CA3 bouton contains a single active zone at the center of a long face. Unless mentioned, the active zone contains seven vesicles in the RRP. Each vesicle has associated calcium sensors: synaptotagmin 1 and 7. Voltage-dependent calcium channels are placed on the plasma membrane in a small cluster of size 100 nm across at a center-to-center distance of about 350 nm from the active zone [Nadkarni et al., 2010]. This distance and cluster size is explicitly mentioned wherever they differ from above mentioned values. The number of calcium channels in the cluster has been varied from 40 to 160 depending on the simulation and is mentioned wherever needed.

Surface of the endoplasmic reticulum uniformly hosts SERCA pumps with a density of 5500 μm^{-2}. These pumps are modeled to implicitly incorporate calcium leakage

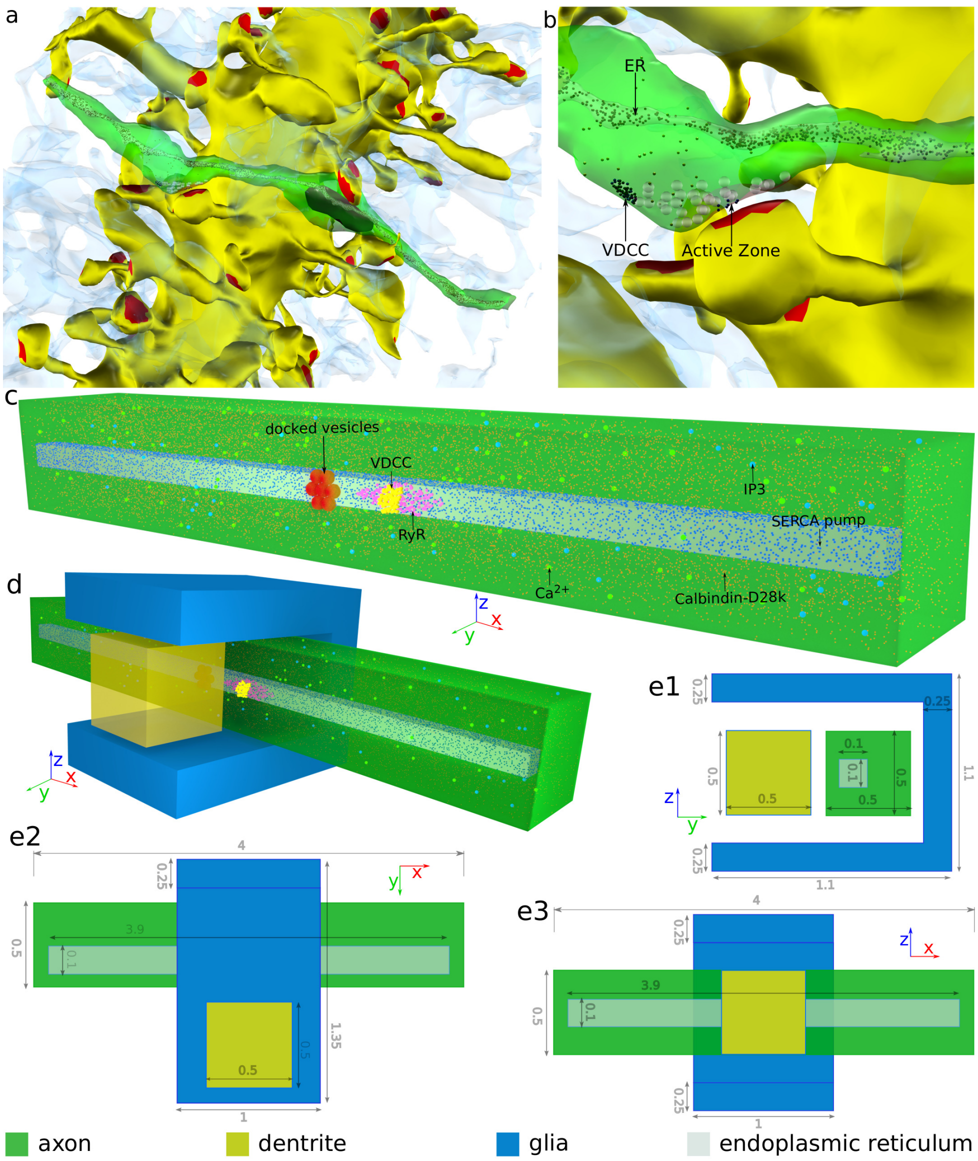
a
b
ER
VDCC
Active Zone
c
docked vesicles
VDCC
IP3
RyR
SERCA pump
Ca2+
Calbindin-D28k
d
z
x
y
e1
0.25
0.25
0.1
0.1
0.5
0.5
0.5
0.5
1.1
1.1
0.25
z
y
e2
4
0.25
y
x
3.9
0.5
0.1
1.35
0.5
0.5
1
e3
4
0.25
z
x
3.9
0.5
0.1
0.25
1
🟩 axon
🟩 dentrite
🟦 glia
⬜ endoplasmic reticulum

FIGURE 4.1. **Model of the CA3 neuron bouton. a.** Reconstruction of CA3–CA1 neuropil in rat hippocampus. The dendrite of a CA1 pyramidal neuron is shown in yellow with red patches, indicating the postsynaptic densities. An axon of CA3 pyramidal neuron is shown in green (other axons in the vicinity have been made transparent for clarity). ER inside the axon is shown in gray. Astrocytes are shown as translucent blue structures. **b.** An en passant synapse formed by a CA3 axon onto a CA1 dendrite. **c.** Presynaptic terminal of the 3D canonical model showing the placement of key molecules. **d.** The complete view of the canonical model showing the relative arrangement of glia, presynaptic and postsynaptic terminals. **e1–3.** Dimensions (in μm) of the model in orthographic projection. ER: endoplasmic reticulum, VDCC: voltage-dependent calcium channel, RyR: ryanodine receptor, IP3: inositol (1,4,5)-trisphosphate.

across the ER membrane. Depending on the simulation, 150 ryanodine receptors and 50 Inositol tris-phosphate receptors are present on the ER surface juxtaposed to the VDCC cluster.

Cytosol contains calbindin-D28k, a fast calcium buffer at a concentration of 45 μM, consistent with experimental observations [Müller et al., 2005]. In addition to calbindin-D28k, PMCA pumps are present on the plasma membrane with a density of 180 μm^{-2}. Together with SERCA pumps, calbindin and PMCA pumps maintain a steady-state concentration of 100 nM calcium ions and 250 μM in ER, assuming 2 mM extracellular calcium concentration.

Kinetic details of each of the components are mentioned in the section "Molecular components". The complete model code can be accessed at `https://github.com/CNLiiserp/CA3bouton`.

4.1.1 Simulations

All simulations had a time-step of 1 sec. In simulations for paired-pulse stimulus, 5000 trials were used to calculate average response for VDCC=40-60, 2000 trials were used for VDCC=70-90 and 1000 trials for VDCC=100-160. Release probability in response to an AP is calculated by counting the number of trials that resulted in vesicular release within 20 ms after initiation of AP, divided by the total number of trials. This is in accordance with the definition of vesicle release probability: probability that at least one vesicle is released. Error in release probability was calculated using 1000 resampling with replacement and then mean and standard error was calculated from the resampled data. Simulations were run for varied times depending on the stimulus protocols used. For paired-pulse protocol, total simulation time was 30 ms + ISI. For a train stimulus of 10 Hz, 20 Hz and 50 Hz, total simulation time was for 1.050 s, 2.050 s and 450 ms, respectively. On average, simulating a single trial of 50 ms requires about 20 minutes.

4.2 Hippocampal mossy fiber

The model for the hippocampal mossy fiber bouton was built in three parts: spatial model of mossy fiber bouton, stochastic point model for vesicle release via synaptotagmins (1 and 7) and point model of CA3 pyramidal neuron and CA3 interneuron to simulate postsynaptic response.

4.2.1 Spatial model of mossy fiber bouton

The model of MF bouton has dimensions $4.1\mu m \times 2.5\mu m \times 0.8\mu m$ (see Figure 4.2). Multiple active zones are placed with an inter-AZ distance of 450 nm at the center of the synaptic surface in a hexagonal grid. Depending on the simulation, the number of active zones vary between 7 and 29. Each active zone has an associated readily releasable pool that varies between 5 and 40, based on mossy fiber EM reconstructions [Rollenhagen et al., 2007].

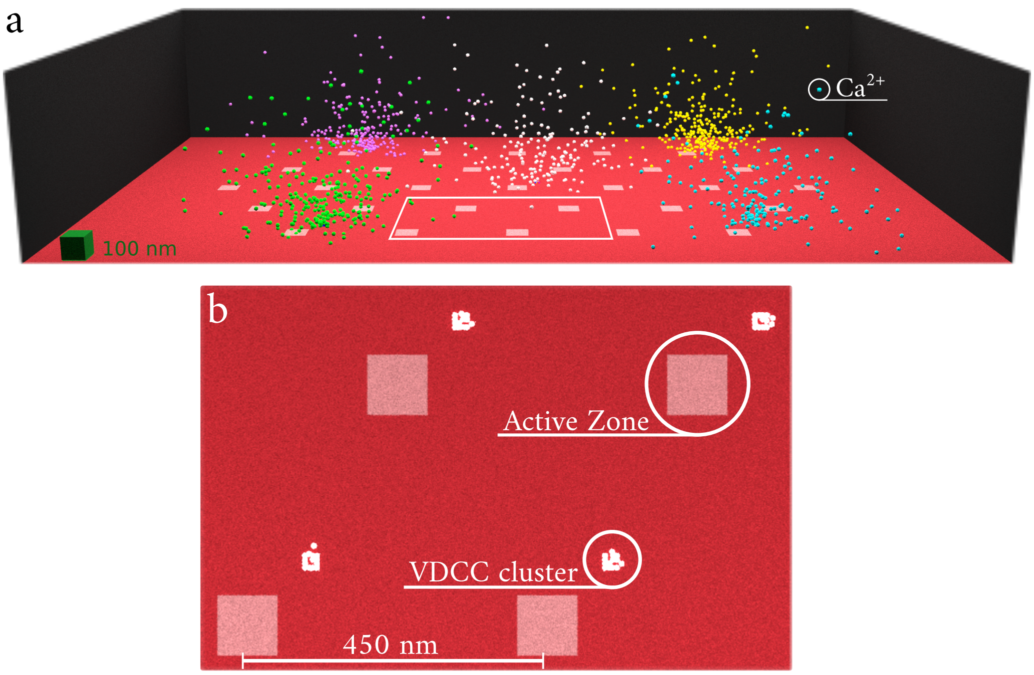

FIGURE 4.2. **Model of the mossy fiber bouton. a.** MF bouton from an oblique perspective. The two front surfaces have been made transparent. The red surface hosts active zones shown as white patches of squares. Calcium influx from 5 representative VDCC clusters is shown in different colours. **b.** The area enclosed in white boundary in **a** is zoomed in and shown here. Scale is represented by the green cube of 100 nm.

Each vesicle has calcium sensors — synaptotagmins (1 and 7), which are modeled in the next part as described below. Bouton is populated with calcium buffers, calbindin-D28k, at a concentration of 40 μM [Müller et al., 2005]. PMCA is present on the plasma membrane with a density of 180 μm^{-2}. Unsaturating buffer is implemented by assuming a constant buffer concentration and multiplying it with buffer rate constants. Voltage-dependent calcium channels are placed on the plasma membrane in small clusters, 20 nm across. Each active zone has an associated VDCC cluster.

Each cluster constitutes up to 14 channels and center-to-center distance between the active zone and its associated VDCC cluster ranges from 60 nm to 220 nm, depending on the simulation. The interplay between PMCA pumps and calcium buffers maintain a steady-state calcium concentration of 100 nm in the cytosol. The model was built using MCell, described in the "Tools used in the study" section.

4.2.2 Stochastic model of vesicle release

The model for calcium sensors (synaptotagmin 1 nad 7) for synchronous and asynchronous neurotransmitter release at MFB has been taken from our previous work [Nadkarni et al., 2010]. It is implemented using STEPS. This model incorporates calcium dependent fast synchronous and slow asynchronous, and calcium independent spontaneous modes of vesicle release (see Figure 4.3g and table Table 4.1). The local calcium concentrations at each active zone were measured from the MCell model These calcium concentrations were then fed to the stochastic model of the calcium sensors (synaptotagmin 1 and 7), and individual releases are recorded.

4.2.3 CA3 phenomenological model

CA3 neurons were based on the observed active and passive electrical properties of the neuron [Kowalski et al., 2016].

$$C_m \frac{dv}{dt} = -g_m(v - V_L) - I_{ampa} - I_{gabaA} - I_{gabaB}$$

$$I_{ampa} = g_{maxampa} \times g_{ampa} dv$$

$$\frac{dg_{ampa}}{dt} = -\frac{g_{ampa}}{tau_{gampa}}$$

$$\frac{dd}{dt} = \frac{1-d}{tau_d}$$

$$I_{gabaA} = g_{gabaA} \times f_{gabaA} \times (v - V_{gabaA})$$

$$\frac{df_{gabaA}}{dt} = A1 \times nt \times (1 - f_{gabaA}) - A2 f_{gabaA}$$

$$I_{gabaB} = \frac{g_{gabaB} G^4}{(G^4 + 100)(v - V_{gabaB})}$$

$$\frac{df_{gabaB}}{dt} = B1 \times nt \times (1 - f_{gabaB}) - B2 \times f_{gabaB}$$

$$\frac{dG}{dt} = K1 \times f_{gabaB} - K2 \times G$$

$V_L = -60mV, V_{AMPA} = 0mV, C_m = 25pF, g_m = 500pS, g_{maxampa} = 1nsiemens,$
$tau_{gampa} = 10ms, tau_d = 50*ms, A1 = 5/(mM-ms), A2 = 0.18/ms, g_{gabaA} = 1nsiemens,$
$V_{gabaA} = -85mV, B1 = 0.09/(mM*ms), B2 = 0.0012/ms, K1 = 0.18/ms, K2 = 0.034/ms,$
$g_{gabaB} = 3nsiemens, V_{gabaB} = -95mV$

AP was recorded at $V_{thr} = -42mV$ and membrane voltage was reset to $V_{reset} = -65mV$ with a refractory period $\tau_{rp} = 5ms$. Input from the presynaptic terminal is fed to the model as synaptic conductance, calculated as $g_{AMPA} = \sum_i K(t - t_i), t_i$ are the vesicle release times. $K(t)$ is a 15 ms biexponential kernel optimized to generate experimentally observed mEPSC. We assumed each active zone has an independent cluster of AMPA receptors.

4.2.4 CA3 inhibitory interneuron model

$$\frac{dv}{dt} = -gm_{in}(v - Vin_{rest}) - I_{ampa})/Cm_{in}$$

$$I_{ampa} = gInmax_{ampa} \times gIn_{ampa} \times v$$

$$\frac{dgIn_{ampa}}{dt} = -\frac{gIn_{ampa}}{tau_{gInampa}}$$

$Cm_{in} = 0.1nF, gm_{in} = 4.0nS, tau_{rpin} = 1ms, Vin_{rest} = -57.0mV,$
$Vin_{thr} = -50.0mV, Vin_{reset} = -60.0mV, gInmax_{ampa} = 3nS, tau_{gInampa} = 5ms$

4.3 Molecular components

4.3.1 Voltage-dependent calcium channels

We have used kinetic models of high-threshold Cav2.1, Cav2.2 and Cav2.3 type voltage-dependent calcium channels in our models. Membrane depolarisation during an action potential activates these channels that mediates neurotransmitter release via large calcium influx. These are based on Cav2.1 (P/Q-type) as characterized by [Bischofberger et al., 2002]. The microscopic rate constants α_i and β_i (i = 1, 2, 3, 4) have exponential dependence on voltage (see Figure 4.3e). The extracellular calcium concentration assumed in our model is 2.0 mM, consistent with the experimental studies [Jonas et al., 1993; Murthy et al., 2001, 1997].

4.3.2 Calcium sensors (synaptotagmin 1 and 7)

Synaptotagmin 1 and 7 are the major calcium sensors for neurotransmitter release at active zones in CA3 and mossy fiber boutons. Their kinetic scheme has been adopted from Nadkarni et al. [2010]. This model incorporates calcium-dependent fast synchronous (synaptotagmin 1) and slow asynchronous (synaptotagmin 7), and calcium independent spontaneous modes of neurotransmitter release (see Figure 4.3g). Synchronous, asynchronous and spontaneous release rates, γ, $a\gamma$ and δ, respectively were obtained using experimental data. Refractory period was implemented with a time constant, ϵ. See table Table 4.1 for the values used in the model.

4.3.3 Ryanodine receptor

The model for ryanodine receptors incorporates its low and high activity states as described by Saftenku et al. [2001] (see Figure 4.3g). $O1_L$, $O2_L$, $O3_L$, $O1_H$, $O2_H$ are the open states of ryanodine receptors in response to calcium binding . See table Table 4.2 for reaction rates.

4.3.4 IP3 receptor

The model for IP3 receptors was implemented using the kinetic study by De Young and Keizer [1992]. The IP3 receptor has three binding sites represented by the subscripts i,j and k in S_{ijk} (see Figure 4.3g). IP3 bound to i-binding site is represented as i=1 and j=1 represents Ca^{2+} bound to activating site j, while k=1 represents Ca^{2+} bound to receptor inhibiting site k. Consequently, S_{110} is the open IP3 receptor state. See table Table 4.2 for reaction rates.

4.3.5 SERCA pumps

The four state model for the SERCA pump described by Higgins et al. [2006] is used. For MCell implementation, each Ca^{2+} binding step was explicitly incorporated, making it a 6-state model (see Figure 4.3c). Rate constants X0Y0, Y0X0, X2Y2 and Y2X2 were modified from the original values for consistent ER calcium-refilling rate constant of ~10s and maintain a steady $[Ca^{2+}]_{ER}$ at ~250 μM [Solovyova et al., 2002; Verkhratsky, 2002]. SERCA surface density of 5500 μm^{-2} was calculated based on [Higgins et al., 2006]. See table Table 4.2 for reaction rates.

4.3.6 Calbindin-D28k

Calbindin-D28k was modeled according to the study by Nägerl et al. [2000]. The model maintains two high affinity and two medium affinity calcium binding sites (see Figure 4.3f). See table Table 4.1 for reaction rates.

4.3.7 Plasma membrane calcium ATPase pump

Kinetic model for the PMCA pump has been incorporated from Brini and Carafoli [2009]; Penheiter et al. [2003]. It implicitly incorporates calcium leak across the plasma membrane (see Figure 4.3d). See table Table 4.1 for reaction rates.

Table 4.1: Reaction rates for the kinetic schemes used in simulations.

PMCA pump	Brini and Carafoli [2009]; Penheiter et al. [2003]
Association rate (kpm1)	$1.5\times10^{8}M^{-1}s^{-1}$
Dissociation rate (kpm2)	$20\ s^{-1}$
Transition rates (kpm3, kpm4)	$100,\ 1.0\times10^{5}s^{-1}$
Leakrate (kpmleak)	$12.5\ s^{-1}$
VDCC	
$a_i(V) = a_{i0}exp(V/V_i)$	
and $b_i(V) = b_{i0}exp(-V/Vi)$	Bischofberger et al. [2002]
a10, a20, a30, a40	4.04, 6.70, 4.39, 17.33 ms^{-1}
b10, b20, b30, b40	2.88, 6.30, 8.16, 1.84 ms^{-1}
V1, V2, V3, V4	49.14, 42.08, 55.31, 26.55 mV
KFlux_VDCC(V)	$\frac{AVN_A[B-e^{-V/C}]}{2F[1-e^{V/C}]}$
	$A = 3.72pS, B = 0.3933, C = 80.36mV$
Calbindin-D28k	Nägerl et al. [2000]
kh+, km+	$0.55\times10^{7},\ 4.35\times10^{7}M^{-1}s^{-1}$
kh-, km-	$2.6,\ 35.8\ s^{-1}$
Calcium sensor model	Nadkarni et al. [2010]
Association rates (ks+, ka+)	$0.612\times10^{8},\ 3.82\times10^{6}M^{-1}s^{-1}$
Dissociation rates (ks-, ka-)	$2.32\times10^{3}, 13s^{-1}$
a, b	0.025, 0.25
γ, δ, ϵ	$2\times10^{3}s^{-1},\ 0.417\times10^{-3}s^{-1}$, 6.34 ms

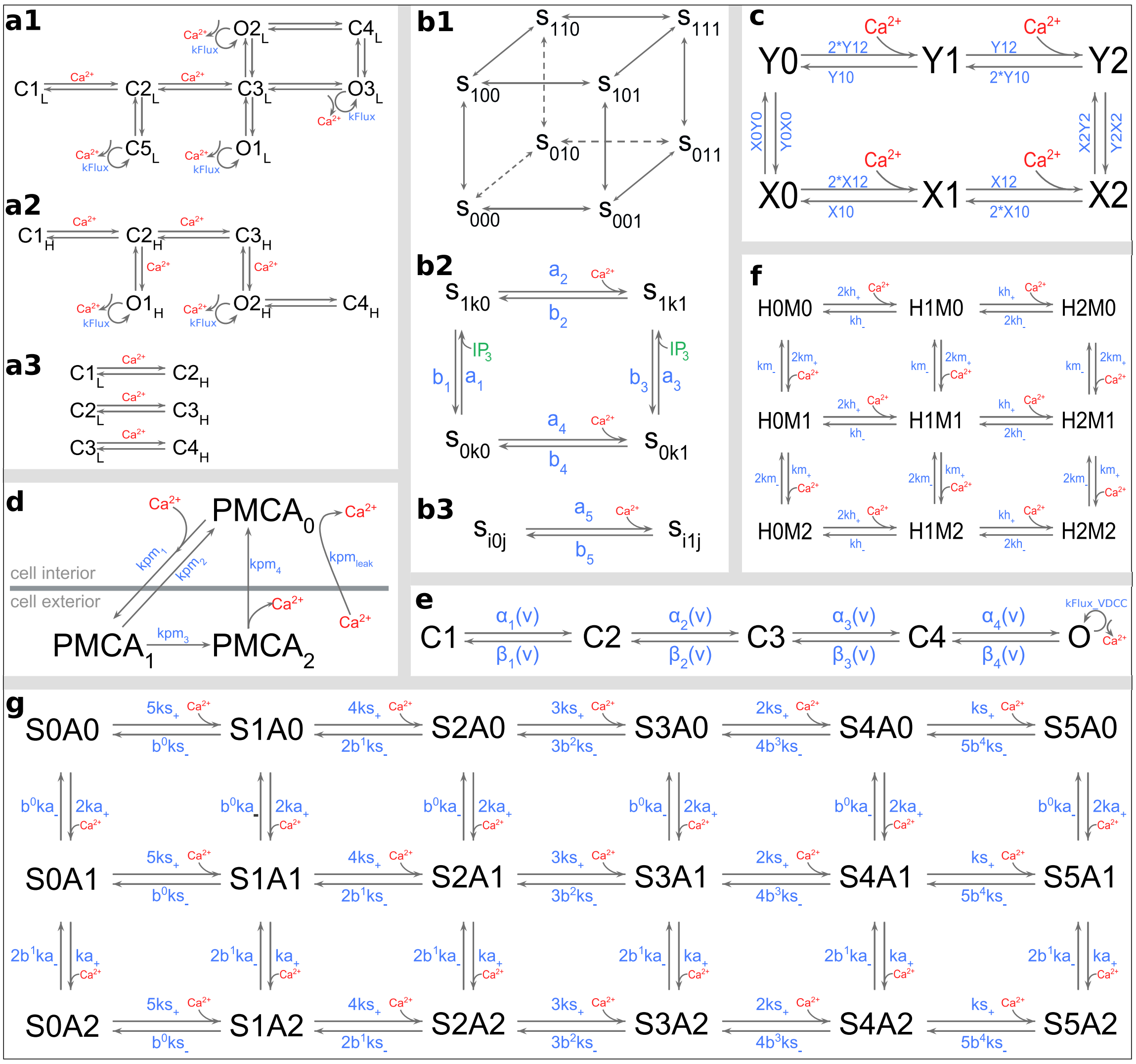
a1
C1L
C2L
C3L
O2L
C4L
O3L
C5L
O1L
Ca2+
kFlux
a2
C1H
C2H
C3H
O1H
O2H
C4H
a3
C1L C2H
C2L C3H
C3L C4H
b1
S110
S111
S100
S101
S010
S011
S000
S001
b2
S1k0
S1k1
S0k0
S0k1
a2
b2
b1
a1
b3
a3
a4
b4
IP3
b3
Si0j
Si1j
a5
b5
c
Y0
Y1
Y2
X0
X1
X2
2*Y12
Y10
Y12
2*Y10
2*X12
X10
X12
2*X10
X0Y0
Y0X0
X2Y2
Y2X2
d
PMCA0
PMCA1
PMCA2
kpm1
kpm2
kpm3
kpm4
kpmleak
cell interior
cell exterior
e
C1
C2
C3
C4
O
α1(v)
β1(v)
α2(v)
β2(v)
α3(v)
β3(v)
α4(v)
β4(v)
kFlux_VDCC
f
H0M0
H1M0
H2M0
H0M1
H1M1
H2M1
H0M2
H1M2
H2M2
2kh+
kh-
kh+
2kh-
km-
2km+
2km-
km+
g
S0A0
S1A0
S2A0
S3A0
S4A0
S5A0
S0A1
S1A1
S2A1
S3A1
S4A1
S5A1
S0A2
S1A2
S2A2
S3A2
S4A2
S5A2
5ks+
4ks+
3ks+
2ks+
ks+
b0ks-
2b1ks-
3b2ks-
4b3ks-
5b4ks-
b0ka-
2ka+
2b1ka-
ka+

Figure 4.3: **Kinetic schemes. a1-3.** RyR-L mode, RyR-H mode and transition between 'L' and 'H' modes of RyR. **b1-3.** IP3 receptor. Lines connecting a state of IP3 receptor in panel b1 represents the possible states it can transition to. Corresponding transition rates are mentioned in panel b2 and b3, where i, j and k can take values 0 and 1. S_{110} is the open state. **c.** SERCA pumps. Binding sites described by 'X' is on the cytosolic side while 'Y' is on the ER side. Calcium is transported across the membrane via transition between 'X2' and 'Y2'. **d.** PMCA pump. The scheme also incorporates the calcium leakage across the plasma membrane. **e.** High-threshold voltage-dependent calcium channel. 'O' is the open state that conducts calcium. **f.** Calcium buffer, calbindin-D28k. It is modelled to have two calcium binding units, termed as, high 'H' and medium 'M', each of which binds two calcium ions. **g.** Calcium sensor for vesicle release with two subunits, 'S' for fast synchronous release with 5 calcium binding sites and 'A' for slow asynchronous release with two calcium binding sites. Release can take place via either the synchronous or the asynchronous unit. Reaction rates are described Table 4.1 and Table 4.2.

Table 4.2: Reaction rates for the kinetic schemes of ER components.

Ryanodine receptor	Saftenku et al. [2001]
$\text{C1}_L - C2_L$, $C2_L - C1_L$	$1.24\times10^6 M^{-1}s^{-1}$, $13.6\ s^{-1}$
$\text{C2}_L - C3_L$, $C3_L - C2_L$	$2.98\times10^7 M^{-1}s^{-1}$, $3867\ s^{-1}$
$\text{C2}_L - C5_L$, $C5_L - C2_L$	1.81, $3.63\ s^{-1}$
$\text{C3}_L - O1_L$, $O1_L - C3_L$	731.2, $4183\ s^{-1}$
$\text{C3}_L - O2_L$, $O2_L - C3_L$	24.5, $156.5\ s^{-1}$
$\text{C3}_L - O3_L$, $O3_L - C3_L$	8.5, $111.7\ s^{-1}$
$\text{C4}_L - O2_L$, $O2_L - C4_L$	415.3, $1995\ s^{-1}$
$\text{C4}_L - O3_L$, $O3_L - C4_L$	43.3, $253.3\ s^{-1}$
$\text{C1}_H - C2_H$, $C2_H - C1_H$	$3.26\times10^6 M^{-1}s^{-1}$, $116\ s^{-1}$
$\text{C2}_H - C3_H$, $C3_H - C2_H$	$6.6\times10^5 M^{-1}s^{-1}$, $163\ s^{-1}$
$\text{C2}_H - O1_H$, $O1_H - C2_H$	$7.86\times10^6 M^{-1}s^{-1}$, $1480\ s^{-1}$
$\text{C3}_H - O2_H$, $O2_H - C3_H$	$7.77\times10^6 M^{-1}s^{-1}$, $330\ s^{-1}$
$\text{C4}_H - O2_H$, $O2_H - C4_H$	2390, $298\ s^{-1}$
$\text{C1}_L - C2_H$, $C2_H - C1_L$	6.6×10^2, $0.083\ s^{-1}$
$\text{C2}_L - C3_H$, $C3_H - C2_L$	6.6×10^2, $0.083\ s^{-1}$
$\text{C3}_L - C4_H$, $C4_H - C3_L$	6.6×10^2, $0.083\ s^{-1}$
kFlux	$1.09\times10^9 M^{-1}s^{-1}$
IP3 receptor	De Young and Keizer [1992]
a1, a2, a3, a4, a5	4×10^8, 2×10^5, 4×10^8, 2×10^5, $2\times10^7\ \mu M^{-1}s^{-1}$
b1, b2, b3, b4, b5	52, 0.21, 377.2, 0.029, $1.64\ s^{-1}$
kFlux_IP3R	$1.19\times10^8 M^{-1}s^{-1}$
SERCA pump	Higgins et al. [2006]
X0Y0, Y0X0	0.022, $7.2\ s^{-1}$
X2Y2, Y2X2	10.8, $75.08\ s^{-1}$
X10, Y10	83.67, $30.012\ s^{-1}$
X12, Y12	1×10^8, $1\times10^5\ M^{-1}s^{-1}$

4.4 Tools used in the study

4.4.1 MCell

MCell (Monte Carlo cell, version 3.2.1, `https://mcell.org`) is a program written in C++ that uses spatially realistic 3D cellular models and specialized Monte Carlo algorithms to simulate the movements and reactions of molecules within and between cells. It tracks the diffusion of each chemical species present either on a surface or in a confined volume and carries out user-specified molecular reactions in the system [Kerr et al., 2008; Stiles et al., 2001, 1996].

4.4.2 STEPS

STEPS (version 3.5.0, short for STochastic Engine for Pathway Simulation, `http://steps.sourceforge.net/STEPS/default.php`) is a stochastic reaction-diffusion simulator developed with an emphasis on simulating biochemical signaling pathways accurately and efficiently. It supports use of complex boundaries represented as 3D tetrahedral meshes. Interface is through Python programming language that facilitates model construction and simulation control. The backend simulation implements the composition and rejection method, a variation of the Gillespie SSA [Hepburn et al., 2012].

4.4.3 Brian

Brian (version 2.3.0.2, `https://briansimulator.org/`) is a simulator for spiking neural networks, written in the Python programming language [Stimberg et al., 2019]. It is designed with the idea to keep it "easy to learn and use, highly flexible and easily extensible."

4.4.4 Python, gnuplot, GNU parallel

Python (version 3.6) is a dynamic programming language. Gnuplot is a freely distributed, portable command-line driven graphing utility. It was originally created to allow scientists and students to visualize mathematical functions and data interactively, but has grown to support non-interactive scripting. GNU Parallel is a UNIX shell tool for running jobs in parallel making efficient use of multiple cores available in a system.

4.5 Computing facility

All simulations were performed on a high-performance computing cluster (HP PROLIANT SL230s Gen8 as compute nodes, each with 2 CPUs containing 10 cores each. CPU: Intel(R) Xeon(R) CPU E5-2860 v2 α 2.80GHz) with 1464 processing units. This supercomputing facility is housed in IISER Pune.

CHAPTER 5

DISCUSSION

This thesis arises out of a simple idea. The brain is a complicated structure riddled with intricate networks of interaction that can be investigated at various levels. Different regions of the brain interact with each other in myriad ways. So do individual neurons. Even within a neuron, many chemicals dance in a complex, dynamic choreography.

Understanding the brain's working is indeed an arduous task, and for better or worse, requires investigation at all levels. We chose to start at the lowest level: subcellular molecular dynamics within a neuron. We explored the form and function of two hippocampal synapses that may prove significant in furthering our understanding of neurons, both, in health and disease.

5.1 Summary

Endoplasmic reticulum (ER) processes, surprisingly, innervate even small boutons of Schaffer collateral synapses. SERCA pumps, present on the ER, refill it with calcium. In addition to this ascribed function, we found that SERCA kinetics also allow it to quickly buffer calcium ions which is essential for short-term plasticity. They lower the calcium concentration at the active zone, thereby maintaining a low release probability. At the same time, they raise residual calcium by releasing a part of their bound calcium after the signal has subsided.

Mossy fibers, on the other hand, are a whole different form of creature. They host a bunch of active zones, which are uncoupled and maintain a low level of excitation during low levels of activity. This helps in filtering out intrinsic, stochastic low frequency noise. However, when a high frequency signal stimulates the bouton, the active zones quickly shift gear and collaborate via calcium signals to turn the synapse into a high fidelity transmission line. Moreover, they do so in a manner that enables temporal separation, by decorrelating similar activity patterns.

My approach has been to build a prototype of the CA3 neuron terminal and mossy fiber bouton to carry out in-silico experiments and make quantitative (not merely qualitative) predictions. This is especially valuable since direct measurements of crucial molecular signals, such as local calcium at the active zone in these important synapses is difficult. The model accounts for the observed rise- and decay time of vesicle release; calcium affinities of the calcium sensors for vesicle release; effective calcium diffusion; the time-scale of calcium transient decay; the rate at which the ER refills; and the steady-state value of ER calcium concentration [Nadkarni et al., 2010; Solovyova et al., 2002; Verkhratsky, 2002]. PPR is a high-dimensional measure of plasticity and is determined by several interdependent synaptic components (residual calcium, RRP size, buffering capacity, calcium sensors among others). It is reasonable to assume that a biophysical model that quantitatively agrees with measurement of PPR for a wide range of protocols is physiologically realistic. Several studies have shown that a biological system can achieve a specific goal using multiple sets of parameters [Marder and Taylor, 2011; Mukunda and Narayanan, 2017]. Given the profuse degeneracy seen in biological systems, our aim was not to arrive at an idealized set of parameters. By demonstrating that our model makes a number of non-trivial ‘post-dictions’ [Abbott, 2008], we argue that our main prediction on the role played by ER in Schaffer collaterals, and complex interaction of active zones, buffers and synaptotagmins in MFs in short-term plasticity is also accurate.

As evidenced in the previous chapters, synaptic design critically determines short-term plasticity, within hippocampal neurons. Therefore, needless to say, STP can be used to study synaptic design of neurons. These studies provide insights into new mechanisms that may be employed in a neuron for STP and the ideas can be repurposed to investigate the inner workings of other neurons.

5.2 Computational approaches to problems in neuroscience

There are multiple ideologies behind computational approaches. Which method to use depends on the specific details of the problem at hand. Take an example of trying to understand the dynamics of network computations performed by various neurons in a region of the brain. Phenomenological models of individual neurons can replicate the neuron's activity. Intracellular biophysical dynamics that give these neurons their properties, can often be safely ignored in the model. Abstract parameters of the models can be tweaked to match the neuron's activity.

However, building a good phenomenological model requires in-depth knowledge of the intracellular mechanisms. Within a neuron various chemical cascades interact with each other. These interactions can be tricky to probe in an experimental setup, especially in small spaces. In such a situation a different approach can be taken. Dynamics or kinetics of individual participating components are incorporated in the model. Such a model can, then, simulate the complex interactions between the various components. Instead of building phenomenological models with precisely tuned parameters, we model the biophysical properties of the components which are available in experimental literature. No tweaking is required. Once the model is built, in-silico experiments can be performed. Unlike experiments, each and every step can be observed to trace out the mechanism. This is exactly the kind of approach we have employed in our study.

Building these models is a crucial aspect of my research, akin to setting up experiments. Every aspect needs to work properly, else results may not be faithful. As the saying goes, "all models are wrong, but some are useful." And, building a useful model is quite a challenge. Although this aphorism was first said in the context of statistical models, it applies to all scientific models. It does not seem helpful just to say that all models are wrong. The very word model implies simplification and idealization. The idea that complex physical, biological or sociological systems can be exactly described by a few formulae is patently absurd. The construction of idealized representations that capture important stable aspects of such systems is, however, a vital part of general scientific analysis and statistical models, especially substantive ones, do not seem essentially different from other kinds of model. A model is a simplification or approximation of reality and hence will not reflect all of reality. The aim is not to build an exact replica but to represent the system in minimal detail that can be used to provide insights into the working of the system. The key idea is to collate and build upon multiple experimental studies to probe questions that are beyond the limits of experiments.

5.3 Future prospects of the study

Synaptic transmission is played out by three major components: pre and postsynaptic terminal, and the encompassing astrocytes. One of the logical next steps would be to incorporate postsynaptic and astrocytic dynamics to have a holistic understanding of not only individual components, but of their interactions also.

Studies probing the calcium hypothesis of Alzheimer's disease have indicated many possible pathways of calcium dysregulation. A comprehensive computational model has the potential to disambiguate between various hypotheses and provide predictions for further experimentations. Such complex diseases as Alzheimers', I believe, will require both experiments and theory to continuously work with each other.

Our CA3-CA1 model does not describe the contribution of presynaptic ER to long-term potentiation (LTP) and the long-term costs of loss of STP as seen in AD, as these are beyond the scope of this present study. We do note that low Pr and high PPR in CA3 boutons correspond to higher magnitude of LTP [Letellier et al., 2016] and potentially describes a relationship between STP and LTP. We hope to study these issues in future extensions of the current work.

PUBLICATIONS

Singh N, Bartol T, Levine H, Sejnowski T, Nadkarni S. Presynaptic endoplasmic reticulum regulates short-term plasticity in hippocampal synapses. Communications biology. 2021; 4(1), 1-13. doi: `https://doi.org/10.1038/s42003-021-01761-7`.

BIBLIOGRAPHY

Abbott LF. Theoretical neuroscience rising. Neuron. 2008; 60(3):489–495. doi: https://doi.org/10.1016/j.neuron.2008.10.019.

Abbott LF, Nelson SB. Synaptic plasticity: taming the beast. Nature neuroscience. 2000; 3(11):1178–1183.

Abbott LF, Varela J, Sen K, Nelson S. Synaptic depression and cortical gain control. Science. 1997; 275(5297):221–224. doi: https://doi.org/10.1126/science.275.5297.221.

Abbott L, Regehr WG. Synaptic computation. Nature. 2004; 431(7010):796. doi: https://doi.org/10.1038/nature03010.

Abraham WC, Jones OD, Glanzman DL. Is plasticity of synapses the mechanism of long-term memory storage? NPJ science of learning. 2019; 4(1):1–10. doi: https://doi.org/10.1038/s41539-019-0048-y.

Acsady L, Kamondi A, Sık A, Freund T, Buzsáki G. GABAergic cells are the major postsynaptic targets of mossy fibers in the rat hippocampus. Journal of neuroscience. 1998; 18(9):3386–3403. doi: https://doi.org/10.1523/jneurosci.18-09-03386.1998.

Ahmed OJ, Mehta MR. The hippocampal rate code: anatomy, physiology and theory. Trends in neurosciences. 2009; 32(6):329–338. doi: https://doi.org/10.1016/j.tins.2009.01.009.

Amaral DG, Ishizuka N, Claiborne B. Chapter Neurons, numbers and the hippocampal network. Progress in brain research. 1990; 83:1–11. doi: https://doi.org/10.1016/S0079-6123(08)61237-6.

Association A, et al. 2018 Alzheimer's disease facts and figures. Alzheimer's & Dementia. 2018; 14(3):367–429. doi: https://doi.org/10.1016/j.jalz.2018.02.001.

Baba-Aïissa F, Raeymaekers L, Wuytack F, De Greef C, Missiaen L, Casteels R. Distribution of the organellar Ca2+ transport ATPase SERCA2 isoforms in the cat brain. Brain research. 1996; 743(1-2):141–153. doi: https://doi.org/10.1016/s0006-8993(96)01037-2.

Baba-Aïssa F, Raeymaekers L, Wuytack F, Callewaert G, Dode L, Missiaen L, Casteels R. Purkinje neurons express the SERCA3 isoform of the organellar type Ca2+-transport ATPase. Molecular brain research. 1996; 41(1-2):169–174. doi: https://doi.org/10.1016/0169-328x(96)00088-5.

Bacaj T, Wu D, Yang X, Morishita W, Zhou P, Xu W, Malenka RC, Südhof TC. Synaptotagmin-1 and synaptotagmin-7 trigger synchronous and asynchronous phases of neurotransmitter release. Neuron. 2013; 80(4):947–959. doi: https://doi.org/10.1016/j.neuron.2013.10.026.

Barria A, Muller D, Derkach V, Griffith LC, Soderling TR. Regulatory phosphorylation of AMPA-type glutamate receptors by CaM-KII during long-term potentiation. Science. 1997; 276(5321):2042–2045. doi: https://doi.org/10.1126/science.276.5321.2042.

Berridge MJ. Calcium hypothesis of Alzheimer's disease. Pflügers Archiv-European Journal of Physiology. 2010; 459(3):441–449. doi: https://doi.org/10.1007/s00424-009-0736-1.

Bezprozvanny I, Mattson MP. Neuronal calcium mishandling and the pathogenesis of Alzheimer's disease. Trends in neurosciences. 2008; 31(9):454–463. doi: https://doi.org/10.1016/j.tins.2008.06.005.

Bhalla US. Synaptic input sequence discrimination on behavioral timescales mediated by reaction-diffusion chemistry in dendrites. Elife. 2017; 6:e25827. doi: https://doi.org/10.7554/eLife.25827.

Bir SC, Ambekar S, Kukreja S, Nanda A. Julius Caesar Arantius (Giulio Cesare Aranzi, 1530–1589) and the hippocampus of the human brain: history behind the discovery. Journal of neurosurgery. 2015; 122(4):971–975. doi: https://doi.org/10.3171/2014.11.JNS132402.

Bird CM, Burgess N. The hippocampus and memory: insights from spatial processing. Nature Reviews Neuroscience. 2008; 9(3):182–194. doi: https://doi.org/10.1038/nrn2335.

Bischofberger J, Geiger JR, Jonas P. Timing and efficacy of Ca2+ channel activation in hippocampal mossy fiber boutons. Journal of Neuroscience. 2002; 22(24):10593–10602. doi: https://doi.org/10.1523/jneurosci.22-24-10593.2002.

Blatow M, Caputi A, Burnashev N, Monyer H, Rozov A. Ca2+ buffer saturation underlies paired pulse facilitation in calbindin-D28k-containing terminals. Neuron. 2003; 38(1):79–88.

Bliss TV, Collingridge GL. Expression of NMDA receptor-dependent LTP in the hippocampus: bridging the divide. Molecular brain. 2013; 6(1):1–14. doi: https://doi.org/10.1186/1756-6606-6-5.

Bliss TV, Collingridge GL. A synaptic model of memory: long-term potentiation in the hippocampus. Nature. 1993; 361(6407):31–39. doi: https://doi.org/10.1038/361031a0.

Bouchard R, Pattarini R, Geiger JD. Presence and functional significance of presynaptic ryanodine receptors. Progress in neurobiology. 2003; 69(6):391–418. doi: https://doi.org/10.1016/s0301-0082(03)00053-4.

Bourne JN, Harris KM. Balancing structure and function at hippocampal dendritic spines. Annu Rev Neurosci. 2008; 31:47–67. doi: https://doi.org/10.1146/annurev.neuro.31.060407.125646.

Brini M, Carafoli E. Calcium pumps in health and disease. Physiological reviews. 2009; 89(4):1341–1378. doi: https://doi.org/10.1152/physrev.00032.2008.

Burgess N, Maguire EA, O'Keefe J. The Human Hippocampus and Spatial and Episodic Memory. Neuron. 2002; 35(4):625–641. doi: https://doi.org/10.1016/S0896-6273(02)00830-9.

Carter AG, Vogt KE, Foster KA, Regehr WG. Assessing the role of calcium-induced calcium release in short-term presynaptic plasticity at excitatory central synapses. Journal of Neuroscience. 2002; 22(1):21–28. doi: https://doi.org/10.1523/jneurosci.22-01-00021.2002.

Chamberland S, Evstratova A, Tóth K. Interplay between synchronization of multivesicular release and recruitment of additional release sites support short-term facilitation at hippocampal mossy fiber to CA3 pyramidal cells synapses. Journal of Neuroscience. 2014; 34(33):11032–11047. doi: https://doi.org/10.1523/jneurosci.0847-14.2014.

Chamberland S, Evstratova A, Tóth K. Short-term facilitation at a detonator synapse requires the distinct contribution of multiple types of voltage-gated calcium channels. Journal of Neuroscience. 2017; 37(19):4913–4927. doi: https://doi.org/10.1523/JNEUROSCI.0159-17.2017.

Chamberland S, Timofeeva Y, Evstratova A, Volynski K, Tóth K. Action potential counting at giant mossy fiber terminals gates information transfer in the hippocampus. Proceedings of the National Academy of Sciences. 2018; 115(28):7434–7439. doi: https://doi.org/10.1073/pnas.1720659115.

Chan SL, Mayne M, Holden CP, Geiger JD, Mattson MP. Presenilin-1 mutations increase levels of ryanodine receptors and calcium release in PC12 cells and cortical neurons. Journal of Biological Chemistry. 2000; 275(24):18195–18200. doi: https://doi.org/10.1074/jbc.M000040200.

Chater TE, Goda Y. The role of AMPA receptors in postsynaptic mechanisms of synaptic plasticity. Frontiers in cellular neuroscience. 2014; 8:401. doi: https://doi.org/10.3389/fncel.2014.00401.

Chawla M, Guzowski J, Ramirez-Amaya V, Lipa P, Hoffman K, Marriott L, Worley P, McNaughton B, Barnes CA. Sparse, environmentally selective expression of Arc RNA in the upper blade of the rodent fascia dentata by brief spatial experience. Hippocampus. 2005; 15(5):579–586. doi: https://doi.org/10.1002/hipo.20091.

Citri A, Malenka RC. Synaptic plasticity: multiple forms, functions, and mechanisms. Neuropsychopharmacology. 2008; 33(1):18–41. doi: https://doi.org/10.1038/sj.npp.1301559.

Cook DL, Schwindt PC, Grande LA, Spain WJ. Synaptic depression in the localization of sound. Nature. 2003; 421(6918):66. doi: https://doi.org/10.1038/nature01248.

Covington NV, Brown-Schmidt S, Duff MC. The Necessity of the Hippocampus for Statistical Learning. Journal of Cognitive Neuroscience. 2018 05; 30(5):680–697. doi: https://doi.org/10.1162/jocn_a_01228.

De Young GW, Keizer J. A single-pool inositol 1, 4, 5-trisphosphate-receptor-based model for agonist-stimulated oscillations in Ca2+ concentration. Proceedings of the National Academy of Sciences. 1992; 89(20):9895–9899. doi: https://doi.org/10.1073/pnas.89.20.9895.

Deng PY, Klyachko VA. The diverse functions of short-term plasticity components in synaptic computations. Communicative & integrative biology. 2011; 4(5):543–548.

Dimsdale-Zucker HR, Ritchey M, Ekstrom AD, Yonelinas AP, Ranganath C. CA1 and CA3 differentially support spontaneous retrieval of episodic contexts within human hippocampal subfields. Nature communications. 2018; 9(1):1–8. doi: https://doi.org/10.1038/s41467-017-02752-1.

Dobrunz LE. Release probability is regulated by the size of the readily releasable vesicle pool at excitatory synapses in hippocampus. International journal of developmental neuroscience. 2002; 20(3-5):225–236. doi: https://doi.org/10.1016/s0736-5748(02)00015-1.

Dobrunz LE, Huang EP, Stevens CF. Very short-term plasticity in hippocampal synapses. Proceedings of the National Academy of Sciences. 1997; 94(26):14843–14847. doi: https://doi.org/10.1073/pnas.94.26.14843.

Dobrunz LE, Stevens CF. Heterogeneity of release probability, facilitation, and depletion at central synapses. Neuron. 1997; 18(6):995–1008. doi: https://doi.org/10.1016/s0896-6273(00)80338-4.

Eichenbaum H. Prefrontal–hippocampal interactions in episodic memory. Nature Reviews Neuroscience. 2017; 18(9):547. doi: https://doi.org/10.1038/nrn.2017.74.

Escobar ML, Derrick B. Long-term potentiation and depression as putative mechanisms for memory formation. Neural Plasticity and Memory: From Genes to Brain Imaging. 2007; p. 15–47.

Fortune ES, Rose GJ. Short-term synaptic plasticity contributes to the temporal filtering of electrosensory information. Journal of Neuroscience. 2000; 20(18):7122–7130. doi: https://doi.org/10.1523/JNEUROSCI.20-18-07122.2000.

Franks KM, Sejnowski TJ. Complexity of calcium signaling in synaptic spines. Bioessays. 2002; 24(12):1130–1144.

Ge Y, Dong Z, Bagot RC, Howland JG, Phillips AG, Wong TP, Wang YT. Hippocampal long-term depression is required for the consolidation of spatial memory. Proceedings of the National Academy of Sciences. 2010; 107(38):16697–16702. doi: https://doi.org/10.1073/pnas.1008200107.

Geiger JR, Jonas P. Dynamic control of presynaptic Ca2+ inflow by fast-inactivating K+ channels in hippocampal mossy fiber boutons. Neuron. 2000; 28(3):927–939. doi: https://doi.org/10.1016/S0896-6273(00)00164-1.

Goldman MS, Maldonado P, Abbott L. Redundancy reduction and sustained firing with stochastic depressing synapses. Journal of Neuroscience. 2002; 22(2):584–591.

Hanse E, Gustafsson B. Paired-pulse plasticity at the single release site level: an experimental and computational study. Journal of Neuroscience. 2001; 21(21):8362–8369. doi: https://doi.org/10.1523/JNEUROSCI.21-21-08362.2001.

Hanse E, Gustafsson B. Release dependence to a paired stimulus at a synaptic release site with a small variable pool of immediately releasable vesicles. Journal of Neuroscience. 2002; 22(11):4381–4387.

Harris KD, Mrsic-Flogel TD. Cortical connectivity and sensory coding. Nature. 2013; 503(7474):51–58. doi: https://doi.org/10.1038/nature12654.

Harris KM, Spacek J, Bell ME, Parker PH, Lindsey LF, Baden AD, Vogelstein JT, Burns R. Open Connectome Project; 2015, doi: http://dx.doi.org/10.7281/T11Z429Q.

Harris KM, Spacek J, Bell ME, Parker PH, Lindsey LF, Baden AD, Vogelstein JT, Burns R. A resource from 3D electron microscopy of hippocampal neuropil for user training and tool development. Scientific data. 2015; 2:150046. doi: https://doi.org/10.1038/sdata.2015.46.

Hartter D, Burton P, Laveri L. Distribution and calcium-sequestering ability of smooth endoplasmic reticulum in olfactory axon terminals of frog brain. Neuroscience. 1987; 23(1):371–386. doi: https://doi.org/10.1016/0306-4522(87)90297-1.

Hennig MH. Theoretical models of synaptic short term plasticity. Frontiers in computational neuroscience. 2013; 7:45. doi: https://doi.org/10.3389/fncom.2013.00045.

Henze DA, Wittner L, Buzsáki G. Single granule cells reliably discharge targets in the hippocampal CA3 network in vivo. Nature neuroscience. 2002; 5(8):790–795. doi: https://doi.org/10.1038/nn887.

Hepburn I, Chen W, Wils S, De Schutter E. STEPS: efficient simulation of stochastic reaction–diffusion models in realistic morphologies. BMC systems biology. 2012; 6(1):1–19. doi: https://doi.org/10.1186/1752-0509-6-36.

Higgins ER, Cannell MB, Sneyd J. A buffering SERCA pump in models of calcium dynamics. Biophysical journal. 2006; 91(1):151–163. doi: https://doi.org/10.1529/biophysj.105.075747.

Jackman SL, Turecek J, Belinsky JE, Regehr WG. The calcium sensor synaptotagmin 7 is required for synaptic facilitation. Nature. 2016; 529(7584):88–91. doi: https://doi.org/10.1038/nature16507.

Jensen TP, Zheng K, Cole N, Marvin JS, Looger LL, Rusakov DA. Multiplex imaging relates quantal glutamate release to presynaptic Ca 2+ homeostasis at multiple synapses in situ. Nature communications. 2019; 10(1):1–14. doi: https://doi.org/10.1038/s41467-019-09216-8.

Jonas P, Major G, Sakmann B. Quantal components of unitary EPSCs at the mossy fibre synapse on CA3 pyramidal cells of rat hippocampus. The Journal of physiology. 1993; 472(1):615–663.

Jurado S, Biou V, Malenka RC. A calcineurin/AKAP complex is required for NMDA receptor–dependent long-term depression. Nature neuroscience. 2010; 13(9):1053–1055. doi: https://doi.org/10.1038/nn.2613.

Kerr RA, Bartol TM, Kaminsky B, Dittrich M, Chang JCJ, Baden SB, Sejnowski TJ, Stiles JR. Fast Monte Carlo simulation methods for biological reaction-diffusion systems in solution and on surfaces. SIAM journal on scientific computing. 2008; 30(6):3126–3149. doi: https://doi.org/10.1137/070692017.

Kesner RP, Kirk RA, Yu Z, Polansky C, Musso ND. Dentate gyrus supports slope recognition memory, shades of grey-context pattern separation and recognition memory, and CA3 supports pattern completion for object memory. Neurobiology of learning and memory. 2016; 129:29–37. doi: https://doi.org/10.1016/j.nlm.2015.08.010.

Khachaturian ZS. Calcium, membranes, aging, and Alzheimer's disease: Introduction and Overview. Annals of the New York Academy of Sciences. 1989; 568(1):1–4. doi: https://doi.org/10.1111/j.1749-6632.1989.tb12485.x.

Kitamura T, Ogawa SK, Roy DS, Okuyama T, Morrissey MD, Smith LM, Redondo RL, Tonegawa S. Engrams and circuits crucial for systems consolidation of a memory. Science. 2017; 356(6333):73–78. doi: https://doi.org/10.1126/science.aam6808.

Klyachko VA, Stevens CF. Excitatory and feed-forward inhibitory hippocampal synapses work synergistically as an adaptive filter of natural spike trains. PLoS biology. 2006; 4(7):e207. doi: https://doi.org/10.1371/journal.pbio.0040207.

Knierim JJ, Neunuebel JP. Tracking the flow of hippocampal computation: Pattern separation, pattern completion, and attractor dynamics. Neurobiology of learning and memory. 2016; 129:38–49. doi: https://doi.org/10.1016/j.nlm.2015.10.008.

Ko H, Hofer SB, Pichler B, Buchanan KA, Sjöström PJ, Mrsic-Flogel TD. Functional specificity of local synaptic connections in neocortical networks. Nature. 2011; 473(7345):87–91. doi: https://doi.org/10.1038/nature09880.

Konorski J. Conditioned reflexes and neuron organization. . 1948; doi: ttps://doi.org/10.1002/1097-4679(195001)6:1<107::AID-JCLP2270060132>3.0.CO;2-0.

Kowalski J, Gan J, Jonas P, Pernía-Andrade AJ. Intrinsic membrane properties determine hippocampal differential firing pattern in vivo in anesthetized rats. Hippocampus. 2016; 26(5):668–682. doi: https://doi.org/10.1002/hipo.22550.

Kwon HB, Castillo PE. Long-term potentiation selectively expressed by NMDA receptors at hippocampal mossy fiber synapses. Neuron. 2008; 57(1):108–120. doi: https://doi.org/10.1016/j.neuron.2007.11.024.

LaFerla FM. Calcium dyshomeostasis and intracellular signalling in Alzheimer's disease. Nature Reviews Neuroscience. 2002; 3(11):862–872. doi: https://doi.org/10.1038/nrn960.

Lawrence JJ, Grinspan ZM, McBain CJ. Quantal transmission at mossy fibre targets in the CA3 region of the rat hippocampus. The Journal of physiology. 2004; 554(1):175–193.

Lee HK, Barbarosie M, Kameyama K, Bear MF, Huganir RL. Regulation of distinct AMPA receptor phosphorylation sites during bidirectional synaptic plasticity. Nature. 2000; 405(6789):955–959. doi: https://doi.org/10.1038/35016089.

Lee I, Jerman TS, Kesner RP. Disruption of delayed memory for a sequence of spatial locations following CA1- or CA3-lesions of the dorsal hippocampus. Neurobiology of Learning and Memory. 2005; 84(2):138–147. doi: https://doi.org/10.1016/j.nlm.2005.06.002.

Lee I, Kesner RP. Encoding versus retrieval of spatial memory: double dissociation between the dentate gyrus and the perforant path inputs into CA3 in the dorsal hippocampus. Hippocampus. 2004; 14(1):66–76. doi: https://doi.org/10.1002/hipo.10167.

Letellier M, Park YK, Chater TE, Chipman PH, Gautam SG, Oshima-Takago T, Goda Y. Astrocytes regulate heterogeneity of presynaptic strengths in hippocampal networks. Proceedings of the National Academy of Sciences. 2016; p. 201523717. doi: https://doi.org/10.1073/pnas.1523717113.

Leutgeb JK, Leutgeb S, Moser MB, Moser EI. Pattern separation in the dentate gyrus and CA3 of the hippocampus. science. 2007; 315(5814):961–966. doi: https://doi.org/10.1126/science.1135801.

Lindsey JD, Ellisman MH. The neuronal endomembrane system. I. Direct links between rough endoplasmic reticulum and the cis element of the Golgi apparatus. Journal of Neuroscience. 1985; 5(12):3111–3123. doi: https://doi.org/10.1523/jneurosci.05-12-03111.1985.

Lu L, Leutgeb JK, Tsao A, Henriksen EJ, Leutgeb S, Barnes CA, Witter MP, Moser MB, Moser EI. Impaired hippocampal rate coding after lesions of the lateral entorhinal cortex. Nature neuroscience. 2013; 16(8):1085. doi: https://doi.org/10.1038/nn.3462.

Luo F, Südhof TC. Synaptotagmin-7-Mediated Asynchronous Release Boosts High-Fidelity Synchronous Transmission at a Central Synapse. Neuron. 2017; 94(4):826–839.e3. doi: https://doi.org/10.1016/j.neuron.2017.04.020.

Madar AD, Ewell LA, Jones MV. Pattern separation of spiketrains in hippocampal neurons. Scientific reports. 2019; 9(1):1–20. doi: https://doi.org/10.1038/s41598-019-41503-8.

Mahajan G, Nadkarni S. Intracellular calcium stores mediate metaplasticity at hippocampal dendritic spines. The Journal of physiology. 2019; 597(13):3473–3502. doi: https://doi.org/10.1113/jp277726.

Malenka R, Kauer J, Perkel D, Nicoll R. The impact of postsynaptic calcium on synaptic transmission—its role in long-term potentiation. Trends in neurosciences. 1989; 12(11):444–450. doi: https://doi.org/10.1016/0166-2236(89)90094-5.

Malenka RC, Bear MF. LTP and LTD: an embarrassment of riches. Neuron. 2004; 44(1):5–21. doi: https://doi.org/10.1016/j.neuron.2004.09.012.

Malenka RC, Nicoll, A R. Long-term potentiation–a decade of progress? Science. 1999; 285(5435):1870–1874. doi: https://doi.org/10.1126/science.285.5435.1870.

Marder E, Taylor AL. Multiple models to capture the variability in biological neurons and networks. Nature neuroscience. 2011; 14(2):133. doi: https://doi.org/10.1038/nn.2735.

Mattson MP, LaFerla FM, Chan SL, Leissring MA, Shepel PN, Geiger JD. Calcium signaling in the ER: its role in neuronal plasticity and neurodegenerative disorders. Trends in neurosciences. 2000; 23(5):222–229. doi: https://doi.org/10.1016/s0166-2236(00)01548-4.

McGraw CF, Somlyo AV, Blaustein MP. Localization of calcium in presynaptic nerve terminals. An ultrastructural and electron microprobe analysis. The Journal of cell biology. 1980; 85(2):228–241. doi: https://doi.org/10.1083/jcb.85.2.228.

McHugh TJ, Jones MW, Quinn JJ, Balthasar N, Coppari R, Elmquist JK, Lowell BB, Fanselow MS, Wilson MA, Tonegawa S. Dentate gyrus NMDA receptors mediate rapid pattern separation in the hippocampal network. Science. 2007; 317(5834):94–99. doi: https://doi.org/10.1126/science.1140263.

McNaughton BL, Battaglia FP, Jensen O, Moser EI, Moser MB. Path integration and the neural basis of the'cognitive map'. Nature Reviews Neuroscience. 2006; 7(8):663–678. doi: https://doi.org/10.1038/nrn1932.

Miller JF, Neufang M, Solway A, Brandt A, Trippel M, Mader I, Hefft S, Merkow M, Polyn SM, Jacobs J, et al. Neural activity in human hippocampal formation reveals the spatial context of retrieved memories. Science. 2013; 342(6162):1111–1114. doi: https://doi.org/10.1126/science.1244056.

Ming Gl, Song H. Adult neurogenesis in the mammalian brain: significant answers and significant questions. Neuron. 2011; 70(4):687–702. doi: https://doi.org/10.1016/j.neuron.2011.05.001.

Mongillo G, Barak O, Tsodyks M. Synaptic theory of working memory. Science. 2008; 319(5869):1543–1546. doi: https://doi.org/10.1126/science.1150769.

Moore KA, Nicoll RA, Schmitz D. Adenosine gates synaptic plasticity at hippocampal mossy fiber synapses. Proceedings of the National Academy of Sciences. 2003; 100(24):14397–14402. doi: https://doi.org/10.1073/pnas.1835831100.

Mukunda CL, Narayanan R. Degeneracy in the regulation of short-term plasticity and synaptic filtering by presynaptic mechanisms. The Journal of physiology. 2017; 595(8):2611–2637. doi: https://doi.org/10.1113/jp273482.

Müller A, Kukley M, Stausberg P, Beck H, Müller W, Dietrich D. Endogenous Ca2+ buffer concentration and Ca2+ microdomains in hippocampal neurons. Journal of Neuroscience. 2005; 25(3):558–565. doi: https://doi.org/10.1523/jneurosci.3799-04.2005.

Murphy MP, LeVine III H. Alzheimer's disease and the amyloid-β peptide. Journal of Alzheimer's disease. 2010; 19(1):311–323.

Murthy VN, Schikorski T, Stevens CF, Zhu Y. Inactivity produces increases in neurotransmitter release and synapse size. Neuron. 2001; 32(4):673–682. doi: https://doi.org/10.1016/s0896-6273(01)00500-1.

Murthy VN, Sejnowski TJ, Stevens CF. Heterogeneous release properties of visualized individual hippocampal synapses. Neuron. 1997; 18(4):599–612. doi: https://doi.org/10.1016/s0896-6273(00)80301-3.

Murthy VN, Stevens CF. Reversal of synaptic vesicle docking at central synapses. Nature neuroscience. 1999; 2(6):503. doi: https://doi.org/10.1038/9149.

Nadkarni S, Bartol TM, Sejnowski TJ, Levine H. Modelling vesicular release at hippocampal synapses. PLoS computational biology. 2010; 6(11):e1000983. doi: https://doi.org/10.1371/journal.pcbi.1000983.

Nägerl UV, Novo D, Mody I, Vergara JL. Binding kinetics of calbindin-D28k determined by flash photolysis of caged Ca2+. Biophysical Journal. 2000; 79(6):3009–3018.

Nelson O, Tu H, Lei T, Bentahir M, De Strooper B, Bezprozvanny I, et al. Familial Alzheimer disease–linked mutations specifically disrupt Ca 2+ leak function of presenilin 1. The Journal of clinical investigation. 2007; 117(5):1230–1239. doi: https://doi.org/10.1172/JCI30447.

Neunuebel JP, Knierim JJ. CA3 retrieves coherent representations from degraded input: direct evidence for CA3 pattern completion and dentate gyrus pattern separation. Neuron. 2014; 81(2):416–427. doi: https://doi.org/10.1016/j.neuron.2013.11.017.

Neunuebel JP, Yoganarasimha D, Rao G, Knierim JJ. Conflicts between local and global spatial frameworks dissociate neural representations of the lateral and medial entorhinal cortex. Journal of Neuroscience. 2013; 33(22):9246–9258. doi: https://doi.org/10.1523/JNEUROSCI.0946-13.2013.

Nicoll RA, Schmitz D. Synaptic plasticity at hippocampal mossy fibre synapses. Nature Reviews Neuroscience. 2005; 6(11):863–876. doi: https://doi.org/10.1038/nrn1786.

O'reilly RC, McClelland JL. Hippocampal conjunctive encoding, storage, and recall: Avoiding a trade-off. Hippocampus. 1994; 4(6):661–682. doi: https://doi.org/10.1002/hipo.450040605.

Penheiter AR, Bajzer Ž, Filoteo AG, Thorogate R, Török K, Caride AJ. A model for the activation of plasma membrane calcium pump isoform 4b by calmodulin. Biochemistry. 2003; 42(41):12115–12124. doi: https://doi.org/10.1021/bi027098+.

Per A, Richard M, Amaral DG, Tim B, O'Keefe KJ. The hippocampal formation. In: *The hippocampus book* Oxford University Press; 2009.doi: https://doi.org/10.1093/acprof:oso/9780195100273.003.0001.

Pfister JP, Dayan P, Lengyel M. Synapses with short-term plasticity are optimal estimators of presynaptic membrane potentials. Nature neuroscience. 2010; 13(10):1271. doi: https://doi.org/10.1038/nn.2640.

Popugaeva E, Pchitskaya E, Bezprozvanny I. Dysregulation of intracellular calcium signaling in Alzheimer's disease. Antioxidants & redox signaling. 2018; 29(12):1176–1188.

Regehr WG. Short-term presynaptic plasticity. Cold Spring Harbor perspectives in biology. 2012; 4(7):a005702. doi: https://doi.org/10.1101/cshperspect.a005702.

Rollenhagen A, Sätzler K, Rodríguez EP, Jonas P, Frotscher M, Lübke JH. Structural determinants of transmission at large hippocampal mossy fiber synapses. Journal of Neuroscience. 2007; 27(39):10434–10444. doi: https://doi.org/10.1523/JNEUROSCI.1946-07.2007.

Rolls E. The mechanisms for pattern completion and pattern separation in the hippocampus. Frontiers in systems neuroscience. 2013; 7:74. doi: https://doi.org/10.3389/fnsys.2013.00074.

Rolls ET. A computational theory of episodic memory formation in the hippocampus. Behavioural brain research. 2010; 215(2):180–196. doi: https://doi.org/10.1016/j.bbr.2010.03.027.

Rosenbaum RS, Köhler S, Schacter DL, Moscovitch M, Westmacott R, Black SE, Gao F, Tulving E. The case of K.C.: contributions of a memory-impaired person to memory theory. Neuropsychologia. 2005; 43(7):989–1021. doi: https://doi.org/10.1016/j.neuropsychologia.2004.10.007.

Rosenbaum R, Rubin J, Doiron B. Short term synaptic depression imposes a frequency dependent filter on synaptic information transfer. PLoS computational biology. 2012; 8(6):e1002557. doi: https://doi.org/10.1371/journal.pcbi.1002557.

Saftenku E, Williams AJ, Sitsapesan R. Markovian models of low and high activity levels of cardiac ryanodine receptors. Biophysical journal. 2001; 80(6):2727–2741. doi: https://doi.org/10.1016/s0006-3495(01)76241-8.

Salin PA, Scanziani M, Malenka RC, Nicoll RA. Distinct short-term plasticity at two excitatory synapses in the hippocampus. Proceedings of the National Academy of Sciences. 1996; 93(23):13304–13309. doi: https://doi.org/10.1073/pnas.93.23.13304.

Schmidt-Hieber C, Häusser M. Cellular mechanisms of spatial navigation in the medial entorhinal cortex. Nature neuroscience. 2013; 16(3):325. doi: https://doi.org/10.1038/nn.3340.

Schneggenburger R, Sakaba T, Neher E. Vesicle pools and short-term synaptic depression: lessons from a large synapse. Trends in neurosciences. 2002; 25(4):206–212. doi: https://doi.org/10.1016/s0166-2236(02)02139-2.

Selkoe DJ. Alzheimer's disease is a synaptic failure. Science. 2002; 298(5594):789–791. doi: https://doi.org/10.1126/science.1074069.

Sharp AH, McPherson PS, Dawson TM, Aoki C, Campbell KP, Snyder SH. Differential immunohistochemical localization of inositol 1, 4, 5-trisphosphate-and ryanodine-sensitive Ca2+ release channels in rat brain. Journal of Neuroscience. 1993; 13(7):3051–3063. doi: https://doi.org/10.1523/jneurosci.13-07-03051.1993.

Shepherd GM, Harris KM. Three-dimensional structure and composition of CA3-CA1 axons in rat hippocampal slices: implications for presynaptic connectivity and compartmentalization. Journal of Neuroscience. 1998; 18(20):8300–8310. doi: https://doi.org/10.1523/JNEUROSCI.18-20-08300.1998.

Solovyova N, Veselovsky N, Toescu E, Verkhratsky A. Ca2+ dynamics in the lumen of the endoplasmic reticulum in sensory neurons: direct visualization of Ca2+-induced Ca2+ release triggered by physiological Ca2+ entry. The EMBO journal. 2002; 21(4):622–630.

Stevens CF, Wang Y. Changes in reliability of synaptic function as a mechanism for plasticity. Nature. 1994; 371(6499):704. doi: https://doi.org/10.1073/pnas.93.12.5747.

Stiles JR, Bartol TM, et al. Monte Carlo methods for simulating realistic synaptic microphysiology using MCell. Computational neuroscience: realistic modeling for experimentalists. 2001; p. 87–127.

Stiles JR, Van Helden D, Bartol T, Salpeter EE, Salpeter MM. Miniature endplate current rise times< 100 s from improved dual recordings can be modeled with passive acetylcholine diffusion from a synaptic vesicle. Proceedings of the National Academy of Sciences. 1996; 93(12):5747–5752. doi: https://doi.org/10.1073/pnas.93.12.5747.

Stimberg M, Brette R, Goodman DF. Brian 2, an intuitive and efficient neural simulator. Elife. 2019; 8:e47314. doi: https://doi.org/10.7554/eLife.47314.

Strange BA, Witter MP, Lein ES, Moser EI. Functional organization of the hippocampal longitudinal axis. Nature Reviews Neuroscience. 2014; 15(10):655–669. doi: https://doi.org/10.1038/nrn3785.

Stutzmann GE, Caccamo A, LaFerla FM, Parker I. Dysregulated IP3 signaling in cortical neurons of knock-in mice expressing an Alzheimer's-linked mutation in presenilin1 results in exaggerated Ca2+ signals and altered membrane excitability. Journal of Neuroscience. 2004; 24(2):508–513. doi: https://doi.org/10.1523/jneurosci.4386-03.2004.

Thibault O, Gant JC, Landfield PW. Expansion of the calcium hypothesis of brain aging and Alzheimer's disease: minding the store. Aging cell. 2007; 6(3):307–317. doi: https://doi.org/10.1111/j.1474-9726.2007.00295.x.

Toth K, Suares G, Lawrence JJ, Philips-Tansey E, McBain CJ. Differential mechanisms of transmission at three types of mossy fiber synapse. Journal of Neuroscience. 2000; 20(22):8279–8289. doi: https://doi.org/10.1523/JNEUROSCI.20-22-08279.2000.

Treves A, Rolls ET. Computational analysis of the role of the hippocampus in memory. Hippocampus. 1994; 4(3):374–391. doi: https://doi.org/10.1002/hipo.450040319.

Treves A, Tashiro A, Witter MP, Moser EI. What is the mammalian dentate gyrus good for? Neuroscience. 2008; 154(4):1155–1172. doi: https://doi.org/10.1016/j.neuroscience.2008.04.073.

Tsukita S, Ishikawa H. Three-dimensional distribution of smooth endoplasmic reticulum in myelinated axons. Microscopy. 1976; 25(3):141–149.

Tu H, Nelson O, Bezprozvanny A, Wang Z, Lee SF, Hao YH, Serneels L, De Strooper B, Yu G, Bezprozvanny I. Presenilins form ER Ca2+ leak channels, a function disrupted by familial Alzheimer's disease-linked mutations. Cell. 2006; 126(5):981–993. doi: https://doi.org/10.1016/j.cell.2006.06.059.

Van Strien N, Cappaert N, Witter M. The anatomy of memory: an interactive overview of the parahippocampal–hippocampal network. Nature reviews neuroscience. 2009; 10(4):272–282. doi: https://doi.org/10.1038/nrn2614.

Vandecaetsbeek I, Trekels M, De Maeyer M, Ceulemans H, Lescrinier E, Raeymaekers L, Wuytack F, Vangheluwe P. Structural basis for the high Ca2+ affinity of the ubiquitous SERCA2b Ca2+ pump. Proceedings of the National Academy of Sciences. 2009; 106(44):18533–18538. doi: https://doi.org/10.1073/pnas.0906797106.

Verkhratsky A. The endoplasmic reticulum and neuronal calcium signalling. Cell calcium. 2002; 32(5-6):393–404. doi: https://doi.org/10.1016/s0143416002001896.

Villegas R, Martinez NW, Lillo J, Pihan P, Hernandez D, Twiss JL, et al. Calcium release from intra-axonal endoplasmic reticulum leads to axon degeneration through mitochondrial dysfunction. Journal of Neuroscience. 2014; 34(21):7179–7189.

Vyleta NP, Borges-Merjane C, Jonas P. Plasticity-dependent, full detonation at hippocampal mossy fiber–CA3 pyramidal neuron synapses. Elife. 2016; 5:e17977. doi: https://doi.org/10.7554/elife.17977.

Vyleta NP, Jonas P. Loose coupling between Ca2+ channels and release sensors at a plastic hippocampal synapse. Science. 2014; 343(6171):665–670. doi: https://doi.org/10.1126/science.1244811.

Westrum LE, Gray EG. New observations on the substructure of the active zone of brain synapses and motor endplates. Proc R Soc Lond B. 1986; 229(1254):29–38. doi: https://doi.org/10.1371/journal.pone.0114033.

Witter MP, Groenewegen HJ, Lopes da Silva FH, Lohman AHM. Functional organization of the extrinsic and intrinsic circuitry of the parahippocampal region. Progress in Neurobiology. 1989; 33(3):161–253. doi: https://doi.org/10.1016/0301-0082(89)90009-9.

Wu B, Yamaguchi H, Lai FA, Shen J. Presenilins regulate calcium homeostasis and presynaptic function via ryanodine receptors in hippocampal neurons. Proceedings of the National Academy of Sciences. 2013; 110(37):15091–15096. doi: https://doi.org/10.1073/pnas.1304171110.

Wu XS, Wu LG. The yin and yang of calcium effects on synaptic vesicle endocytosis. Journal of Neuroscience. 2014; 34(7):2652–2659. doi: https://doi.org/10.1523/jneurosci.3582-13.2014.

Xu J, Mashimo T, Südhof TC. Synaptotagmin-1, -2, and -9: Ca2+ Sensors for Fast Release that Specify Distinct Presynaptic Properties in Subsets of Neurons. Neuron. 2007; 54(4):567–581. doi: https://doi.org/10.1016/j.neuron.2007.05.004.

Yalçın B, Zhao L, Stofanko M, O'Sullivan NC, Kang ZH, Roost A, Thomas MR, Zaessinger S, Blard O, Patto AL, et al. Modeling of axonal endoplasmic reticulum network by spastic paraplegia proteins. Elife. 2017; 6:e23882. doi: https://doi.org/10.7554/eLife.23882.

Yang SN, Tang YG, Zucker RS. Selective induction of LTP and LTD by postsynaptic [Ca2+] i elevation. Journal of neurophysiology. 1999; 81(2):781–787. doi: https://doi.org/10.1152/jn.1999.81.2.781.

Zalutsky RA, Nicoll RA. Comparison of two forms of long-term potentiation in single hippocampal neurons. Science. 1990; 248(4963):1619–1624. doi: https://doi.org/10.1126/science.2114039.

Zhang C, Wu B, Beglopoulos V, Wines-Samuelson M, Zhang D, Dragatsis I, Südhof TC, Shen J. Presenilins are essential for regulating neurotransmitter release. Nature. 2009; 460(7255):632.

Zhang H, Sun S, Herreman A, De Strooper B, Bezprozvanny I. Role of presenilins in neuronal calcium homeostasis. Journal of Neuroscience. 2010; 30(25):8566–8580. doi: Role of presenilins in neuronal calcium homeostasis.

Zhang S, Zhang M, Cai F, Song W. Biological function of Presenilin and its role in AD pathogenesis. Translational neurodegeneration. 2013; 2(1):1–13.